The Impact of Climate Change and Soil Management on Root System Architecture and rhizosphere processes in Winter Wheat ¿ Insight from an Ecotron experiment

Auteur : Kirbas, Gaëlle
Promoteur(s) : Delaplace, Pierre; Michel, Jennifer
Faculté : Gembloux Agro-Bio Tech (GxABT)
Diplôme : Master en bioingénieur : sciences agronomiques, à finalité spécialisée
Année académique : 2024-2025
URI/URL : http://hdl.handle.net/2268.2/23227

LIÈGE université
Gembloux
Agro-Bio Tech

The Impact of Climate Change and Soil Management on Root System Architecture and rhizosphere processes in Winter Wheat

–

Insight from an Ecotron experiment.

Gaëlle Kirbas

Master thesis submitted in order to obtain the Bioengineering Master's Degree in Agricultural Sciences

-

Co-promotors: Delaplace Pierre & Michel Jennifer

Academic year 2024-2025

LIÈGE université
Gembloux
Agro-Bio Tech

The Impact of Climate Change and Soil Management on Root System Architecture and rhizosphere processes in Winter Wheat

–

Insight from an Ecotron experiment.

Gaëlle Kirbas

Master thesis submitted in order to obtain the Bioengineering Master's Degree in Agricultural Sciences

-

Co-promotors: Delaplace Pierre & Michel Jennifer

Academic year 2024-2025

Host institution

This master thesis was conducted within the 'Plant Genetics and Rhizosphere Processes laboratory' (PGRP) of the 'Plant Biology' laboratory at the faculty Gembloux Agro Bio Tech from ULiège. All the equipment necessary for this research were provided by this laboratory, namely the flatbed scanner, the backlit imaging system, the RhizoVision Explorer software, the spectrophotometric microplane reader, precision balance, various chemical products, and their corresponding user manuals and analysis protocols.

Acknowledgements

Je tiens à remercier toutes les personnes ayant contribué à ce que ce travail de fin d'études voit enfin le jour, que ce soit au travers de conseils, de discussions motivantes sur le sujet, d'encouragements, ou de toutes formes d'intérêt. Je tiens à remercier particulièrement mes co-promoteurs Jennifer Michel et Pierre Delaplace pour m'avoir guidée tout au long de ce travail, ainsi que tous les membres du laboratoire de physiologie végétale pour m'avoir partagé leurs pratiques et précieux conseils sur l'étude passionnante des systèmes racinaires. Je remercie Sok Lay, Jimmy Bin, Sébastien Cougnet, Simon Biver, Adrien Blum, et Quentin Guidosse pour leurs aides occasionnelles et surtout pour l'accueil bienveillant qu'ils m'ont réservé au sein de leur environnement de travail. Je remercie aussi M. Patrick Dujardin pour m'avoir donné ce goût pour l'étude des plantes. Je remercie toutes les personnes que j'ai rencontrés à Gembloux Agro Bio Tech ou ailleurs ayant ponctué mon cycle d'études de joies diverses et moments mémorables. Je remercie bien-sûr les membres de ma famille qui n'ont pas baissé les bras devant ma motivation parfois défaillante. Je remercie Joachim pour son soutien inébranlable et sa présence inconditionnelle. Enfin, je remercie toutes les personnes de mon entourage qui ont cru en moi du début à la fin, et qui m'ont poussée à aller jusqu'au bout de ce long et ardu voyage personnel de l'adolescence à l'âge adulte. Puis, je me remercie moi-même pour avoir finalement franchi cette ligne d'arrivée qui tardait à apparaître.

Résumé

Le changement climatique (CC) représente un défi majeur pour la sécurité alimentaire mondiale actuelle et future en affectant considérablement la productivité des systèmes agricoles. Le blé d'hiver est un aliment de base largement consommé et produit en Europe qui est particulièrement vulnérable au CC. Or, la production de blé mondiale doit être augmentée de 70 Mt d'ici 2050 pour pouvoir nourrir une population estimée à 9.8 milliards d'ici la moitié du siècle. La compétition pour les ressources et la terre, couplée à la dégradation de l'environnement par l'agriculture intensive, imposent de développer des systèmes agricoles plus efficients en ressources capables de maintenir la productivité des agroécosystèmes sur le long terme. C'est dans ce contexte qu'il faut trouver de nouvelles pratiques agricoles pouvant accroître la résilience du blé sous les contraintes du CC, tout en préservant l'environnement. Ce mémoire de fin d'étude étudie les relations entre architecture racinaire du blé, microbes de la rhizosphère et indicateurs de rendement, sous des climats futurs simulés, et deux types de gestion du sol contrastés (apports faibles vs. élevés en matière organique), afin de déterminer quelles pratiques agricoles peuvent améliorer la résilience du blé au CC. Les résultats obtenus indiquent que les climats futurs favorisent plutôt la production de biomasse aérienne par rapport aux racines chez le blé d'hiver, bien que les réponses racinaires sont non-linéaires : la prolifération racinaire est accrue dans le climat de 2068 mais réduite dans le climat de 2085, témoignant de la complexité des réponses adaptatives du blé face au CC. Des systèmes racinaires plus profonds ont été observés dans les sols à haute teneur en matière organique, mais cela n'a pas conféré d'avantages de rendement. À l'inverse, les plants de blé dans le sol à faible teneur en matière organique ont favorisé des systèmes racinaires plus superficiels donnant un meilleur rendement, mais qui ont probablement accru le risque de lessivage des nitrates. Ces résultats corroborent le besoin de sélectionner des plants de blé ayant un système dimorphique capable de se développer autant en profondeur qu'en surface, afin d'allier rendement agricole et réduction de la pollution des écosystèmes. Des essais long-terme en champs sont nécessaires pour valider les résultats obtenus dans cette étude, ce afin de guider au mieux une production de blé résiliente au CC.

Mots-clés: Froment d'hiver; Triticum aestivum; Changement climatique; Architecture racinaire (RSA); cycle du carbone; cycle de l'azote; allocation du carbone; lessivage des nitrates; santé du sol; rhizosphère; agriculture durable; gestion des sols; résilience.

Abstract

Climate change (CC) poses significant challenges to global food security by affecting crop productivity. Winter wheat (Triticum aestivum L.), a major staple food consumed in Europe, is particularly vulnerable to CC. Yet, wheat production must increase by 70 Mt by 2050 to feed the projected 9.8 billion people. Competition for land and resources coupled with the degradation of the environment by intensive agriculture demands resource-efficient agricultural systems that maintain agroecosystems' ability to provide goods and services in the long run. In this context, sustainable agricultural strategies that enhance wheat resilience under CC are urgently needed. This study investigates the interactions between Root System Architecture (RSA), rhizosphere processes, and wheat performance under simulated future climate scenarios and contrasting soil management practices (low vs. high organic matter input) in order to identify potential innovative farming practices that simultaneously sustain wheat yield and preserve the environment under the challenges of CC. Results indicate that elevated CO_2 and warming influence carbon allocation in wheat, by promoting shoot over root biomass. However, RSA responses to climate stress were non-linear: root proliferation increased under the 2068 scenario but declined under the more extreme 2085 climate, indicating complex adaptative responses of wheat under CC. Deeper RSA traits were observed in high-SOM soils, yet these did not confer yield advantages, likely due to increased microbial competition for nitrogen. Conversely, low-SOM soils promoted shallower roots with consistently higher grain yield but increased the risk of nitrate leaching. These findings highlight the need of breeding dimorphic wheat ideotypes capable of forming both shallow and deep roots to ally the needs of sustaining wheat yield increases, with the preservation of the environment. Future long-term field trials are essential to validate these insights and guide a more resilient wheat production in the face of CC.

Keywords: Winter wheat; Triticum aestivum; Climate change; root rystem architecture (RSA); carbon cycling; nitrogen cycling; carbon allocation; nitrate leaching; soil health; rhizosphere; sustainable agriculture; soil management; resilience.

Table of content

List of figures

List of tables

List of acronyms

- **ANOVA** – Analysis of Variance
- **AMF -** Arbuscular Mycorrhizal Fungi
- **BIOFAIR** – BIOdiversity of soils and FArming Innovations for improved Resilience in European wheat agrosystems
- **BNF -** Biological Nitrogen Fixation
- **CA** – Conservation Agriculture
- **CER** – Controlled Environment Room
- **CIM** – Cardy Ion Meter
- **CC** – Climate Change
- **CLD** – Compact Letter Display
- **DAS** – Days After Sowing
- **EMMeans** – Estimated Marginal Means
- **ES** – Ecosystem Service
- **GHG** – Greenhouse Gas
- **GNC** – Grain Nitrogen Content
- **GxABT** – Gembloux Agro Bio Tech
- **GY** – Grain Yield
- **IFP** – Innovative Farming Practices
- **INM** – Integrated Nutrient Management
- **IQR** – Interquartile Range
- **LMM** – Linear Mixed Model
- **MANOVA** – Multivariate Analysis of Variance
- **MBC** – Microbial Biomass Carbon
- **OM** – Organic Matter
- **OF** – Organic Farming
- **PCA** – Principal Component Analysis
- **PC** – Principal Component
- **PGPM** – Plant Growth Promoting Microorganisms
- **pPCA** – Probabilistic Principal Component Analysis
- **RCP** – Representative Concentration Pathway
- **RSA** – Root System Architecture
- **SOM** – Soil Organic Matter
- **SW** – Spring Wheat
- **TRL** – Total Root Length
- **TRL_log** – log-transformed Total Root Length
- **WHC** – Water Holding Capacity
- **WRB** – World Reference Base for Soil Resources
- **WW** – Winter Wheat

1. Introduction

Climate Change (CC) is one of the most talked-about issues of our time notably because of its uncertain consequences on crop production worldwide and its related food insecurity (Lobell et al., 2013). Global population growth reaching 9.8 billion people by 2050 puts additional pressure on agricultural systems to provide enough food for everyone (DESA, 2017). Competition for land, water and energy further complicates the problem by limiting the resources available for agriculture (Godfray et al., 2010). Intensification of agricultural systems is therefore indispensable (Parry et al., 2011; Reynolds et al., 2011) but this has to be achieved without compromising agriculture's long-term viability.

Past agricultural intensification strategies deployed under the 'Green Revolution' have led to large-scale environmental degradation including increased soil erosion, biodiversity loss, declining soil fertility, and greenhouse gas (GHG) emissions, all of which undermine the capacity of ecosystems to sustain food production in the long run (Foley et al., 2005). Novel strategies such as 'Sustainable agriculture' or 'Agroecology' propose to integrate natural biological cycles and ecological interactions into farming systems while making an efficient use of nonrenewable resources and preserving the environment (Altieri, 2018; Doval, 2018). This way, we ensure the long-term ability of agroecosystems to provide goods and services, and secure a safe, sufficient, and sustainable food supply for future generations.

Wheat (*Triticum Aestivum L*.) is the fourth most cultivated cereal worldwide after rice and maize ("FAOSTAT," 2023), contributing approximately 20% of total dietary calories and protein intake globally, which makes it a cornerstone of worldwide food security (Shiferaw et al., 2013). Over the next decade, wheat production is assumed to increase by 70 Mt to meet the 21% yield growth target necessary for a Zero Hunger world, along with a 6% reduction in GHG emissions (OECD et al., 2022). However, climate change will impact wheat production in ways that hamper such productivity growth (Myers et al., 2018).

In Europe, CC is modifying the geographical distribution of agro-climatic zones by lengthening the crops' growing season, thereby altering crop growth suitability (Ceglar et al., 2019). Since 1990, warming and precipitation changes have contributed to continent-wide reductions in wheat yields (Moore et al., 2015; van der Velde et al., 2018), a trend which is expected to intensify in the coming decades (Ben-Ari et al., 2018). Given that Europe produces 33% of global wheat yield, 25% of which is exported to third-party countries, maintaining high yields is critical for global food security (Shiferaw et al., 2013; "FAOSTAT," 2023; Palacin, 2024).

Initiatives such as "**BIO**diversity of soils and **FA**rming **I**nnovations for improved **R**esilience in European wheat agrosystems" ("BIOFAIR," 2023) help to achieve this goal by seeking ways to enhance wheat yields under the constraints of climate change. Central to this approach is the study of the soil microbiome within the wheat rhizosphere, which is a key factor of crop performance (Cangioli et al., 2022). Soil microbes enhance plant growth and resilience to biotic and abiotic stresses (Vandenkoornhuyse et al., 2015). However, they are themselves vulnerable to CC, as abiotic factors influence their composition and function (Agler et al., 2016). Understanding how these respond and adapt to CC is therefore crucial for seeking ways to sustain their beneficial roles on agricultural productivity in the future.

This brings the subject of my master's thesis which investigates the interactions between Root System Architecture (RSA) of WW and soil microbes under various climate scenarios and soil management strategies. RSA, which refers to the spatiotemporal organization of root organs, plays a crucial role in determining wheat's ability to acquire soil resources (Lynch, 2022). Under suboptimal water and nutrient availability, roots can alter their phenotype to optimize soil resource uptake, a phenomenon described to as root architectural plasticity (Lynch, 2019).

RSA plasticity enables plants to adapt to environmental stress, but the extent to which plant-microbe interactions contribute to this process remains unclear. Plant-growth promoting microorganisms (PGPM) can cause changes in root architecture through the secretion of plant growth regulators. In turn, plants exposed to abiotic stress can recruit specific microbes that help them acquire more of the limiting resource through the exudation of specific compounds (Rengel et al., 2000; Micallef et al., 2009; Castrillo et al., 2017).

Linking root architecture with carbon rhizodeposition is thus important to understand the benefits plants gain to establish plant-microbial associations for soil resource capture (Galindo-Castañeda et al., 2022). This study aims to (1) evaluate how variations in RSA emerge under simulated future climates and contrasting soil management regimes (conventional vs. organic), (2) investigate whether these traits are associated with enhanced rhizodeposition in the wheat rhizosphere, (3) identify which root traits are best correlated with wheat yield and nutritional value, and (4) determine which soil management regime is most interesting to enhance wheat's resilience in the face of CC. By linking RSA, rhizodeposition, and yield, this study will provide insights into soil management strategies that sustain wheat's productivity while maintaining soil health and fertility under future climates.

2. State-of-the-art

2.1. Climate Change

Climate Change is defined as the long-term shift in weather patterns of the Earth's climates according to the NASA ("What Is Climate Change?,", n.d.). Although changes in climate patterns occur naturally, as when volcanoes erupt or the sun's activity varies, Earth's global climate has seen an alarming disruption since the 20th century when humans began using fossil fuels as their main source of energy (Nations, n.d.). Today, it is overall agreed that human activities have caused global warming through the emissions of GHG (Calvin et al., 2023). The total anthropogenic increase in global surface temperature between pre-industrial levels (1850-1900) and the last decade (2010-2019) is between 0.8°C and 1.3°C (Calvin et al., 2023).

This rise in temperature has already caused widespread adverse impacts across the globe, mainly through the increased frequency of extreme events like hurricanes, wildfires, heatwaves, droughts, heavy precipitation, and floods. Climate-sensitive sectors such as agriculture and energy have already exposed millions of people to food insecurity (Calvin et al., 2023). However, regions of the world are not equally affected, with mid- and low-latitude regions experiencing more negative impacts than high-latitude regions (Calvin et al., 2023).

In Europe, rising temperatures will shift the geographical distribution of climate zones (European Commission, n.d.). Agricultural yields may decline due to higher temperatures, more frequent heavy precipitation, and increased agricultural droughts. Southern Europe is particularly vulnerable to CC, as they face considerable declines in overall rainfall and more severe droughts. In contrast, Northern and Western Europe are expected to receive more annual rainfall, though not all models agree on such assumption (Figure 1) (Jacob et al., 2014; "Impact drivers," 2024). Nevertheless, uneven seasonal distribution of precipitation will likely lead to more extreme droughts and heavy rainfall events, posing serious threats to crop growth and yield, especially if these occur at critical growth stages (Zampieri et al., 2017).

In its Fifth Assessment Report AR5, the Intergovernmental Panel on Climate Change (IPCC) developed fours scenarios of climate evolution for the end of the 21st century, termed the Representative Concentration Pathways (RCPs) (Pachauri et al., 2015). These scenarios describe distinct GHG emissions pathways with their associated impacts on the biosphere and human societies, based on various socio-economic and mitigation assumptions (Calvin et al., 2023). RCP8.5 represents the highest-emission scenario inducing a radiative forcing of 8.5 W.m^{-2} (~1370 ppm CO2 eq) by 2100 (Riahi et al., 2011). It is often called the 'business as usual' pathway, as it assumes no mitigation efforts are taken to reduce GHG emissions. Under this trajectory, the projected increase in global mean surface temperature between pre-industrial levels and the end of the century is between 3.15 and 5.47 °C (Pachauri et al., 2015).

2.2. Winter wheat

Winter wheat (WW) dominates wheat production in Europe, accounting for 96% of the total annual yield (Eurostat, n.d.; USDA, n.d.), largely due to the temperate climate of Europe which provides a period of vernalization necessary for WW growth. Specifically, WW must be exposed to cold temperatures, ranging from 0° to 5°C, before heading takes (B.C. Curtis, n.d.). Therefore, WW is sown in autumn to allow it to grow sufficiently before winter. In spring, WW resumes its growth rapidly, outperforming spring wheat (SW), which is only sown in spring due to its higher frost sensitivity. Both WW and SW are harvested between April and September, depending on location and variety (B.C. Curtis, n.d.). Although WW and SW differ in several ways, they belong to the same species: common wheat (*Triticum Aestivum L.*).

Common wheat is the most cultivated wheat species in the world due to its high yield potential, strong nutritional value and excellent baking qualities (Biel et al., 2020). It contains essential minerals, vitamins and lipids essential for the human nutrition, besides being a great source of carbohydrates (Biel et al., 2020). It also has a high protein content, especially in the form gluten which is responsible for the raising of the dough during bread making. In comparison, *Triticum Durum L.* is a harder wheat species, that is more appropriate for pasta and semolina production. Beyond human consumption, wheat also provides valuable by-products: wheat straw serves for feedstock, bedding of livestock and soil amendment, while spent grain is used as a key ingredient in beer production (B.C. Curtis, n.d.).

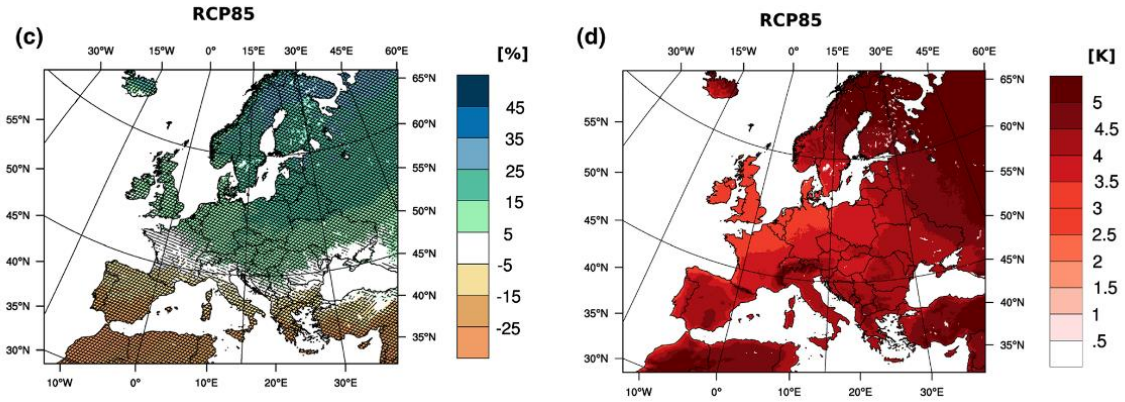

Figure 1 :*Projected changes of total annual precipitation (%) (left) and annual mean temperature [K] (right) for 2071–2100 compared to 1971–2000, for RCP8.5 (Jacob et al., 2014).*

The optimal growth and tillering temperature for WW ranges from 15 to 20°C, and the growth temperature threshold is situated between 4°C to 30°C (FAO, 2025; B.C. Curtis, n.d.). The growing period lasts 180 to 250 days, depending on location (FAO, 2025). Under the high-emission RCP8.5 scenario, Western Europe is projected to be warmer of 3°C by 2100, receive an additional +140 mm of precipitation and see CO_2 concentrations rise by +375 ppm (Jacob et al., 2014; IPCC, 2021), though variability is seen between regions (Figure 1).

Rising temperatures will disrupt the normal development of wheat, accelerating its growth period, and negatively impacting yield and nutritional grain quality (Zampieri et al., 2017; Khan et al., 2020). Extreme heat events happening at sensitive stages of plant development, such as flowering (BBCH 61-69) or grain-filling (BBCH 71-79), may considerably reduce grain yield, especially if they are prolonged (Figure 2) (Riedesel et al., 2023). When combined with

drought, the effects of heat stress are even more pronounced (Pradhan et al., 2012). Drought is most problematic during the stem elongation and booting phases (BBCH 31–50) (Figure 2) (Riedesel et al., 2023). Wheat is also highly sensitive to excess water as it leads to pest and disease proliferation, nutrient leaching, and anoxic soil conditions that hinder root respiration (Zampieri et al., 2017). In other words, wheat is vulnerable to summer drought during grain filling and winter waterlogging during establishment, which pose serious risks to future yields, as Western and Central Europe will experience drier summers and wetter winters (IPCC, n.d.).

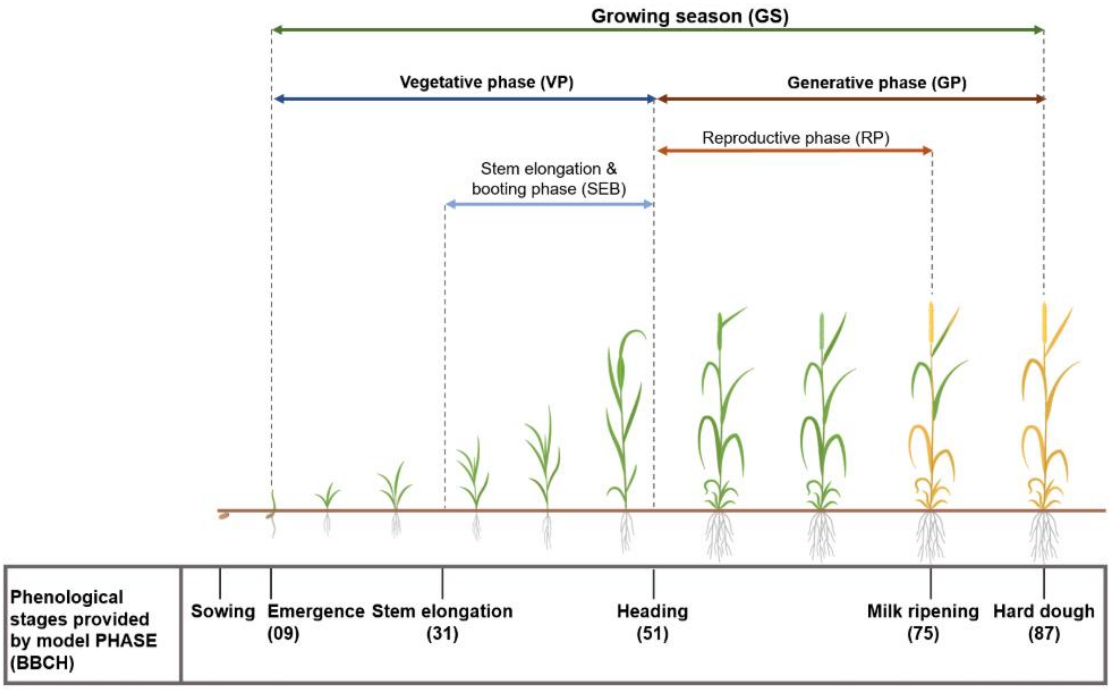

***Figure 2**: Phenological stages of winter wheat growing season, as provided by the PHASE model, with values relating to the BBCH scale throughout the vegetation period (Riedesel et al., 2023).*

While increased carbon dioxide atmospheric concentrations could enhance wheat yield through the CO_2-fertilization effect, this benefit would only be realized if nutrients are not limiting and temperature is optimal (Porter et al., 2014; Terrer et al., 2020). Extreme temperatures can rapidly offset CO_2-induced crop growth, with each 100-ppm CO_2 increase being lost with an increase of about 2°C (Asseng et al., 2019).

Strikingly, water-limited plants tend to benefit more from elevated CO_2 levels than irrigated plants, since they reduce their stomatal conductance as a consequence of CO2 abundance, which improves their water-use efficiency (Asseng et al., 2004; Porter et al., 2014). McGrath et al. (2013) showed that yield gains in rain-fed systems were greater in dry years than in wet years. However, reduced evapotranspiration could also potentially reduce plant nutrient uptake, leading to lower protein and vitamin concentrations in the grains (Myers et al., 2014).

The combined effects of increased temperature, elevated CO_2 concentrations, and shifting rainfall patterns under the RCP8.5 scenario suggest that protein yield will decline even when grain yield increase (Asseng et al., 2019). However, European countries won't be affected the same way, with low- and mid-latitude locations experiencing mostly negative yield impacts from CC, whereas higher-latitude areas may see some positive impacts. The nature of extreme weather events will also differ by region : Norther Europe will face higher risks of excessive

wet conditions from sowing to flowering while Southern Europe will face more frequent and longer droughts during the growing season (Zampieri et al., 2017; Mäkinen et al., 2018). As a result, yield reductions will be more severe in the south, while the north may experience smaller losses and even yield gains (Figure 3) (Rama et al., 2023).

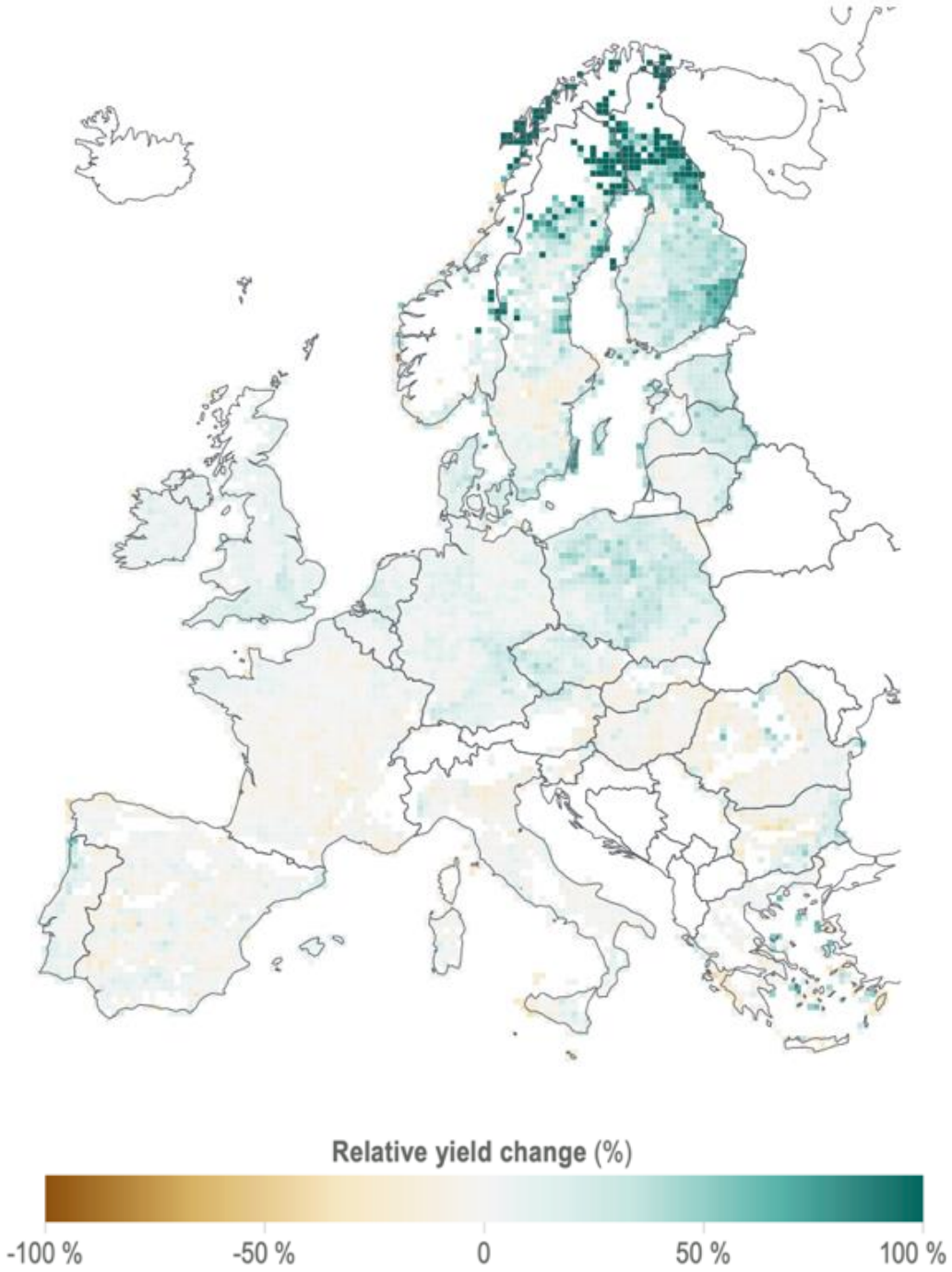

Figure 3: *Map showing relative wheat yield changes in 2055 compared to 1955 under CC and elevated CO2 for current rain-fed production systems under the RCP4.5(Rama et al., 2023).*

2.3. Soil Degradation

Today's agriculture relies mainly on external inputs such as pesticides, mineral fertilizers, irrigation, or intense tillage to achieve high crop yields. These practices directly derive from the Green Revolution heritage of the 1960s which enabled astonishing increases in crop yields. However, they have caused vast environmental damage, ranging from local consequences, such as increased erosion, lower soil fertility, and reduced biodiversity; to regional damage, such as water pollution and eutrophication; and global damage such as the disruption of Earth's hydrological and biogeochemical cycles (Matson et al., 1997). Although these modern agricultural techniques boost yields in the short term, they ultimately threaten the capacity of agroecosystems to sustain food production in the long run.

Central to this problem is soil's ability to deliver long-term goods and services. Soils provide 98.8% of humanity's total food besides offering other regulating services, such as carbon storage, greenhouse gas regulation, flood mitigation, and filtering of nutrients and contaminants, among others (Kopittke et al., 2019). Their importance in sustaining humanity is well captured by the striking quote "soil is the thin layer covering the planet that stands between us and starvation" (Karlen et al., 2014). Despite their critical role, soils are increasingly threatened by intensive agriculture, which provokes soil degradation through the loss of organic matter and biodiversity, contamination, erosion, and acidification (Kopittke et al., 2019). Worldwide, 52% of agricultural soils are estimated to be moderately to severely degraded, costing the global economy $400 billion annually (Noel et al., 2015; FAO, 2021).

Soil degradation is driven by two main mechanisms : the loss of organic matter and erosion (Karlen et al., 2015). Soil organic matter (SOM) is a key determinant of soil health and fertility: it enhances cation exchange capacity, improves water infiltration and retention, serves as a slow-release reservoir of nutrients and provides habitat for beneficial soil micro-organisms (Kopittke et al., 2019). Yet, long-term agricultural production depletes SOM stocks by removing crop residues and exporting biomass away from the fields.

Practices such as ploughing and intensive tillage further accelerate SOM loss by oxygenating the soil and stimulating microbial activity and decomposition rates. This ultimately leads to the degradation of soil structure, mainly through crusting, runoff, and erosion. Erosion, in turn, worsens SOM loss in a negative feedback loop by stripping away the most nutrient-rich and OM-dense layer of the soil profile (DeLong et al., 2015).

Conservation tillage, cover crop implementation, and enhanced OM input are often cited as practical ways to reduce erosion risks and increase OM accumulation in soils (Lal, 2015). Furthermore, they enhance soil biological properties such as nutrient cycling and pathogen suppression, while also improving soil aggregate stability and water-holding capacity, strengthening the soil's ability to buffer against climatic extremes and offering great potential for climate change adaptation (DeLong et al., 2015; Kopittke et al., 2019).

2.4. Biogeochemical Cycles

Increasing organic carbon stocks in soils also contribute to climate change mitigation. In fact, the terrestrial biosphere holds the largest carbon reservoir in the form of dead organic matter in litter and soils (1,500–2,400 PgC), far exceeding the carbon stored in living vegetation biomass (450–650 PgC) (Stocker et al., 2013). However, when SOM is lost through microbial respiration, soil's role shifts from a carbon sink to a net emitter of GHG. Although elevated atmospheric CO_2 concentration can foster photosynthesis via the CO_2 fertilization effect and OM input to soils, this is only effective when other nutrients are not limiting, especially nitrogen, which can reduce the CO_2 fertilization effect by ~65% (Terrer et al., 2020).

The biogeochemical cycles of carbon and nitrogen are closely intertwined. For example, when soil carbon stocks decrease, microorganisms lose the substrate necessary for their growth, rendering them unable to perform biological nitrogen fixation (BNF) - a process essential for the conversion of non-reactive atmospheric N_2 into reactive forms like NH_3 or NH_4^+, which are available for plant uptake (Stocker et al., 2013). This ultimately limits the fixation of carbon through photosynthesis and SOM inputs, thereby reinforcing a negative feedback loop.

Since the industrial era, conventional farming practices have substantially depleted soil organic carbon (SOC) stocks, which have affected agricultural BNF and microbial nutrient cycling. To compensate this, the Haber-Bosch process was developed in 1908 to artificially synthesize ammonia NH_3 from N_2, the primary substance used in nitrogen fertilizers. While this innovation exploded crop yields, it also led to an excessive production of reactive nitrogen (Nr) on Earth, leading to disastrous impacts on the environment, including soil and water acidification, eutrophication of waterbodies, and emission of nitrogen oxides NO_x, which are a series of potent GHGs (Figure 4) (Gruber et al., 2008; Stocker et al., 2013).

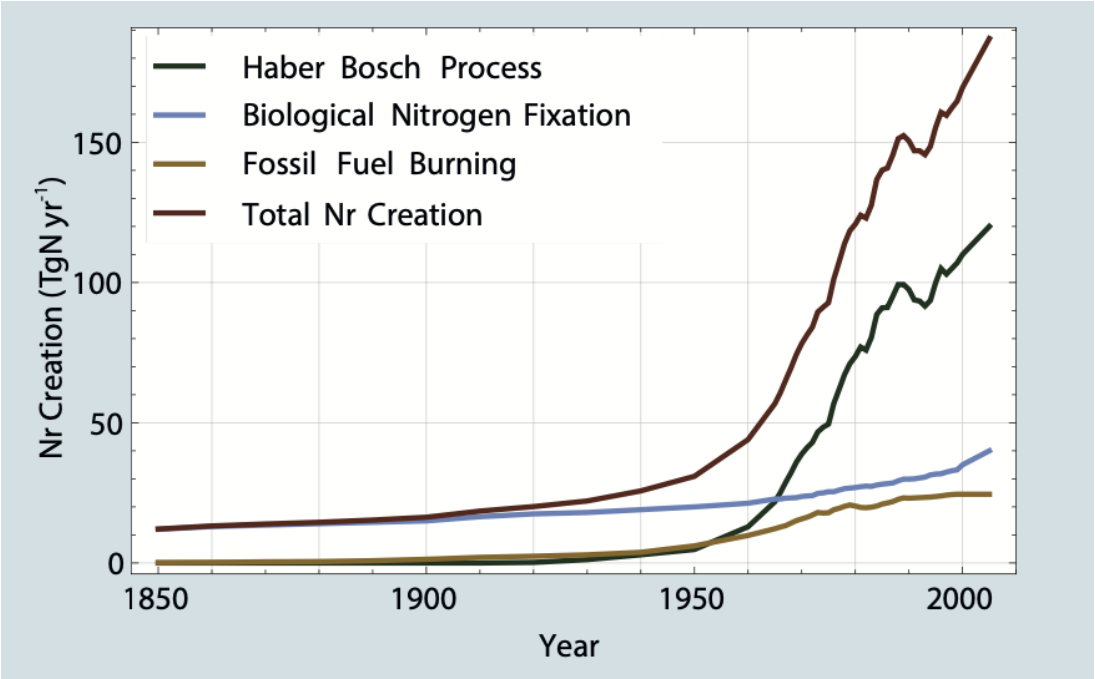

Figure 4: *Anthropogenic reactive nitrogen (Nr) production (in TgN.yr^{-1}) stemming from fossil fuel burning, cultivation-induced biological nitrogen fixation, the Haber–Bosch process, and the totality of it (Gruber et al., 2008; Stocker et al., 2013).*

2.5. Sustainable Agriculture

Given these complexities, it is crucial to adopt more sustainable agricultural systems that focus on optimizing fertilizer use while minimizing environmental harm. However, given that nitrogen availability will constrain terrestrial carbon storage throughout the 21st century, CC mitigation and agricultural productivity will only be feasible if nitrogen is not limiting (Erisman et al., 2011). But simply increasing nitrogen production through the Haber-Bosch process is not the best solution. Practices that restore soil organic matter, promote natural nitrogen fixation, and enhance soil health are actually those that will help to simultaneously mitigate CC and maintain long-term agroecosystem productivity (Chang et al., 2021).

Novel approaches such as Organic Agriculture, Agroecology and Conservation Agriculture emerged in response to the above-mentioned impacts of intensive agriculture on the environment. These promote food production with minimal harm to humans, animals and ecosystems (Hossard et al., 2016). Although each has their particularities, they share a common vision of integrating natural biological cycles and ecological interactions into farming systems, while advocating for the reduction of reliance on nonrenewable resources, the preservation of the environment and the mitigation of contributions to CC (Altieri, 2018; Doval, 2018). Collectively, they fall under the umbrella of *Sustainable Agriculture*.

Organic Farming (OF) is defined by the European Commission as a farming system that relies on ecosystem management rather than external agricultural inputs, such as synthetic fertilizers, pesticides, veterinary drugs, genetically modified organisms, etc. ("Regulation - 889/2008 - EN - EUR-Lex,", n.d.). In comparison, Conservation Agriculture (CA) promotes the combination of Integrated Nutrient Management (INM), minimum mechanical soil disturbance, and retention of crop residue in the form of mulch or cover crop (Lal, 2015).

While CA differs from OF by authorizing the use of external inputs (Hobbs et al., 2008), they both share the same goal of enhancing SOM abundance, support microbial nutrient cycling, and decrease fertilizer use. As SOM abundance increases, changes in size, activity, and composition of soil microbial communities occur, with direct consequences on the cycling and retention of nutrients. Overall, greater biodiversity translates into an increased provision of ecosystem services (ES) (Benayas et al., 2009; Wagg et al., 2014). In a meta-analysis, Rahmann (2011) showed that OF produced more biodiversity than its conventional counterpart, just as CA which proved to promote soil fungi and bacteria, and their related ES (Chen et al., 2020).

Such ES include the regulation of biogeochemical cycles, nutrient retention and delivery to plants, maintenance of soil structure and fertility, pollutant bioremediation, pest and pathogen control, and regulation of plant production through biochemical signaling. Soil mesofauna and macrofauna also contribute to nutrient cycling and soil fertility by transforming SOM into fecal pellets or by fragmenting SOM into pieces available for microbial decomposition (Jackson et al., 2017). Altogether, sustainable agriculture takes advantage of these naturally-occurring biological processes to support adequate yields, maintain soil resources over the long-term, and preserve the environment (Lehman et al., 2015).

2.6. Microbial Nutrient Cycling

One of the most interesting aspects of microbial life is their active contribution to the biogeochemical cycling of nutrients. Soil microorganisms are responsible for mineralizing organic compounds and releasing elements from SOM to make them readily available to plants. They transform all fixed soil carbon and determine its fate, transferring it between the different compartments of the terrestrial biosphere (Figure 5) (Gougoulias et al., 2014a).

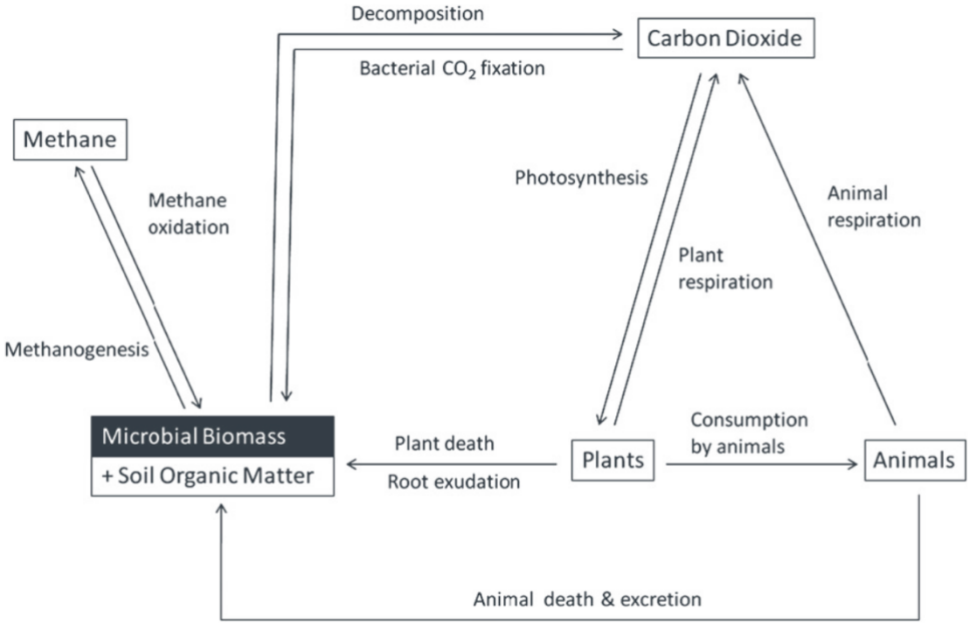

***Figure 5**: Major carbon fluxes mediated by soil microorganisms(Gougoulias et al., 2014a).*

Soil microbes are greatly diversified and exhibit a wide range of physiological capabilities, tolerances, and energy sources. They use various essential nutrients to support their metabolism, utilizing them either as electron donors or acceptors in redox reactions. This leads to the inevitable coupling of carbon cycle with that of other essential nutrients, such as nitrogen as discussed above, and influence the abundance of soil nutrients in complex and dynamic ways, with direct implications for terrestrial plants (Lehman et al., 2015).

Apart from detaining an important role in the breakdown of SOM, soil microbes fuel the nitrogen cycle, either by reducing nitrogen gas (N_2) into ammonia (NH_3) through BNF; converting ammonia to nitrite (NO_2^-) and then to nitrate (NO_3^-) through nitrification; returning nitrate or ammonia to nitrogen gas through denitrification and anammox, respectively; and decomposing nitrogen organic forms into soluble ammonia through ammonification. All of these processes combined determine the productivity of terrestrial ecosystems (Jetten, 2008).

Sustainable agriculture utilizes this remarkable microbial machinery to provide plants with sufficient nutrients for their growth and reduce unnecessary losses in the environment, namely by implementing complex rotations and cover cropping that vary the types of carbon entering the soil, and stimulate microbial groups implied in nitrogen fixation, such as free-living N fixing bacteria, symbiotic N fixers, and obligate plant symbiotic fungi like arbuscular mycorrhizal fungi (AMF) (Drinkwater et al., 2007; Dawson et al., 2008; Smith et al., 2008).

2.7 Root System Architecture

Root System Architecture (RSA) is defined as the 'spatial and temporal configuration of the root system' within the soil, with the overarching function of maximizing the efficiency of soil resource capture (Galindo-Castañeda et al., 2024). In response to suboptimal availability of nutrients and water in terrestrial ecosystems, plants have developed evolutionary mechanisms to strategically deploy their root systems in response to their above-ground metabolic demands for support, defense, and reproduction. The primary goal of RSA is thus to maintain a favorable balance between resource investment in root growth and resource acquisition enabled by this growth (Lynch, 1995). To achieve this, plants adapt their RSA in relation to nutrient patches in the soil, oxygen status, pH, and bulk density.

Roots can sense their environment and respond accordingly by adjusting their meristematic activity and allocating a just balance of resources between absorption or transport functions. This ability to alter their root phenotype in response to environmental stimuli is called *root plasticity*. This process explains why root systems can differ greatly in their architectural configuration within a same species, among genotypes of a given species, and even within a same individual, which in the latter case refers to *root dimorphism* (Lynch, 1995, 2019).

There are two main types of root systems encountered in flowering plants: the dicotyledonous one and the monocotyledonous one. The dicotyledonous one is characterized by a main tap root, from which lateral roots emerge to form a unique primary root system. The monocotyledonous one develops a secondary root system made of shoot-borne roots (i.e., adventitious roots), in parallel to the primary root system. Both types of root systems produce secondary roots that branch extensively, and form a complex network of lateral roots essential for resource acquisition due to their increased absorptive surface area (Figure 6) (Badri et al., 2009; Freschet et al., 2021). Wheat's root system is monocotyledonous.

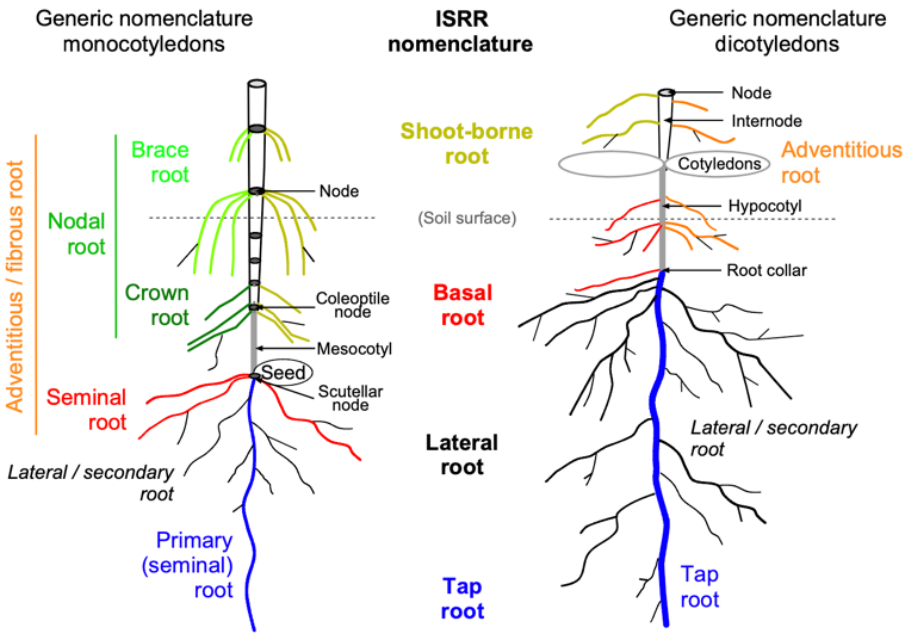

***Figure 6**: Schema of monocotyledonous (left) and dicotyledonous (right) root systems, and their related International Society of Root Research (ISSR) nomenclature (Freschet et al., 2021).*

As roots grow in the soil medium, they differentiate into distinct zones. The very end of the root tip is typically involved in the production of new cells by division, a tissue called meristem in reference to the Greek term 'meristos' meaning 'divisible'. Just above the zone of division is the zone of elongation where cells stop to divide but rather elongate in the longitudinal orientation of roots, pushing forward the root tip in the soil. The latter one is protected by a root cap called the calyptra, which is constantly renewed as it sloughs off by rubbing against soil particles during growth. To aid its passage through the soil, the calyptra secretes a lubricating substance called mucilage, which is subsequently released into the soil, alongside border cells and border-like cells (clusters of border cells) (E. Weaver, 1926).

After elongation, roots enter their maturing phase and specialize in different activities. Some absorb water and nutrients, while some conduct absorbed resources to the leaves. Some store food and others maintain the plant's stance in the soil medium. These functions can only surely be determined anatomically. However, topological, and architectural analysis can make assumptions about the functionality of these roots based on their diameters. Indeed, as plants mature, they induce secondary growth, which makes root diameter an appropriate proxy for root age. Usually, younger and finer roots are involved in absorbing activities while older and thicker roots occupy storage and transport functions (Freschet et al., 2021).

Diameter-based root classification is thus a useful technique to identify a plant's resource allocation strategy, whether it be the proliferation of fine absorbing roots in nutrient-rich areas or the construction of thick and impermeable roots that penetrate deep into the soil in search of limiting resources (Freschet et al., 2021). Past research has shown that roots grow in the direction of moist and oxygen-abundant soil pores, and that they proliferate in nutrient-rich soil patches of phosphate, nitrate, and iron (Badri et al., 2009; Sun et al., 2017).

Conversely, roots respond differently when soil resources are deficient: they grow deep for mobile nutrients that move with water flow like nitrate, whereas they grow shallow for immobile nutrients of poor diffusivity such as phosphorus and iron (Richardson et al., 2009). Nitrogen-deficient plants thus usually adopt a steep foraging strategy, while phosphorus-deficient plants branch profusely in the top soil (Figure 7) (Trachsel et al., 2013).

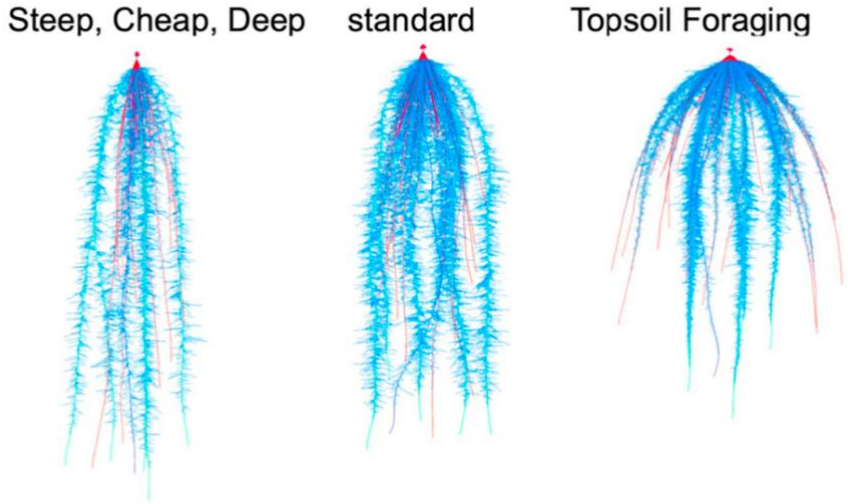

***Figure 7**: 'Steep, Cheap and Deep' and 'Topsoil Foraging' ideotypes in maize, representing the distinct soil exploration strategies of monocotyledonous crops such as wheat (Lynch, 2019).*

2.8 Rhizobiome

Plants support soil microbes by providing organic carbon either through above-ground plant litter or below-ground root litter and exudation - the latter process known as *rhizodeposition*. Rhizodeposition involves the continuous release of carbon-rich compounds from roots into the soil solution, which are typically categorized into two groups: *low-molecular-weight compounds* - including simple sugars, amino acids, sugar alcohols, organic acids, and secondary metabolites involved in plant defense and growth - and *high-molecular-weight compounds* such as mucilage and proteins (Bais et al., 2006). Root exudation accounts for 20-40% of the photosynthetically fixed C and 15% of the plant-assimilated N (Canarini et al., 2019). Glucose represents the dominant component of the exuded carbon, comprising 40-50%, though this proportion varies with genotype, plant growth stage, and environmental conditions (Hütsch et al., 2002; Chaparro et al., 2014; Mönchgesang et al., 2016).

The reason why plants allocate such an amount of photosynthates to the soil is evolutionary: plants exert mutualistic relationships with microorganisms, mostly fungi and bacteria, whereby labile sugar and amino acids are released into the soil solution to attract these microbes through chemotaxis and stimulate them to decompose the SOM around the roots This microbial stimulation is termed as 'priming effect' (Jones et al., 2004; Dijkstra et al., 2013).

There are two ways by which carbon is allocated to soil. The first one is passive and involves the diffusion of exudates from roots to soil along concentration gradients—a process referred to as root *excretion*. The second is active and involves an array of transporters and symporters that facilitate their *secretion* (Bais et al., 2006; Sasse et al., 2018). As a result, soil microbes are attracted from the bulk soil to the area in close vicinity to the roots called the *rhizosphere*. The entirety of microbial organisms living in the rhizosphere compose the *rhizobiome*.

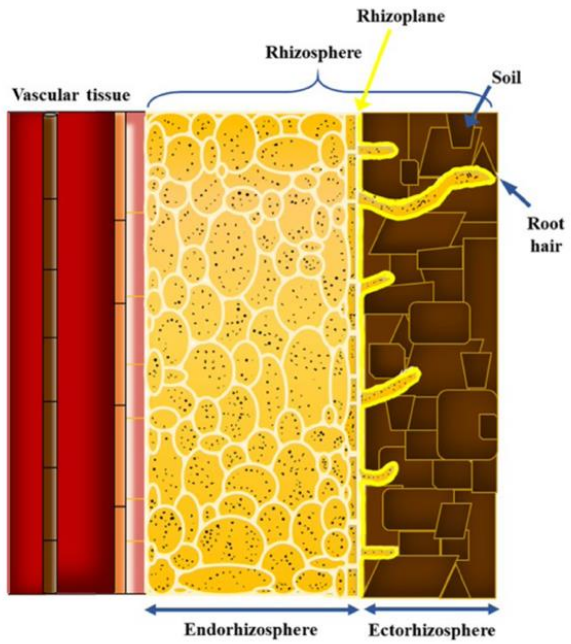

Microbial colonization shows spatial variation in relation to root systems. First, microbes exhibit radial differentiation by colonizing either the *ectorhizosphere*, *rhizoplane*, or *endorhizosphere* – which refer to the internal root tissue, root surface, and external root zone, respectively (Figure 8). Second, microbial communities show lateral differentiation along root segments, with various root regions being colonized by distinct microbial communities (DeAngelis et al., 2009). Kawasaki et al. (2021) demonstrated that the variation in microbial diversity between root classes and along root zones was of the same amplitude as that between different host types of wheat and rice.

***Figure 8**: Scheme of the rhizosphere comprising the endorhizosphere, rhizoplane and ectorhizosphere (Scavo et al., 2019).*

2.9 RSA and exudation patterns

Although root exudation is an inevitable consequence of plant growth, there are clear examples of targeted exudation that attract individual organisms (Jones et al., 2004). In fact, plants under certain stress conditions can recruit specific microbial partners that help them survive better. For example, plants exposed to nutrient deficiencies induce symbioses with mycorrhiza and rhizobia to enhance their acquisition of limiting nutrients (Carvalhais et al., 2013; Castrillo et al., 2017). Similarly, plants exposed to pathogen attacks can selectively attract biocontrol agents to protect them. This targeted recruitment is potentially mediated by the secretion of specific root exudates (Micallef et al., 2009; Rolfe et al., 2019).

Root tips are known to produce more fresh exudates than other root classes, which results in a higher number of active bacteria associated with them. Other root zones, such as the elongation zone and mature root zone harbor distinct microbial communities (Rudrappa et al., 2008; Jones et al., 2009), while shed tissues in the form of border and border-like cells exercise a strong role in plant-microbe interactions by secreting various biochemicals, alongside mucilage (Bais et al., 2006; Sasse et al., 2018). Traits such as root growth angle, rooting depth, and lateral root branching density determine the spatial distribution of root tips in the soil medium, and therefore influence the abundance and location of root exudates, ultimately shaping the composition of microbial communities in soil space (Zai et al., 2021).

Shallow root systems are usually associated with nitrifiers and methanotrophs, as these tolerate better topsoil fluctuations of temperature, moisture, and oxygen levels. On the contrary, deep root systems are rather associated with reductive microbial processes such as denitrification, ammonification, manganese and iron reduction, because these reactions only take place in anaerobic and humid conditions (Galindo-Castañeda et al., 2024).

Just as roots change exudate composition to attract specific microbes in suboptimal availability of nutrients, their architectural configuration can also be modified by soil microbes through the secretion of plant growth regulators, such as cytokinins and auxins, altering the abundance, length and branching frequency of lateral roots, and ultimately enhancing the exudation of carbohydrates for microbial growth (Badri et al., 2009; Wen et al., 2022). Hence, RSA results from a complex and dynamic interaction between the soil, microbes, and roots.

Agricultural practices further modulate these interactions. For example, topsoil of intensively fertilized soils hosts rather acid-tolerant microbes, while liquid fertilizers, which are prone to leaching into deeper soil strata, prompt plants to adopt deeper foraging strategies. Likewise, intensive tillage encourages roots to grow deep and steep in the soil to be able to penetrate through compacted soil layers. All these mechanisms ultimately influence soil microbial composition and their interactions with roots, proving how important IFP are in constructing optimized RSA for wheat performance under future climates (Galindo-Castañeda et al., 2024).

3 Objectives and Methodology

This master thesis is part of the **BIOFAIR** (***BIO****diversity of soils and* ***F****Arming* ***I****nnovations for improved* ***R****esilience in European wheat agrosystems*) project led by several European research institutions that gathered to assess the impact of CC on wheat quality traits, in concert with the study of functional soil microbiome in the wheat rhizosphere, with the overarching goal of identifying agronomic levers that could potentially mitigate the negative impacts of CC on plant productivity, while preserving soil biodiversity and ecosystem services.

BIOFAIR operates under the **BiodivERsA** European Biodiveristy Partnership, a funding agency focusing on the restoration of Europe's Biodiversity ("Biodiversa+," 2024). The project brings together seven research institutes across five European countries, including GxABT (University of Liège), UGent, INRAe, FiBL, and CSIC, among others ("BIOFAIR," 2023). The project is organized into seven work packages (WPs), each addressing a specific research topic aligned with the partners' expertise (Figure 9) ("BIOFAIR," 2023).

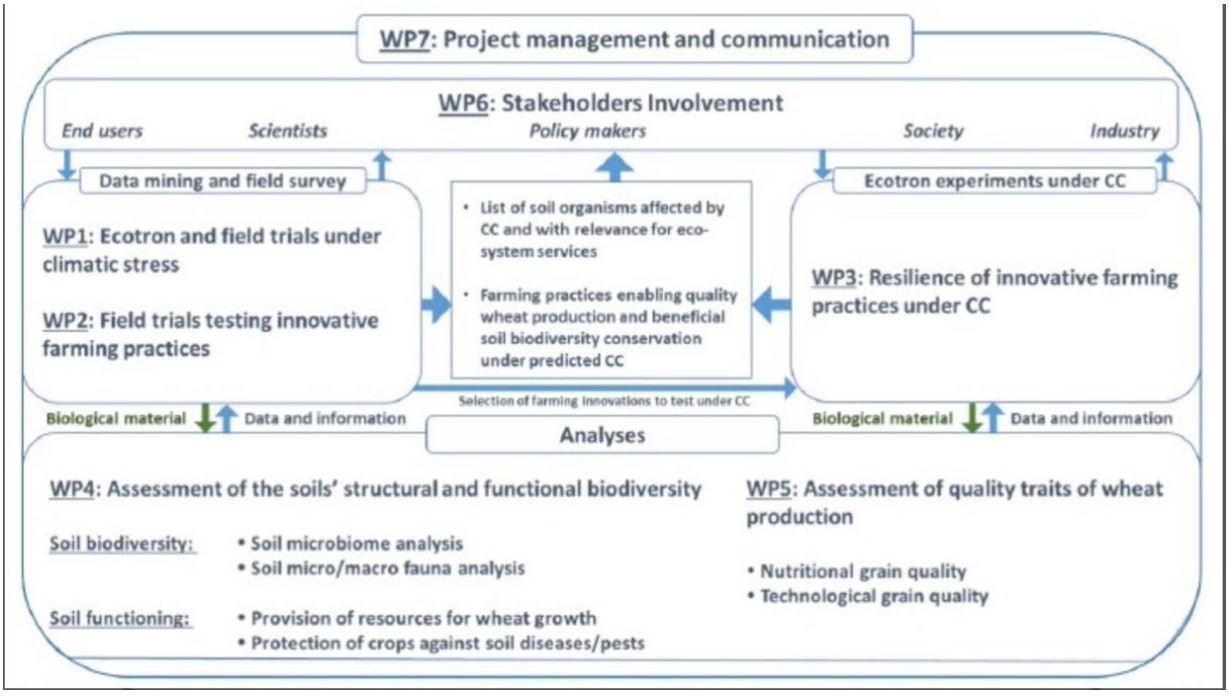

Figure 9*:Overview of work packages and workflow for the BIOFAIR project.*

BIOFAIR combines long-term field trials with controlled mesocosm experiments to measure the impact of CC on wheat yield and quality traits like nutritional and technological quality of the grain, as well as investigate the way soil taxa evolve with CC and how this in turn affects the functional quality of soils in terms of nutrient cycling and disease suppression. Ultimately, the project aims to identify and propose innovative farming practices that enhance the prevalence of beneficial taxa versus pathogenic ones, maintain the production of high-quality grains, and support wheat resilience under future climate scenarios. ("BIOFAIR," 2023).

This master's thesis was conducted within the framework of WP3, taking advantage of its experimental set-up to study the influence of specific root traits and exudation patterns on wheat yield and nutritional value under different climate scenarios and soil management strategies. Precisely, wheat plants were cultivated in controlled environment chambers (CER) that simulated the meteorological conditions of the years 2013, 2068 and 2085.

Wheat plants were grown in soils with contrasting organic matter management (high versus low organic input). Belowground and aboveground plant traits were measured throughout the full growth cycle at three key phenological stages - stem elongation, flowering, and harvest (BBCH30/50/80). Centered on the plants, soil cores were collected and stratified into two horizons (0-10 cm and 10-20 cm) (Figure 10). Additionally, interstitial soil pore water was extracted weekly – unless prevented by drought conditions - to quantify freely available glucose and nitrate equivalents as indicators of rhizosphere microbial processes.

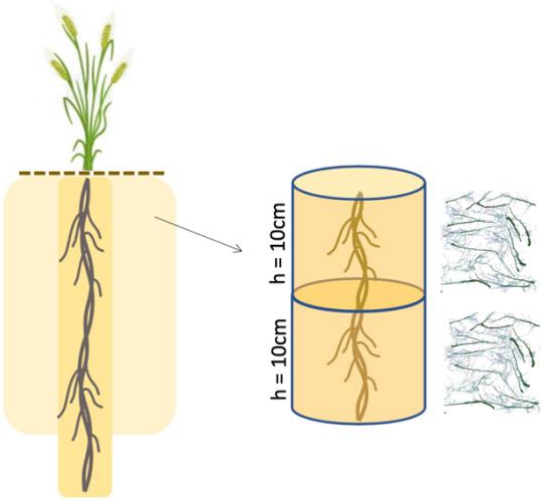

***Figure 10**:Schema of soil coring and stratification*

For root treatment, soil cores were washed on a 1 mm mesh to retrieve plant roots, which were carefully extracted with tweezers. The recovered roots were then stored in Falken tubes filled with a solution of 80% Ethanol until scanning. For imaging, roots were evenly spread in a plastic tray with water to scan them on a flatbed scanner. The obtained scans were subsequently analyzed using *RhizoVizion Explorer* to measure various root architectural traits. Soil pore water concentrations of glucose and nitrate were measured using spectrophotometry and a portable Cardy Ion Meter (CIM), respectively.

To assess "The Impact of Climate Change and Soil Management on Root System Architecture and Sugar Exudation in Winter Wheat ", the following hypotheses were tested:

H1: Root traits will be significantly impacted by different climates and soil types.
H2: Carbon (glucose equivalent) and nitrate concentrations in interstitial soil pore water will be correlated with specific root traits such as number of root tips and total root length.
H3: Root system architecture and rhizosphere chemistry will correlate with wheat nutrient uptake, yield and grain quality (e.g. soil nitrate and grain protein).

The following objectives were pursued to address this question:

- Quantify root traits under different climates and soil regimes.
- Measure exudate production in wheat plants with varying root architectures.
- Correlate root traits and exudate production across climates and soil managements.
- Evaluate the influence of root traits and exudates on wheat yield and grain quality.

4 Materials and Methods

4.1 Experimental set-up

The experiment was conducted in the Ecotron facility of the TERRA Research Center, which pertains to the Gembloux Agro-Bio Tech faculty of the University of Liège. This Ecotron facility has six controlled environment rooms (CERs) which can simulate various climatic scenarios using artificial conditions. Environmental factors such as air temperature, humidity, wind speed, pressure, precipitation, carbon dioxide and ozone levels, photon flux density, soil basal water potential and temperature can all be precisely controlled and monitored within these growth chambers. In this experiment, three specific climates were reproduced to reflect the meteorological conditions of the years 2013, 2068, and 2085.

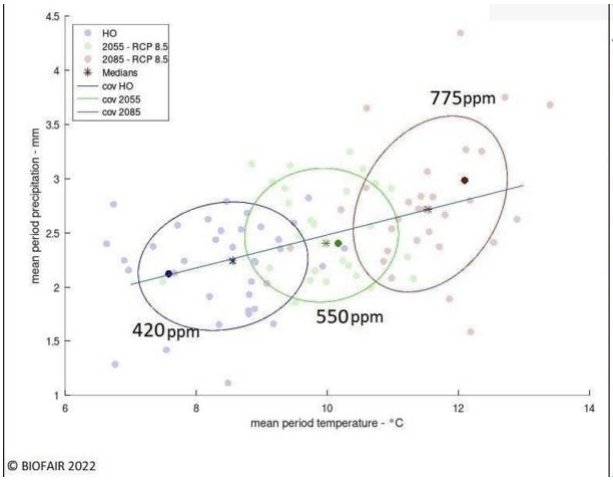

Climatic parameters	2013	2068	2085
Mean CO_2 ppm	420	550	775
Mean radiation µmol m^{-2} s^{-1}	51.81	53.98	54.49
Mean temperature °C d^{-1}	7.6	10.2	12.1
Mean precipitation mm d^{-1}	2.1	2.4	3
Hydrothermal index (rel.)	4	4.5	4.7
Maximum temperature °C	26.5	23.4	22.2
Minimum temperature °C	-7.6	-5.8	3.1
n days temperature ≤ 4°C	94	40	3
n days temperature ≥ 22°C	9	7	2
Maximum precipitation mm	46.3	39.0	47.3
Minimum precipitation mm	0.0	0.0	0.0
n days precipitation ≤ 0mm	135	4	3
n days precipitation ≥ 4mm	57	62	72

Figure 11*: Graphic illustrating the hydrothermal gradient with increasing CO2 concentration levels over time across different periods. The historical observations period is shown in blue, the 2040–2070 period in green, and the 2070–2100 period in red. The three dots represent the past climate (2013), near-future climate (2068), and farther-future climate (2085), with corresponding CO_2 levels of 420, 550, and 775 ppm, respectively. The ellipses show the 95% confidence interval for the Alaro-0 model predictions for future climates and the average synthetic data for the past climate. On the right, the average values of key variables for each climate are shown.*

The past climatic scenario (2013) was recreated using synthetic data derived from historical measurements of climatic variables at the meteorological station of Ernage in Gembloux (50°34'33"N, 4°43'1"E), since 1980. Future climatic scenarios were simulated based on the predictions of the Alaro-0 model for the RCP8.5 $W.m^{-2}$ concerning the respective periods of 2040-2070 and 2070-2100 (IPCC, 2014; Giot et al., 2016). The near-future (2068) and farther-future (2085) climates were selected along a continuous hydrothermal index gradient of increasing temperature, precipitation, and atmospheric CO2-concentrations. Key climatic parameters for the selected years were reproduced in CERs (Figure 11) (Michel et al., 2024).

To ensure reproducibility, each climate had two replicates, utilizing all six CERs. Each CER contained nine mesocosms, resulting in a total of 54 experimental mesocosms. These consisted of 50 × 50 × 50 cm (125 L) containers filled with undisturbed soil monoliths that were sourced from two agricultural fields with differing historical management practices: one received high organic input (S2) and the other low organic input (S1) (Appendices 6.1 & 6.2). Four soil samples from each category were randomly distributed in each CER, while the ninth mesocosm served as an unplanted control (S1 or S2, depending on the CER replicate) aiming

to assess baseline soil activity relative to planted mesocosms (Figure 12). In total, six modalities were established (2013.S1, 2013.S2, 2068.S1, 2068.S2, 2085.S1, 2085.S2), half of which were designated for destructive aboveground and belowground measurements throughout the growth cycle, while the other half was kept for final harvest.

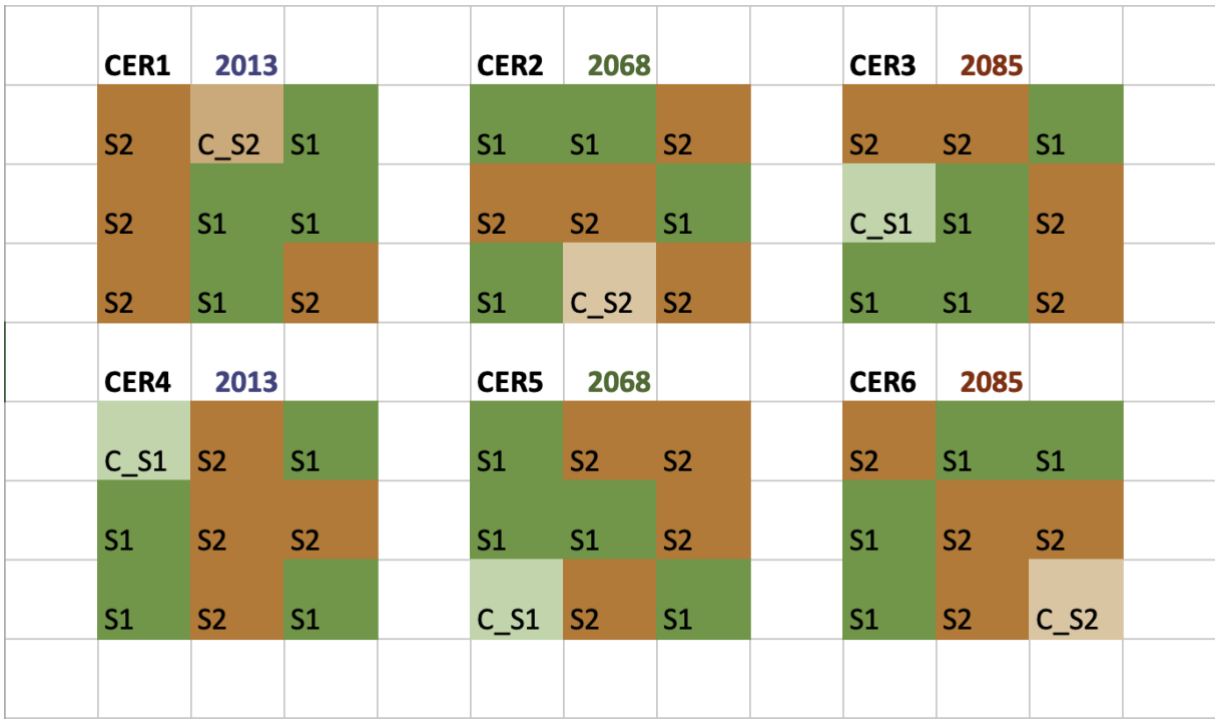

***Figure 12**: Experimental Setup. The 54 mesocosms were distributed between the six CERs. Two soil types were used: S1 (low organic input) and S2 (high organic input). Each CER contained four replicates of each soil type, along with an unplanted control cube. CERs 1 and 4 correspond to the past climate (2013), CERs 2 and 5 to the near-future climate (2068), and CERs 3 and 6 to the farther-future climate (2085). Control cubes are denoted by a 'C' before the soil type (e.g., C_S1, C_S2).*

Winter wheat (*Triticum aestivum (L.) var. Asory*) was sown at a rate of 308 seeds·m^{-2} on 23rd of December 2022, reaching a density of 77 plants per cube. Weeds were removed manually, and no herbicides were applied. To simulate winter conditions, mesocosms were transferred to a winter room 46 days after sowing (DAS) under a temperature of 4°C. They were returned to their respective CERs at 176 DAS for the past climate (2013) and 103 DAS for the near-future climate (2068). The farther-future climate did not require this treatment, as winter temperatures in that climatic scenario remained above 4°C throughout the growing season. Back in CERs, plant development was monitored, including BBCH growth stages (Figure 13).

Environmental variables such as soil matric potential, soil and air temperature, and photonflux density (µmol.m^{-2}.s^{-1}) were also continuously recorded. Fertilization was applied in three doses using ammonium nitrate, following recommendations from *Le Livre Blanc* ("Fumures – Livre Blanc Céréales," n.d.). Applications were made at key growth stages: end of tillering/stem elongation, node formation, and flag leaf stage. The total nitrogen input (kg N·ha^{-1}) was calculated based on pre-existing soil nitrogen levels and crop requirements. Due to its lower initial N stock, S1 received an average of 50 kg N·ha^{-1} more than S2.

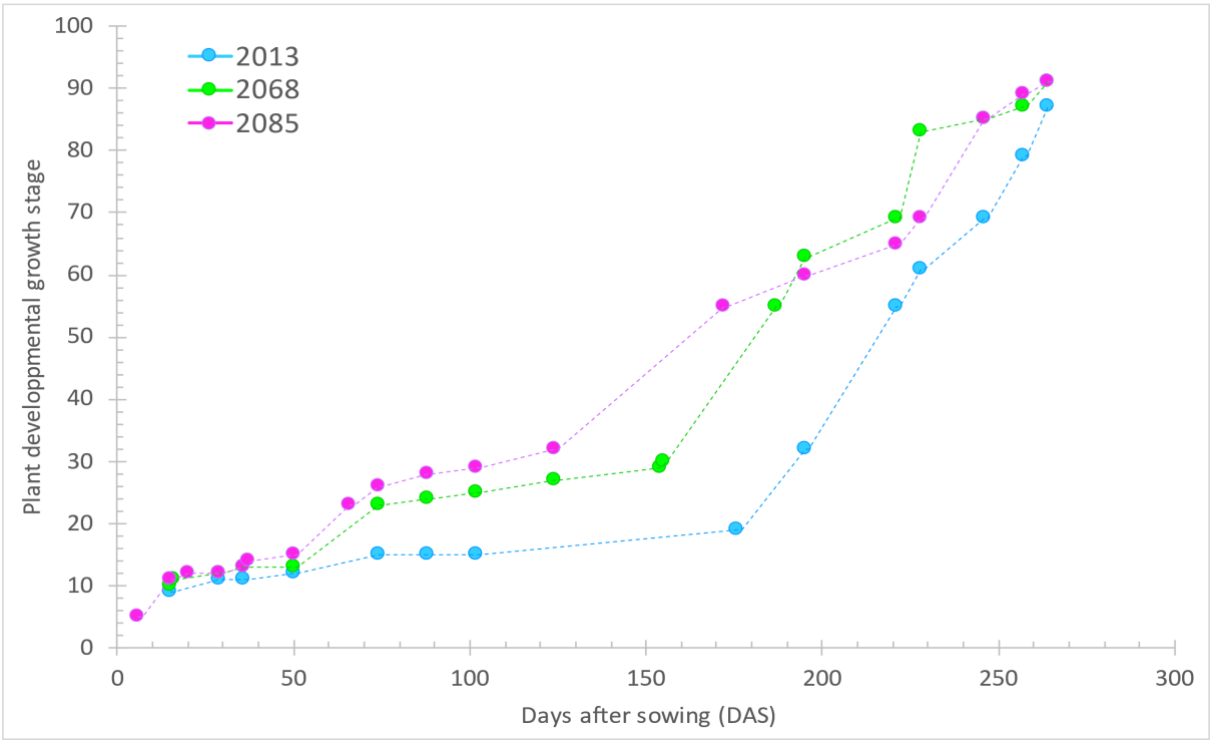

***Figure 13**: Graphical representation of plant growth rate expressed in BBCH phenological stages across the full growth cycle, for each climate. Future climates accelerate winter wheat growth.*

The two soil types are very similar in texture and pedogenesis, as both are classified Aba(b)0 in the Belgian Soil Classification System, and as Luvisols in the World Reference Base for Soil Resources (WRB). These refer to silty loam soils developed in loess which effectively retain water and nutrients due to their clay content (ISRIC, n.d.). The primary difference between the twi soils lies in their precise particle composition: S1 contains more sand than S2 (20.7% vs. 7.6%) but less silt (67.1% vs. 78.8%) (Appendix 9.3). Long-term field management strategies were different for the two soils: S1 received significantly less organic matter input than S2, resulting in a two-fold decrease in humus, phosphorus (P), potassium (K), magnesium (Mg), organic carbon (OC), and nitrogen (N) contents at the start of the experiment (Appendix 9.3). However, pH and C:N ratio remained similar, which suggest comparable soil functionality in terms of microbial activity. Mesofauna abundance was higher in S2 than S1, just as its Maximum Water Holding Capacity (WHC) (64.2 vs. 53.8), likely due to the greater SOM, and increased soil porosity provoked by burrowing activities of soil organisms (Appendix 9.3).

Just before the experiment, the organically managed field S2 was pre-cropped with a radish mix, contributing 10% of the dry weight of the remaining biomass, along with a grass cover (40%) and a dense subsurface mulch layer of wheat straw (40%). No cover crop was sown in the conventional field (S1), although a straw layer (45%) had been incorporated into the soil, and oak leaves (40%) remained present. Despite these similarities, the absolute dry biomasses varied significantly between the two soils, with S2 containing approximately eight times more biomass than S1 (2645g vs. 350 g, respectively) (Appendix 9.3 & 9.4). From now onwards, we will refer to S1 as the “conventional” soil and S2 as the “organic” soil, although this is not completely true, as S2 received chemical protection products that do not respect organic farming legal standards (Appendix 9.2).

4.2 Sampling & measurements

At three timepoints corresponding to stem-elongation, flowering and harvest growth stages (BBCH30/50/80), soil cores centered on wheat plants were collected for half of each modality (four replicates per modality, corresponding to two similar mesocosms per CER), which were used to assess root trait parameters, such as total root length, network area, and root growth angle. Timepoints were selected based on plant phenological stages to ensure accurate comparisons between climates, as these influenced wheat growth rates (Figure 13).

In each mesocosm, two root core replicates were taken. These were further stratified into two depth horizons (0-10 cm and 10-20 cm) to evaluate root growth variability in relation to soil depth (Figure 10). All samples were stored at -20°C until further analysis. Aboveground plant parts were separated from the roots and dried at 45°C for four days to determine the dry weights of leaves, stems, and heads. Roots were also dried and weighed after scanning (see Section Roots treatment & scanning) using the same procedure. Additional yield-related parameters—grain fresh weight, grain moisture, thousand grain weight, and grain nitrogen content—were measured at full plant maturity (BBCH 89) by UGhent collaborators.

Besides, soil pore water was extracted weekly – if water extraction was possible - to measure freely available soil carbon and nitrogen, as indicators of root exudation and nutrient cycling. For this, MacroRhizons were installed in mesocosms (one per mesocosm) to extract pore water through suction with minimal soil disturbance. Collected soil interstitial water was stored in Eppendorf® tubes at -20°C until further analysis.

4.3 Roots treatment & scanning

For root recovery and treatment, the frozen soil cores (n=144) were placed in individual containers with 1L of tap water to facilitate the thawing and washing of soil cores. Given the low clay content (12–13%) of soils, sodium chloride was not added to the suspension for the flocculation of clay particles and dispersion of soil aggregates. Instead, soil samples were manually disintegrated using gloved hands, making sure that gloves were rinsed over each sample to prevent their cross-contamination. While hand manipulation may have slightly damaged root systems - potentially affecting branched root quantification - all samples were treated consistently, which minimizes the risk of introduced bias in the overall results.

Suspended soil-root samples were then poured over a 1mm-mesh sieve to retain roots for further cleaning. The remaining soil particles were rinsed off using a low-pressure hand sprinkler. We expect root losses to be approximately the same for all samples, ensuring the reliability of measurements (Böhm, 1979). Roots were then carefully extracted using tweezers, separating them from stones, aerial plant parts, mosses, and other organic debris also retained on the sieve. The aerial plant parts were dried and included in the total aboveground biomass weights. On average, twenty minutes were needed for the extraction of roots per sample. After the extraction, the sieve was cleaned with a brush to ensure no roots remained for the next sample. Recovered roots were stored in Falken® tubes with a solution of 80% Ethanol, and stored in a 8°C room for several weeks until scanning.

For imaging, roots were first separated from alcohol and placed in a tap water-filled pitcher, where they were cleaned from organic debris using the decantation method of Böhm (1979). Once only roots remained, they were evenly spread in a plastic tray using plastic forceps to prevent scratches. Approximately 400 mL of water was added to the tray to ensure full submersion of roots and their optimal visibility for scanning. A transparent plastic sheet was then placed over the water to flatten the roots, and excess water was removed with a syringe through a hole at the corner of the plastic sheet to eliminate bubbles and shadows.

The prepared tray was then transferred to an *Epson Expression 12000XL* flatbed scanner with a transparency unit and scanned at 600 DPI using *Epson Scan 2* software ("Epson Expression 12000XL Photo Scanner | Products | Epson US," n.d.; "FAQ Article Page | Epson Europe," n.d.). Most scans were A4-sized, but larger samples needed an A3 tray, which is the scanner's maximum supported size. If samples were still too large, multiple scans had to be taken, whose parameters were later aggregated for statistical analysis (Appendix 9.6). Care was taken to avoid placing roots near the tray edges to prevent their cropping from the scan.

After scanning, the tray was cleaned with water to ensure no roots remained for the next scan. Roots were then collected in a paper microfilter to dry them and weigh their dry biomass ("Whatman prepleated qualitative filter paper for technical use, Grade 0858 1/2, grained circles, diam. 320 mm, pack of 100 Whatman paper," n.d.). The scanned images were then analyzed using *RhizoVision Explorer*, an open-source software designed for high-throughput root image processing and automatic measurement of root architectural traits (Seethepalli & York, 2021). In this study, *RhizoVision Explorer* was used on a Surface Windows 10 device.

For root analysis, the 'broken roots' mode was selected to measure architectural traits such as Total Root Length and Branching Frequency. Images were first organized into a single folder to enable a batch analysis, and pre-processing and feature extraction settings were adjusted based on the average characteristics of the scans. Root diameter ranges were defined according to the observed distribution of root segments in the images. Precisely, four diameter ranges were used for feature extraction: [0–0.09] mm, [0.09–0.18] mm, [0.18–0.26] mm, and [0.26 mm and above] to identify variations in diameter distribution across samples.

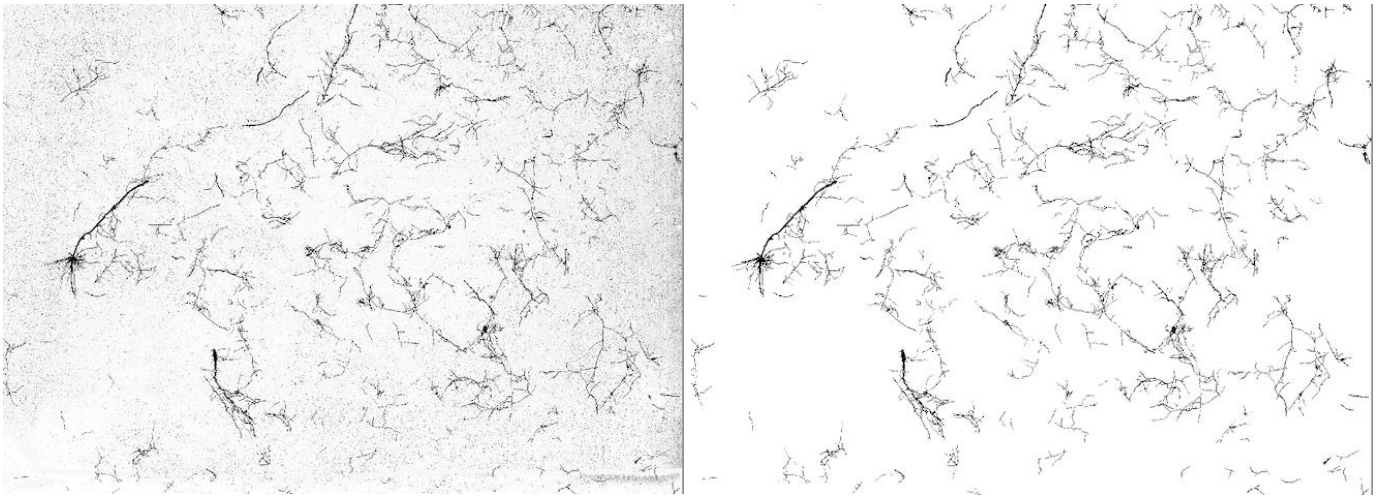

***Figure 14**: Two images of a same sample before (left) and after (right) image segmentation. Non root objects < 1 mm were removed, and root contours were smoothed using a thresholding level of 200. Lateral roots were pruned if their length exceeded the radius of the parent root plus 3 pixels (root pruning = 3).*

Additional preprocessing settings were applied on the scans, including a thresholding level of 200, root pruning set to 3, filtering of background noise components (non-root objects) set to 1 mm, and a pixel-to-physical unit conversion set to 600 DPI (Figure 14). All other preprocessing options were deactivated as they were not necessary in our case. A batch analysis was run, and preprocessing settings were applied to the entire folder of images. A tabular data file was generated containing all the automatically computed root parameters, while a metadata file containing the batch analysis settings was also generated.

4.4 Root crowns imaging

In this study, root crown imaging was conducted to complement broken root data with the measurement of traits related to foraging strategies, such as root angles, rooting depth, and convex hull (Seethepalli, Dhakal, et al., 2021). Root crowns refer to the upper portion of root systems that transitions into the shoots (Christenhusz, 2010), and root crown phenotyping, known as “shovelomics”, is used to study soil resource acquisition strategies of plants grown in specific environments (Seethepalli et al., 2020). In this experiment, only half of the root samples, specifically those stemming from the 0–10 cm depth contained root crowns.

Root crown images were obtained using a different approach than the scanning of broken roots. Imaging was performed using a backlit imaging box made of black profiles isolated from the outside light. A black fabric was placed at the bottom of the box, and a camera was mounted on top of it using a spring clamp, facing downward toward the fabric (*Nikon D3400 with Nikon DX VR AF-P Nikkor 18-55mm f/3.5-5.6G*, 2016). Root crowns were positioned at the camera’s focal point. A white 1-cm wide paper circle was placed in the corner of the fabric to serve as a scale reference for further image analysis. To prevent camera movement and consequent image blur, images were captured remotely via a USB connection on a computer using the DigiCamControl software (DigiCamControl, n.d.).

Camera settings were as follows: ISO 100, shutter speed 1/30, aperture f/5.6, white balance auto, exposure compensation -1.3, and focus mode AF-S. The contrast between the white wheat roots and the black background facilitated the generation of easy-to-process binary images. However, some crowns had already turned brown because of prolonged storage, which made them more challenging to analyze. To address this, post-capture adjustments to brightness and contrast were applied to standardize their appearance with other images.The ‘whole root’ mode was used in RhizoVision Explorer to analyze root crown images. Batch analysis settings were as follows: thresholding level 220, invert images (TRUE), keep largest components (TRUE), edge smoothing threshold 2, root pruning threshold 4, convert pixels to physical units (TRUE), and number of pixels per mm 24.5, while all other settings remained unchecked. The number of pixels per mm setting was obtained by dividing the number of pixels contained in the 1 cm-wide paper circle diameter by 10 mm.

In case where multiple scans were taken for a same sample, the various root parameters were correctly aggregated to accurately represent the root distribution of the whole sample. To achieve this, branching frequency (per mm) was obtained by dividing the number of branch points by TRL, whereas average root diameter was calculated as a weighted average of the TRL found in each sub-sample (Appendix 9.6). Other root traits were summed.

4.5 Soil glucose and nitrate quantification

For the analysis of glucose and nitrogen concentrations in the soil pore water samples, the anthrone test and a cardy-ion meter (CIM) were respectively used. The anthrone test is commonly used to detect hexoses in aqueous solutions. In this study, it was used to measure the total carbohydrate content in soil pore water extracts without distinguishing glucose from other sugar compounds. This is not a concern, as glucose is the primary form of sugar exuded by roots, therefore constituting a reliable indicator of carbon allocation to belowground plant parts (Chantigny et al., 2025). As for the measurement of nitrogen in soil pore water, a portable CIM was used to detect soluble nitrate NO^{3-} in the pore water samples (Folegatti et al., 2005; "LAQUAtwin NO3-11C/NO3-11S/NO3-11,", n.d.). This is not a concern, as nitrate is the primary source of nitrogen for most higher plants (Sun et al., 2017).

The anthrone test involves hydrolyzing carbohydrates into simple monosaccharides in a hot acidic medium, before dehydrating them into hydroxymethyl furfural compounds, which react with the anthrone product to produce a blue-green solution whose concentration can be quantified using a spectrophotometer at an absorption rate of 620/630 nm (Gerwig, 2021). Standard sugar solutions were prepared beforehand and measured to construct calibration curves, later used for the quantitative determination of carbohydrates in the samples (See Appendix 9.5 for more information on the lab protocol). Concerning the use of the CIM for the measurement of nitrate concentration in soil pore water samples, a two-point calibration was proceeded a standard solution. Afterwards, a droplet of each sample was applied directly on the sensor pad to record the nitrate concentrations, taking care to rinse the sensor with distilled water between each measurement. The two-point calibration was repeated regularly to enhance the sensor's accuracy (Folegatti et al., 2005).

4.6 Statistical Analysis

For statistical analysis, a first PCA was conducted to identify which root traits had the same variability patterns. Only representative traits from each principal component were then analyzed by fitting linear mixed models (LMMs), which are in fact more adapted to the specific nature of this experiment as they include both fixed (Climate, Soil, Timepoint, Depth) and random effects (CER, Cube). Indeed, as Cube and CER vary in terms of environmental conditions, they cannot be considered as fully independent replicate experimental units.

Likewise, Timepoint and Depth are not completely independent factors because they include repeated measures on the same experimental units (cubes). Sampling at one timepoint or depth could thus have affected the next one, either by disturbing soil structure, plant stance, or biological activity. This demands hierarchical models that consider Timepoint and Depth as the within-*Cube* factors; and Year and Soil as the *between-Cube* factors. Random slopes were thus added for the Timepoint and Depth effects inside the Cube random factor using (1 + Timepoint | Cube) and (1 + Depth | Cube). For the exudate data, only random intercepts were used for CER and Cube effects, as MacroRhizons weren't moved during the whole experiment, meaning experimental units were not disturbed between successive samplings.

Since the number of observations per population was low, either for root traits than for exudates, checking normality and homoscedasticity on raw variables had little utility. Instead, model assumptions were checked on the residuals of each LMM as recommended by Schützenmeister et al. (2012), and when residuals did not respect such assumptions, appropriate transformations were applied to the raw variables (logarithmic, square root, or Box-Cox transformations), prior to model refitting. Missing values were added as NAs in the datasets to keep the whole experimental structure intact, for the sake of statistical robustness.

Outliers were identified using the interquartile range (IQR) method and were manually inspected to see if these stemmed from natural biological variation or from scanning issues, which in the latter case were corrected. Otherwise, natural outliers were kept in the dataset to avoid modifying the results. In total, 18 samples were missing (out of the 144 = 3 climates x 2 soils x 3 timepoints x 2 depths x 4 replicates), because of uneasy soil core extraction. For the exudate data, outliers were removed (accounted as NAs) as they could not be manually evaluated. Post-hoc comparisons of Year-Soil modalities were then carried out using Estimated Marginal Means (EMMeans) to find out differences between modalities (i.e. interactions between climates [2013/2068/2085] and soil types [S1/S2]), and similarity letters were computed using the Compact Letter Display (CLD) to group significantly close modalities.

Statistical analysis was carried out using R 4.3.3 version (R Core Team, 2024) along with the additional packages 'readxl' (Wickham et al., 2025), 'dplyr' (Müller et al., 2023), 'car' (Fox et al., 2019), 'lme4' (Bates et al., 2015), 'tidyr' (Wickham et al., 2024), 'MASS' (Ripley et al., 2002), 'ggplot2' (Wickham, 2016), 'multcompView' (Piepho et al., 2024), 'lmerTest' (Kuznetsova et al., 2017), 'emmeans' (Lenth, 2024), 'FactoMineR' (Josse et al., 2008), 'factoextra' (Mundt et al., 2020), 'missMDA' (Josse et al., 2016), and 'RVAideMemoire' (Herve, 2025).

5 Results

5.1 The impact of climate and soil management on wheat yield

5.1.1 Grain yield and nitrogen content

To assess the qualitative and quantitative yield of grain production, simple linear models were fitted on both grain nitrogen content (GNC) and grain yield (GY). ANOVA results revealed a significant effect of *Year* on GNC: plants grown under the 2068 climate showed significantly lower GNC compared to 2013, while plants grown under the 2085 climate showed an almost significant decrease in GNC compared to 2013 (Table 1; Figure 15, left). In contrast, 'Year' had no significant effect on GY, whereas the 'Soil' factor had a significant impact: grain yield differed significantly between S1 and S2 under the 2085 climate (Table 1; Figure 15, right).

Term	p.value (GNC)	p.value (GY)
Year	0.033	0.417
Soil	0.302	0.006
Year:Soil	0.792	0.177

Table 1: p-values for the effects of Year and Soil on *grain nitrogen content (%N) and grain yield (t.ha^{-1})*

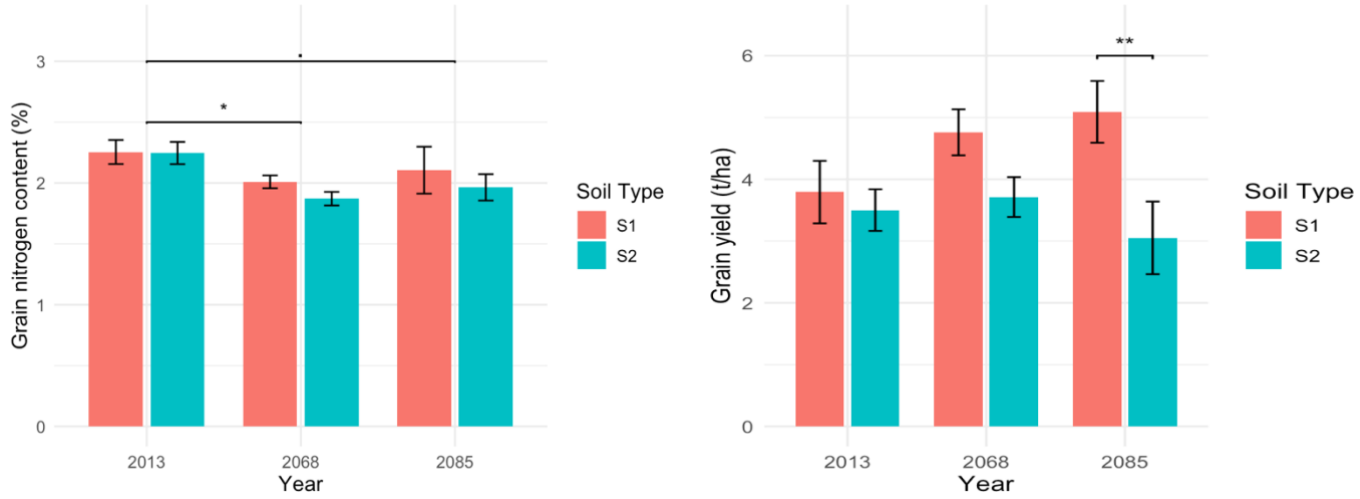

***Figure 15**: Bar plots showing grain nitrogen content (GNC) and grain yield (t/ha) distribution across Year x Soil modalities. Horizontal brackets indicate significant contrasts between climates and soils.*

5.1.2 Root & shoot biomasses

To study the impacts of climatic conditions and soil management on resource partitioning in wheat, bar plots of root and shoot biomass, as well as root-to-shoot ratio were generated for each depth and timepoint. Linear Mixed Models (LMMs) were fitted accordingly, and Compacted Letter Display (CLD) were assigned to modalities using Estimated Marginal Means (EMMeans), based on Tukey-adjusted post-hoc comparisons (alpha=0.05).

Root biomass was significantly lower in climate 2085 compared to other climates at both depths (p-value:…) (Figure 16). No significant differences in root-to-shoot ratio were observed across modalities, although a timepoint effect was found (p-value = 8.69e-05), with a reduced ratio value at the flowering stage (t2) (data not shown).

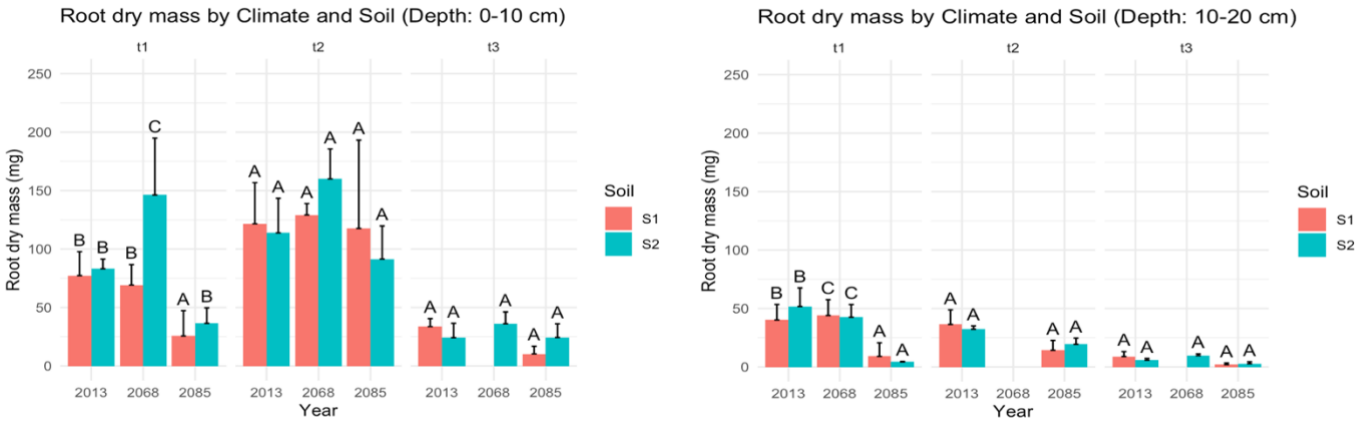

***Figure 16**: Root Dry Weight (in mg) across years and soil types by timepoints for the two soil depths: upper (left) and lower (right). Bars represent means, and only the upper half of the standard deviations is shown (Mean + SD). CLD letters indicate statistically different groups.*

5.2 The impact of climate and soil management on wheat root traits

5.2.1 PCA analysis – Root System Architecture

First, a Principal Component Analysis (PCA) combining root trait parameters, root crown data, and root weight was conducted to summarize the multivariate structure of wheat's RSA. This PCA required to impute missing values for root crown data at lower depths – as these ones were naturally missing – which may have affected the PCA results. This imputation was done in an iterative process, using the imputePCA() function from the missMDA package (Josse et al., 2016). Caution is thus required when interpreting the following findings.

Below is depicted the first factorial plane (PC1 vs. PC2) of the computed PCA (Figure 17). Only three components were considered statistically significant, with three components having eigenvalues exceeding the unit significance threshold (Appendix 9.7 & 9.8). Nevertheless, since the third component explains only 8.4 % of the total variance, compared to 44.6% for PC1 and 24.4% for PC2, only the two first components will be retained for ease of interpretability. The second factorial plane is provided for information in Appendix 9.9.

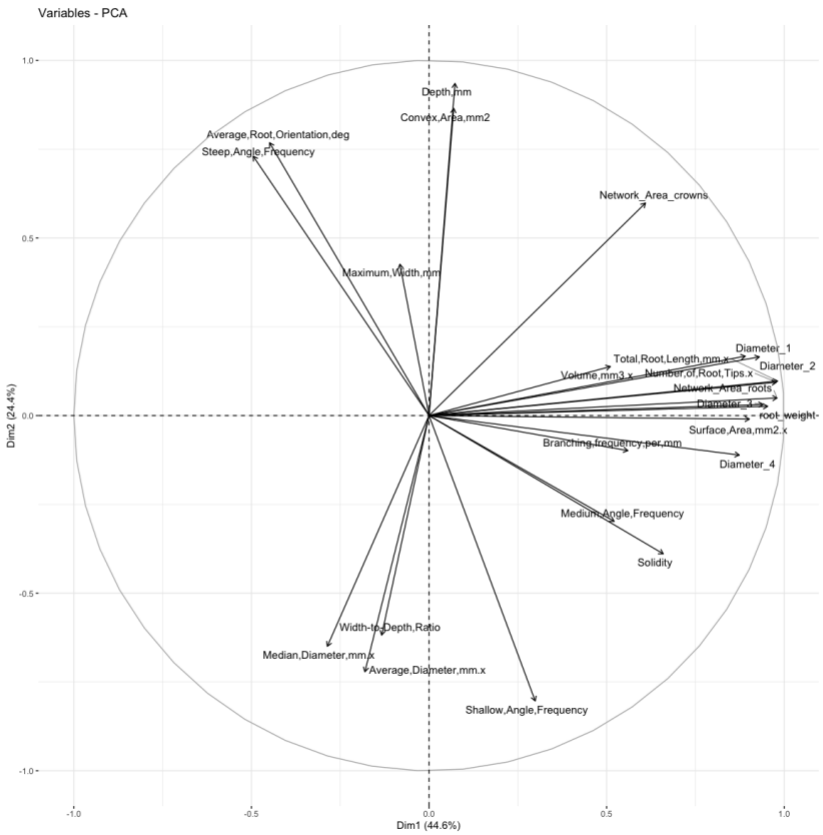

Figure 17*: PCA plot for the first factorial plane (PC1 & PC2). First diameter range represents the diameter class [0–0.09] mm; the second, diameter class [0.09–0.18] mm; the third, diameter class [0.18–0.26] mm; the fourth, diameter class [0.26 mm and above]; Shallow Angle relates to the angular range of [0–30°]; Medium Angle to [30–60°]; and Steep Angle to [60–90°].*

The number of root tips, total root length, network area of broken roots, surface area, the four diameter classes, root weight, network area of root crowns and solidity are strongly explained by the first principal component (PC1), meaning the latter captures overall root system development. Interestingly, average angle orientation and steep angle frequency

seem to go against such root proliferation, though not completely (cor = -0.45 and -0.5, respectively). Branching frequency per mm and root volume are moderately aligned with the first axis (cor = 0.56 and 0.51, respectively), suggesting they don't share similar variability patterns as the former root traits.

Looking at the second principal component, steep, average angle orientation, and crown depth contrast with shallow and medium angle frequencies (positively vs. negatively), as well as width-to-depth ratio and average and median diameters. Interestingly, maximum width goes against width-to-depth ratio. Besides, solidity negatively correlates with PC2 (cor = -0.39), indicating that roots are more concentrated inside shallower root systems (See Appendix 9.12 for the exact meaning of root traits). PC2 thus describes root angle orientation with positive values being associated with steeper, and deeper-penetrating root systems while negative values point to more horizontally spread and shallower root systems.

Bi plotting both individuals and variables on the first factorial plane and grouping them by Year x Soil modality some differential spreading of 95% confidence ellipses can be seen (Figure 18). First, we can note a tendency of climate 2068 soils to promote root proliferation by spreading on the positive side of PC1, though its soil S1 shows a contracted ellipse, possibly due to missing data for this modality. On the other hand, climate 2085 spreads more on the opposite side of root proliferation, specifically in the direction of average and steep angle frequencies. Climate 2013 expands less its ellipses in specific directions, but its S1 soil appears to support shallower root systems, whereas its organic soil S2 is more aligned with steeper root growth.

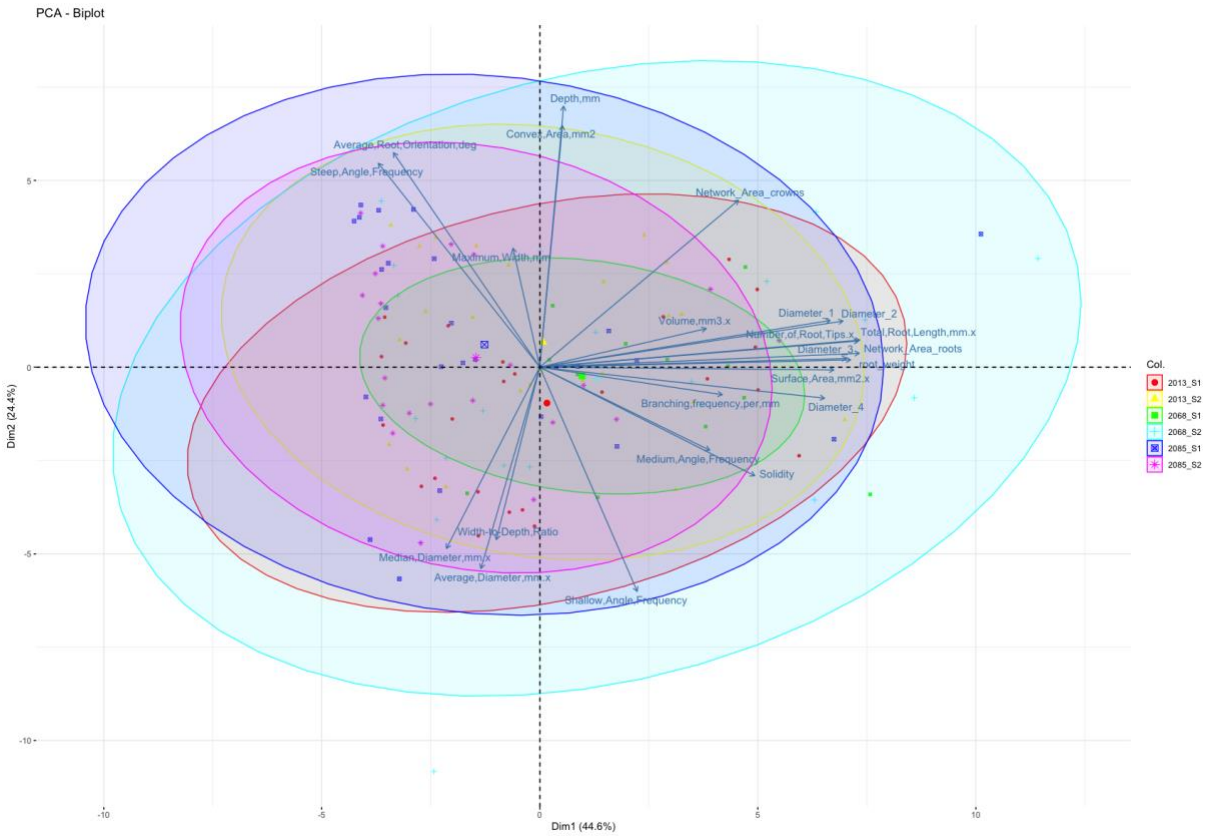

***Figure 18**: PCA biplot (PC1 vs PC2) of variables and individuals grouped by Year × Soil modalities. Each modality is represented by a 95% confidence ellipse.*

To investigate whether these modalities show a significant different clustering along the first two principal components, a Multivariate Analysis of Variance 'MANOVA' was run using the 'Pillai' test. This test detects if the centroids' coordinates of each modality are significantly different from each other in relation to the two first dimensions. The results indicated a statistically significant difference between modalities (p-value = 0.0053).

To determine which modalities were effectively different from each other, post-hoc pairwise comparisons were carried out using a Permutation-based MANOVA test. A Euclidian distance matrix was also generated to quantify the distances between group centroids (Appendix 9.11). Results showed that S1 of 2068 was statistically different from S2 of 2085, while S1 of 2068 was almost statistically different from S1 of 2085 (Appendix 9.10). Overall, soils of climate 2085 are notably distant from those of climate 2068, but they don't differ inside each climate (S1-S2 distance: 0.3 for 2068; 0.4 for 2085). However, soils of climate 2013 are more dissimilar to each other (distance = 1.6) (Appendix 9.11 & 9.14).

For further analysis, total root length (TRL), the number of root tips, volume, branching frequency per mm, average diameter, root orientation classes, root diameter classes, width, depth and width-to-depth ratio will all be retained for descriptive analysis as representative root traits from each principal component.

5.2.2 Descriptive analysis on individual RSA traits

To investigate the potential impacts of future climatic conditions and soil management on the RSA of wheat plants, bar plots of the above-mentioned root traits were generated to study their distribution across Year x Soil modalities, separated by timepoints and depths. Prior to this, a general LMM was fitted on TRL, to observe the effects of the different factors on the response variable. The results of the Type III ANOVA using Satterthwaite's method are shown in Table 2 (Kuznetsova et al., 2017). These results show a strong effect of Depth, and Timepoint on TRL (differences are highly significant), while Year has an almost significant effect on TRL (p-value = 0.0671) but Soil doesn't have a significant effect (Table 2).

Given that the factors *Year* and *Soil* are the main factors of interest, whereas *Depth* and *Timepoint* are factors not central to the main hypotheses, separate linear mixed models were fitted on root traits for each Timepoint × Depth combination to isolate the effects of *Year* and *Soil* on the response variables. Care was taken to transform these variables appropriately if their residuals did not meet assumptions of normality and homogeneity of variance. In these subset models, random slopes were not required anymore, and random intercepts were added as (1 | CER) + (1 | Cube). Estimated Marginal Means (EMMeans) and Compacted Letter Display CLD were added to identify potentially significant differences between *Year* and *Soil* effects in each combination (Appendix 9.16).

Globally, no differences were seen across modalities, except for TRL and the numder of root tips, which were lower in climate 2085 compared to climates 2013 and 2068 at depth 10-20 cm (Figure 19 & 20; Appendix 9.16). No differences were seen for the percentages of root length in each diameter range, except for range 3 which showed a notably higher frequency in S2 of climate 2068 at timepoint t2 and depth 0-10 cm (Appendix 9.16). Visually, we can note a slightly higher frequency of fine diameters (ranges 1 & 2) in S2 compared to S1.

Factor	p_value	Significance
Year	6,71E-02	.
Soil	1,50E-01	ns
Depth	6,71E-12	***
Timepoint	5,20E-11	***
Year:Soil	3,25E-01	ns
Year:Depth	1,66E-03	**
Soil:Depth	3,47E-01	ns
Year:Timepoint	8,76E-05	***
Soil:Timepoint	6,20E-01	ns
Depth:Timepoint	4,02E-01	ns

Table 2**: p-values for the different factors and interaction terms from the linear mixed model run on log-transformed total root length (TRL_log). Only two-way interaction terms were kept in this table while the three- and four- way interaction terms were excluded to enhance interpretability of the results and focus on the most relevant effects. Significance levels are marked as follows: '' for p<0.001; '**' for p<0.01; '*' for p<0.05; '.' for p<0.1 and 'ns' for not significant.*

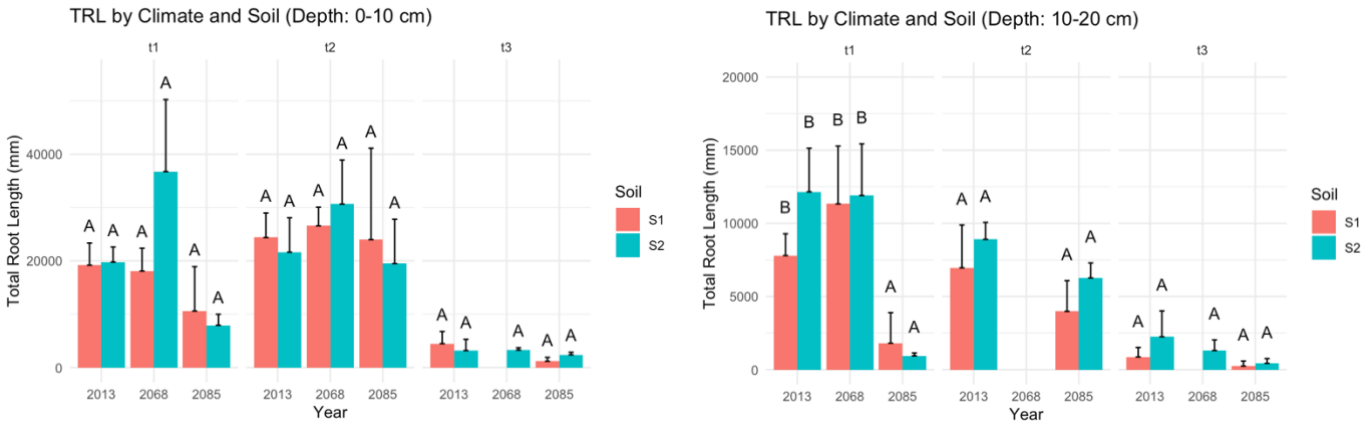

***Figure 19**: bar plots showing Total Root Length (TRL) across years and soil types (S1 = conventional, S2 = organic), segregated between timepoints, and depths (left: 0-10 cm and right: 10-20 cm). Bars represent means, and only the upper half of the standard deviations is shown (Mean + SD). Groups sharing the same letter prove to not be statistically different from each other.*

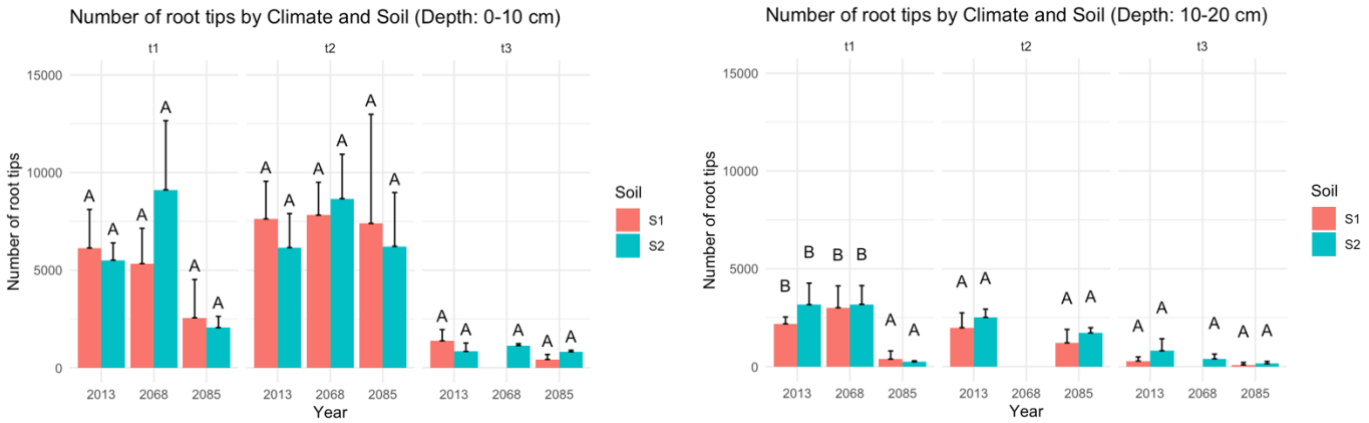

***Figure 20**: bar plots showing the number of root tips across years and soil types (S1 = conventional, S2 = organic), segregated between timepoints, and depths (left: 0-10 cm and right: 10-20 cm).*

5.3 The effects of Climate and Soil management on of glucose and nitrate concentrations patterns in interstitial soil pore water

For the glucose and nitrate data, separate LMMs were run on planted vs. unplanted cubes for each type of compounds. The p-values of the corresponding ANOVA tables are shown in Table x. Concerning glucose content, the factor 'Date' is highly significant in both planted and unplanted cubes, just as the interaction terms Year:Date, Soil:Date, and Year:Soil:Date. However, Year and Soil don't have no effect on glucose soil concentration.

The same results are seen for nitrate concentration in planted cubes where the factor Date, and its interaction terms Year:Date, Soil:Date and Year:Soil:Date are also significant. The third level interaction term could not be tested in unplanted cubes likely due to an insufficient number of observations in the datasubset retrieved for unplanted cubes. Results must be interpreted with care as a lot of Year x Soil x Date combinations were missing from both datasets, meaning p-values might not accurately reflect true significance (Table 3).

	p_planted	p_unplanted
Year	3.189E-01	1.000E+00
Soil	1.108E-01	1.000E+00
Date	7.314E-33	6.804E-16
Year:Soil	4.549E-01	1.000E+00
Year:Date	4.912E-07	1.118E-07
Soil:Date	2.131E-06	1.229E-03
Year:Soil:Date	3.244E-06	1.733E-02

	p_planted	p_unplanted
Year	1.17E-01	5.66E-01
Soil	1.58E-01	8.58E-01
Date	3.69E-15	8.93E-03
Year:Soil	3.79E-01	8.74E-01
Year:Date	2.40E-12	1.21E-01
Soil:Date	2.04E-05	5.66E-01
Year:Soil:Date	1.46E-07	NA

***Table 3**: p-values of the anova results for the LMMs run on planted vs. unplanted cubes, for glucose concentration and nitrate concentration, respectively.*

If we look at the evolution of glucose concentration over time across climates and soil types, we can observe a great temporal variability, as confirmed by the significant effect of the factor 'Date' (Table 3; Figure 21-26). For some periods, similar concentration patterns are seen for the two studied molecules glucose and nitrate across climates, albeit with time lags. To investigate the link between glucose and nitrate concentrations, a Pearson correlation test was conducted, taking care to meet assumptions of normality and homoscedasticity, and to verify the linear relationship between these variables (Appendix 9.17). The results did not indicate a high correlation coefficient (r=0.33) between nitrate and glucose concentrations.

New LMMs were fitted including the *Planted* factor but omitting the *Date* factor to test whether planted cubes showed significant differences compared to unplanted cubes in terms of nitrate and glucose contents. It is important to note that omitting the *Date* factor is delicate because of the significant interaction terms *Year:Date* and *Year:Soil:Date* which possibly indicate a non-existing independent effect of the *Year* factor (Table 3). Type III ANOVA results showed no difference in glucose content between planted and unplanted cubes, whereas nitrate content was significantly lower in planted cubes (p = 0.00083).

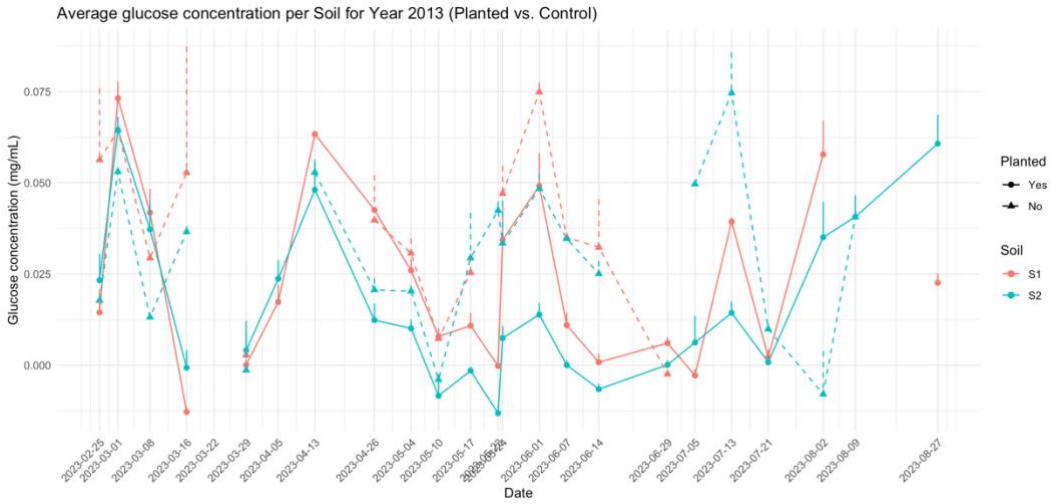

***Figure 21**: Evolution of glucose concentration in soil interstitial pore water (mg.mL^{-1}) over time for climate 2013, for planted and control cubes. Lines represent soil × planted combinations, and error bars indicate standard errors of the means. The number of replicates per modality is comprised between n=1 and n=8.*

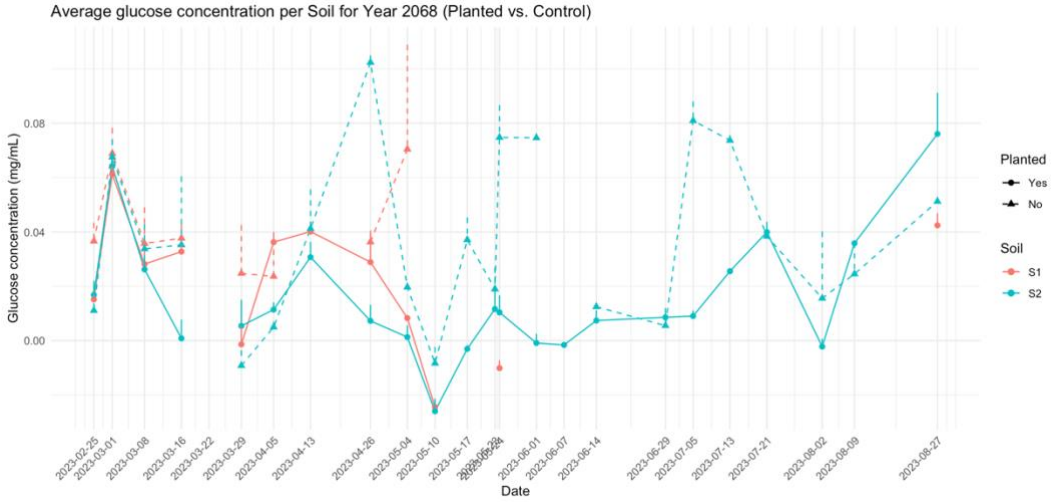

***Figure 22**: Evolution of glucose concentration in soil interstitial pore water (mg.mL^{-1}) over time for climate 2068, for planted and control cubes. Lines represent soil × planted combinations, and error bars indicate standard errors of the means. The number of replicates per modality is comprised between n=1 and n=8.*

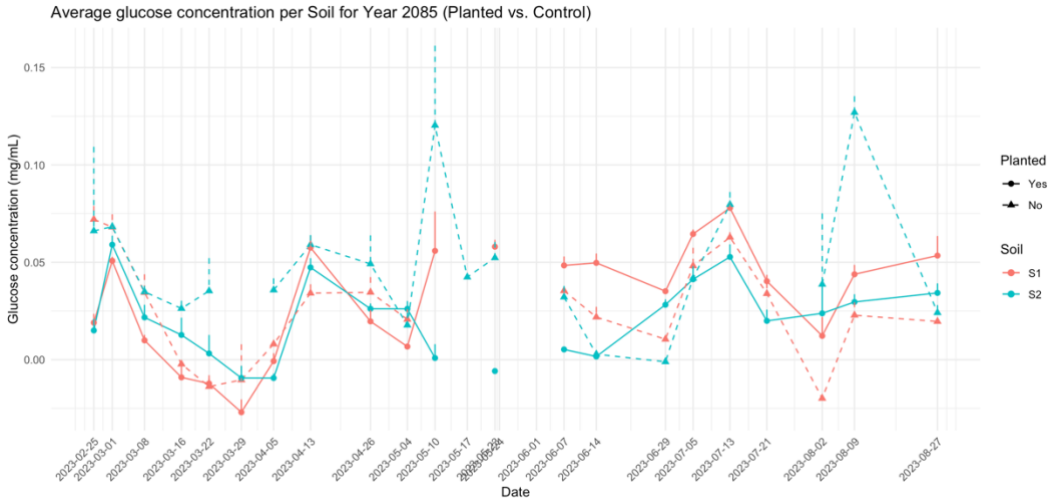

***Figure 23**: Evolution of glucose concentration in soil interstitial pore water (mg mL^{-1}) over time for climate 2085, for planted and control cubes. Lines represent soil × planted combinations, and error bars indicate standard errors of the means. The number of replicates per modality is comprised between n=1 and n=8.*

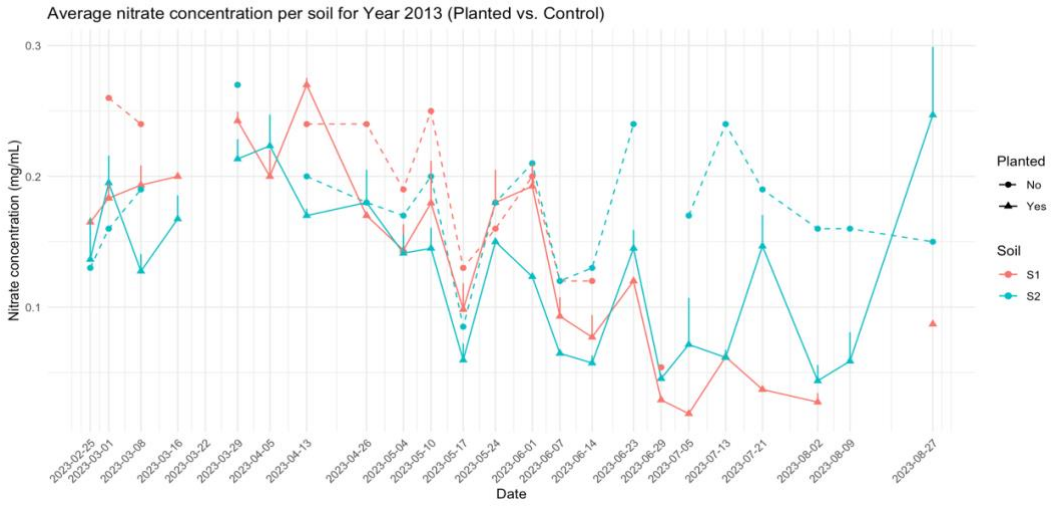

***Figure 24**: Evolution of nitrate concentration in soil interstitial pore water (mg.mL^{-1}) over time for climate 2013, for planted and control cubes. Lines represent soil × planted combinations, and error bars indicate standard errors of the means. The number of replicates per modality is comprised between n=1 and n=8.*

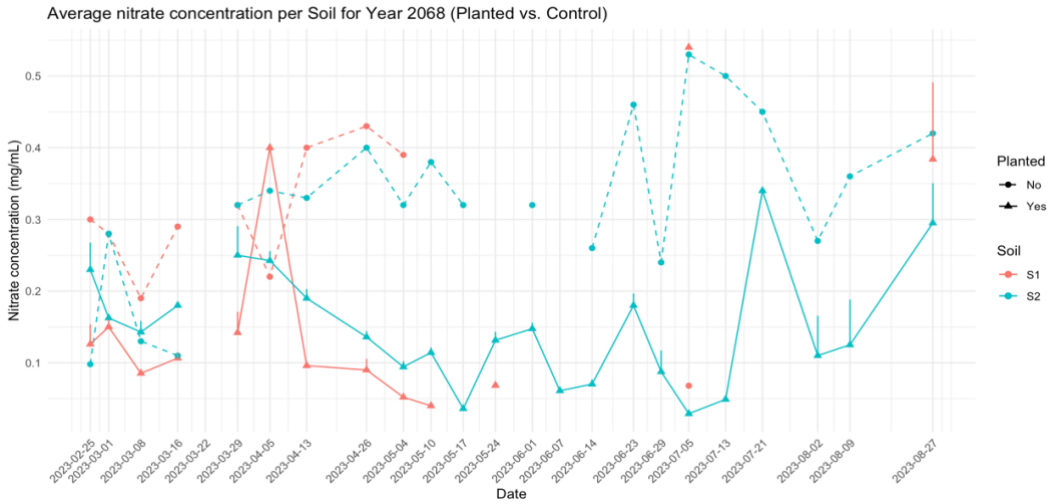

***Figure 25**: Evolution of nitrate concentration in soil interstitial pore water (mg.mL^{-1}) over time for climate 2068, for planted and control cubes. Lines represent soil × planted combinations, and error bars indicate standard errors of the means. The number of replicates per modality is comprised between n=1 and n=8.*

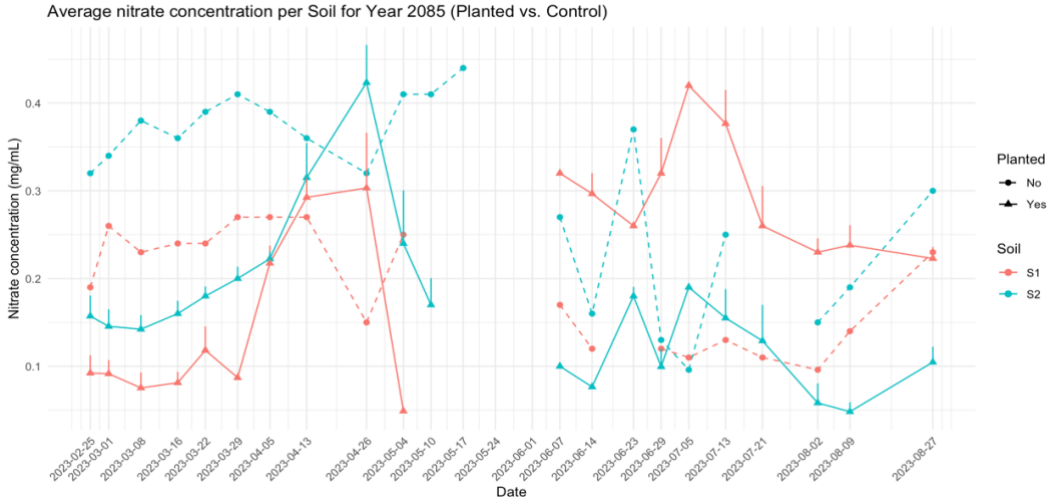

***Figure 26**: Evolution of nitrate concentration in soil interstitial pore water (mg.mL^{-1}) over time for climate 2085, for planted and control cubes. Lines represent soil × planted combinations, and error bars indicate standard errors of the means. The number of replicates per modality is comprised between n=1 and n=8.*

New LMMs comprising the *Soil* and *Year* factors only were run separately on both types of cubes to check differences between Year x Soil modalities in glucose and nitrate contents for each of them. Type III ANOVA results indicated no statistically significant effects of *Year* or *Soil* on glucose nor nitrate, whether it be in planted nor unplanted cubes. However, plotting EMMeans from these LMMs shows slight differences between Soil x Year modalities, with glucose and nitrate contents tending to increase under future climates (2013<2068<2085), a trend particularly encountered in conventional soils (S1) (Figures 27-28). Means and standard errors of nitrate and glucose are available in Tables 4 & 5.

Year	Soil	Mean ± SE (planted)	Mean ± SE (unplanted)
2013	S1	0.0231 ± 0.0027	0.0354 ± 0.0048
	S2	0.0177 ± 0.0023	0.0295 ± 0.0035
2068	S1	0.0257 ± 0.0043	0.0418 ± 0.0061
	S2	0.0146 ± 0.0025	0.0366 ± 0.0049
2085	S1	0.0299 ± 0.0031	0.0253 ± 0.0044
	S2	0.0195 ± 0.0027	0.0476 ± 0.0058

***Table 4**: Means and standard errors of glucose concentration (mg/mL) in planted and unplanted cubes for each Year x Soil combination.*

Year	Soil	Mean ± SE (planted)	Mean ± SE (unplanted)
2013	S1	0.138 ± 0.0106	0.1903 ± 0.0188
	S2	0.1264 ± 0.009	0.1767 ± 0.0098
2068	S1	0.1658 ± 0.0305	0.2888 ± 0.0345
	S2	0.1468 ± 0.0102	0.3256 ± 0.0257
2085	S1	0.2093 ± 0.01459	0.1893 ± 0.01485
	S2	0.168 ± 0.0128	0.307 ± 0.0229

***Table 5**: Means and standard errors of nitrate concentration (mg/mL) in planted and unplanted cubes for each Year x Soil combination.*

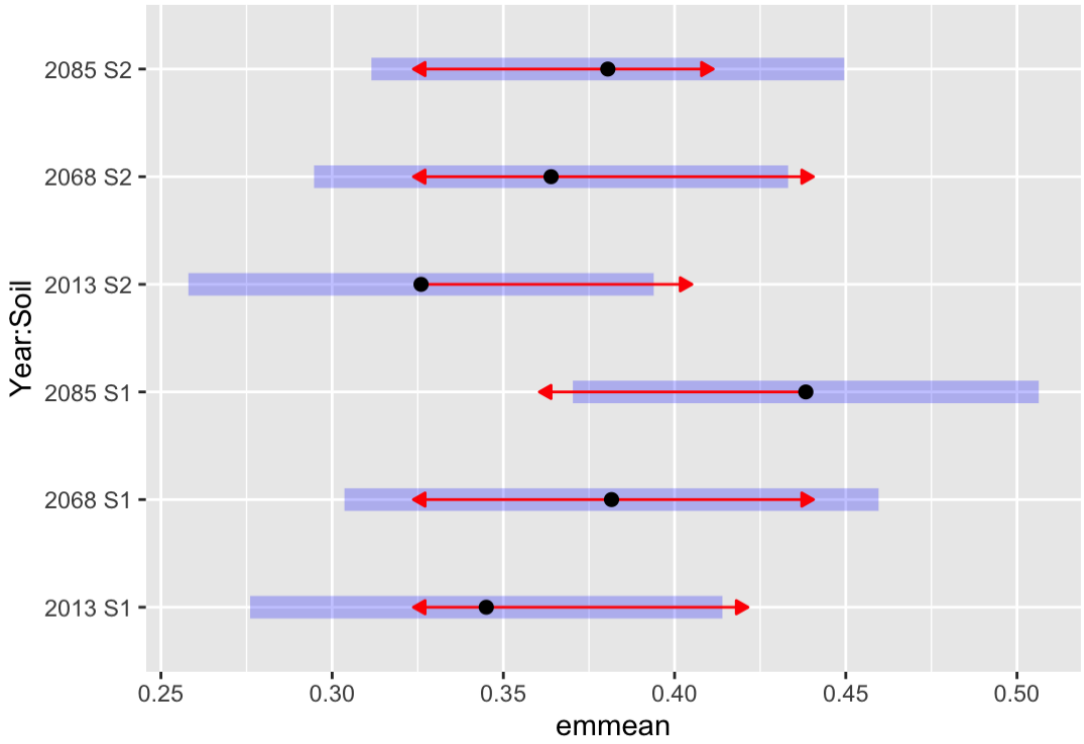

***Figure 27**: Plotted Estimated Marginal Means (EMMeans) of Year × Soil modalities for nitrate concentration in planted cubes. Black dots are the EMMeans, while horizontal blue bars show their 95% confidence intervals. Red arrows represent pairwise comparisons: overlapping arrows indicate no significant difference, while separated arrows suggest statistical significance.*

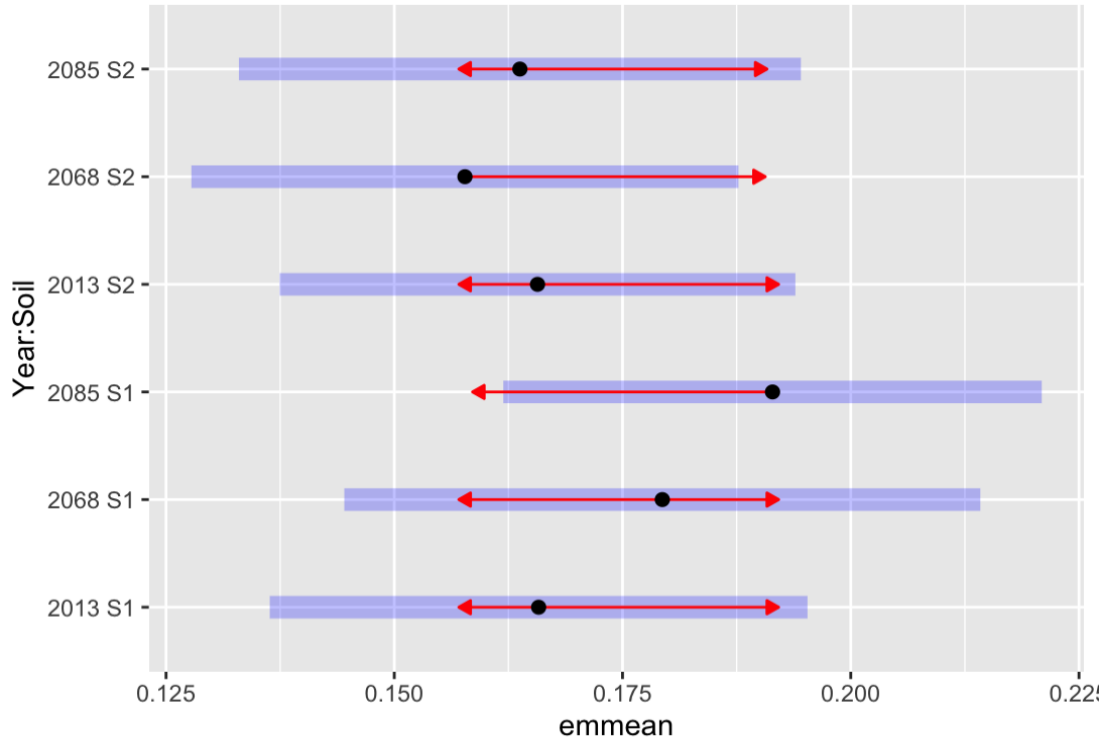

***Figure 28**: Plotted Estimated Marginal Means (EMMeans) of Year × Soil modalities for glucose concentration in planted cubes. Black dots are the EMMeans, while horizontal blue bars show their 95% confidence intervals. Red arrows represent pairwise comparisons: overlapping arrows indicate no significant difference, while separated arrows suggest statistical significance.*

5.4 The impact of climate and soil on microbial biomass carbon

To complement the exudate analysis, Microbial Biomass Carbon (MBC) was also plotted to analyze its distribution across Year x Soil modalities, separately for each depth and timepoint. LMMs were fitted accordingly and CLD were assigned to modalities using the Estimated Marginal Means (EMMeans) with Tukey-adjusted post-hoc comparisons. Modalities sharing same letters are not significantly different from each other. MBC differed significantly between soils at timepoint t1 and 0-10 cm depth, with organic soils (S2) exhibiting enhanced MBC compared to conventional soils (S1). The largest gap between soils is seen in future climatic scenario 2085 gap. The dominance of S2 over S1 in MBC is still visible in t2 but not anymore in t3. At the 10-20 cm depth, trends are similar but of lower amplitude. Overall, MBC is slightly lower at 10-20 cm depth compared to the 0-10 cm depth (Figure 29).

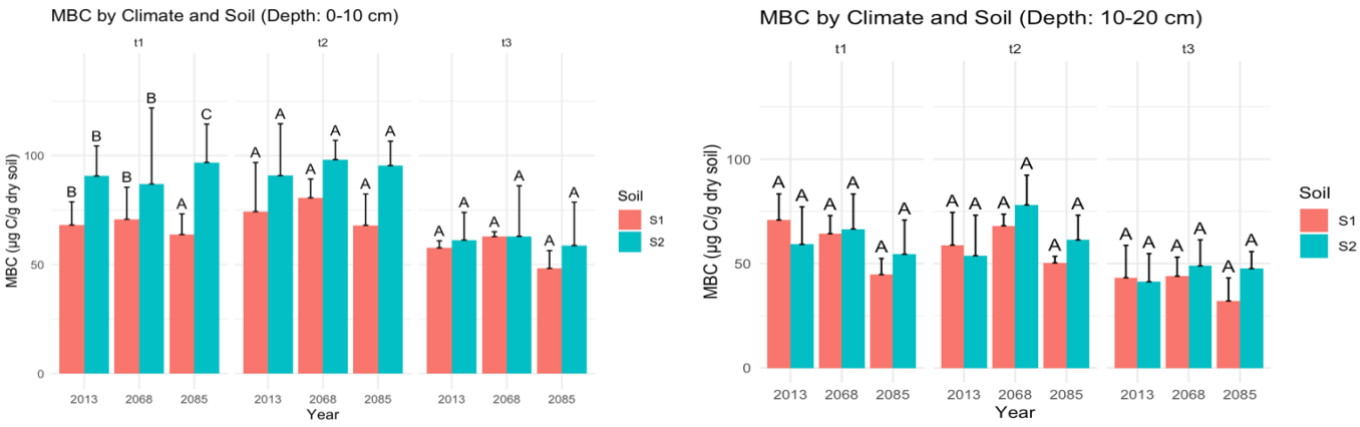

***Figure 29**: MBC (in µg C/g dry soil) across years and soil types by timepoints and for the two soil depths: upper (left) and lower (right). Bars represent means, and only the upper half of the standard deviations is shown (Mean + SD). CLD indicate statistically different groups according to Tukey post-hoc comparisons.*

5.5 Probabilistic PCA over RSA, exudation, and yield parameters

A probabilistic Principal Component Analysis (pPCA) was finally run on the overall data comprising root traits, nitrate and glucose soil interstitial pore water concentrations, yield parameters, and Microbial biomass carbon (MBC). Only two components were retained for ease of interpretation. Altogether, these explained approximately 60% of the overall variability, which is considered satisfactory. Spearman's correlations were also computed between variables, based on the imputed data from the pPCA (Appendix 9.22).

On one hand, PC1 accounts for the largest share of variance (50%) and is mainly associated with belowground traits of root system development and microbial biomass, with high positive loadings being observed for the number of root tips (0.33), root dry mass (0.32), surface area (0.3), root length of the four diameter classes (±0.3), and microbial biomass carbon (MBC: 0.38). This suggest that PC1 represents a gradient of prolific root development along with microbial activity. Spearman correlations support these as root traits and microbial traits strongly co-correlate ($r > 0.90$). On the contrary, soil nitrate concentration is negatively correlated with PC1, indicating a trade-off between root development and nitrate soil concentration in pore interstitial water (Appendix 9.21).

On the other hand, PC2 emphasizes on nutritional quality and root crown foraging strategy. Notably, it has strong positive loadings for grain nitrogen content GNC (0.32), shallow and medium angle frequencies (0.46 and 0.35). However, it negatively correlates with steep angle frequency (–0.57), root crown depth (-0.32), and total root length (–0.24). Traits contributing to PC2 therefore appear to reflect a superficial foraging strategy that yields nutrient-rich grains (Appendix 9.18). Plants grown under the climate 2068 are the most aligned with PC1, while plants grown under the 2085 climate show the least correlation with PC1 (Appendix 9.20), which meets the previous PCA results detecting an enhanced root proliferation under 2068 climate and reduced root development under 2085 climate (Figure 16). Climate 2013 displays a rather balanced profile and does not expand towards either of the axis.

While the soils under each climate share similar centroid coordinates along the first axis (PC1), they differentiate more along the second axis (PC2), with soils S1 systematically taking higher values on PC2 than soils S2, suggesting that conventional soils encourage plants to adopt a topsoil foraging strategy. However, these differences were not statistically significant, and was less pronounced for future climates compared to 2013. Moreover, there is a slight tendency of plants grown under future climates to shift from a topsoil foraging strategy to a steeper one as climates becomes more extreme, but this trend is very subtle. Although soils of each climate don't differentiate much along PC1, the centroid ellipses of soils S2 soils tend to have higher loadings on PC1 than S1 soils, indicating a slightly greater root proliferation in S2 compared to S1. This is especially the case for plants grown in 2085 climate (Figure 30; Appendix 9.21).

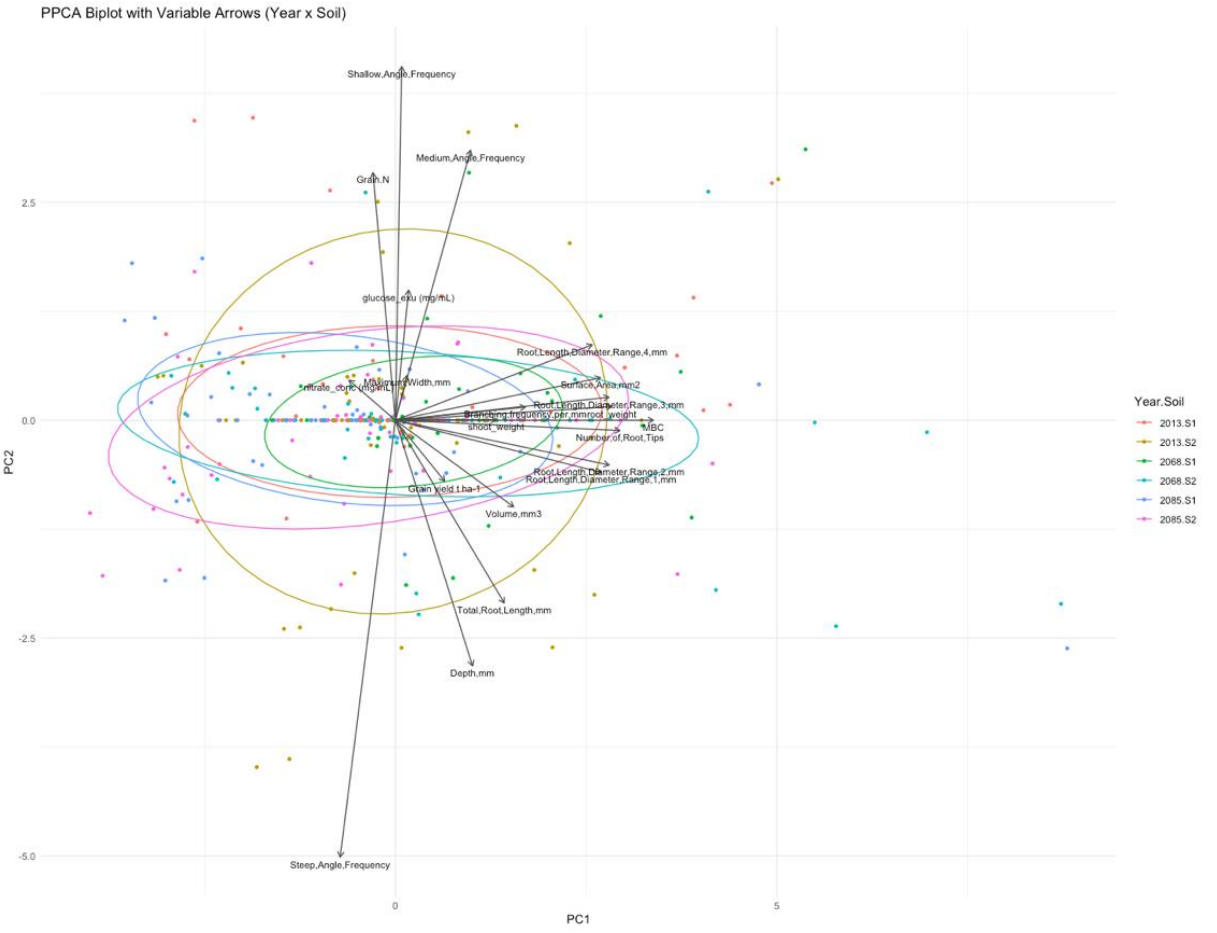

***Figure 30**: pPCA biplot (PC1 vs PC2) of variables and individuals grouped by Year x Soil modality. Each modality is represented by a 95% confidence ellipse.*

6 Discussion

6.1 Climate change and soil management affects wheat yield

Above results indicate significant yield differences of wheat plants grown under future climates compared to the present climate: grain nitrogen content was significantly lower in 2068 and almost significantly lower in 2085 compared to 2013. Within each climate, plants grown in S1 showed slightly higher GNC than those in S2, though this difference was not significant. Besides, grain yield showed differing responses across soils in future climates: it was significantly increased in S1 under both climates 2068 and 2085, while in S2, it was increased only in 2068 but decreased in 2085. Within each climate, S1 showed consistently higher grain yield than S2, although this difference was significant only in the 2085 climate.

These results are supported by other studies which found that the benefits from elevated atmospheric CO_2 concentrations on wheat GNC is usually negated by rising temperature and changes in rainfall patterns, ultimately resulting in an overall decrease in GNC (Asseng et al., 2019). Other studies reported an increase of grain yield under temperature and rainfall increases, tough this increase leads to a reduced protein content in the grains (Qin et al., 2023). The fact that plants in S1 showed higher grain yield and GNC than in S2 likely stems from the fact that the former received slightly more fertilization (50 kg $N \cdot ha^{-1}$) compared to S2, which is in accordance with a Chinese meta-analysis that found consistent increases in wheat grain yield under highly fertilized soils compared to no fertilized soils (An et al., 2024).

6.2 Climate change affects wheat root and shoot biomasses

Belowground, these yield patterns correlated with a significantly reduced root development in climate 2085, and a non-significant increase in 2068 compared to the present climate, either in terms of root biomass, total root length and number of root tips. The contrasting root development responses between climates 2068 and 2085 reflect complex dynamics in root system plasticity and adaptation to future climatic conditions, proving how increasing climatic extremes do not necessarily induce linear responses in root development nor yield traits. In fact, consequences of elevated CO_2 on root growth have shown contrasting results, with some studies finding an enhanced root growth and some a reduced one (Ainsworth et al., 2025).

Aboveground, shoot biomass was progressively reduced under future climates at the stem elongation (t1) and harvest stage (t3), but increased at the flowering stage (t2), showing how wheat plants grown in future climatic conditions react differently to climatic extremes at different growth stages, investing more in aboveground biomass during reproductive phases under future climatic stress. Overall, root-to-shoot ratio tended to decrease with increasing climatic scenarios at all timepoints, implying that future wheat plants globally favor shoot biomass over root biomass. However, root-to-shoot ratio sometimes increased under climate 2068, especially in S2 soils, showing how allocation strategies are complex and stage-specific according to soil types and climates. Globally, it is acknowledged that elevated atmospheric CO_2 levels increase plant above-ground biomass, along with root growth (Han et al., 2023). Bektas et al. (2023) showed that under optimal conditions, an almost linear correlation is observed between root and shoot biomass, which is supported by the positive correlation seen between shoot biomass and root proliferation parameters (>0.6), especially with root

biomass (0.68). However, such a correlation was seen only under 2068 climate, whereas root growth was decoupled from shoot growth in 2085, suggesting a differential allocation strategy under stress conditions. Drought conditions appear to favor root development in place of shoot, while the contrary happens under increasing temperature and precipitations, even if counteracted by elevated CO_2 and drought conditions (Seidel et al. 2024). The compound effects of future climatic stresses may ultimately lead to an enhanced shoot biomass over roots, though this depends greatly on the sensitivity of the wheat cultivar used in the experiment (Bektas et al. 2023). In this study, wheat plants adopted an adaptative response to the 2068 climate by developing more roots, while this strategy may no longer have been viable in 2085, where reduced carbon allocation to roots was needed to be able to maintain aboveground photosynthesis and reproductive functions.

6.3 Wheat RSAs are steeper in S2 compared to S1

The first Principal Component Analysis (PCA) on root parameters showed strong positive correlations between major root development traits such as TRL, number of root tips, and root surface area. However, these were opposed to steep angle frequency, suggesting a trade-off between steeper root systems and root proliferation, which meets previous studies on maize that reported a reduced abundance of lateral roots in steep rooting systems, rather favoring the development of fewer, longer and thinner lateral roots (Lynch, 2019, 2022b).

This is supported by our results which found steep angle frequency was opposed to the root length of thicker diameter class (range 4), and correlated more with diameter ranges 1 and 2, reinforcing the idea that steeper architectures preferentially favor very fine roots over coarse roots. This is supported by the fact that branching frequency – which was most strongly associated with the thinnest diameter class (range 1) - was more correlated with rooting depth than crown width (0.5 vs. 0.25). Altogether, this suggests that even if root length is reduced in steeper root systems, thinner roots are relatively more prevalent than thicker ones, reflecting an economic strategy of steep root systems to allocate carbon in a more efficient way by favoring finer roots over coarser ones which are more costly to build (Lynch, 2019).

Overall, conventional soils showed an enhanced root crown width compared to soils S2 across climates, especially at the stem elongation stage (t1), though this was not statistically confirmed. pPCA results also highlighted a slight predominance of shallower root systems in S1, compared to the deeper ones in organic soils S2, likely due to the looser topsoil of S1 which received more frequent soil tillage compared to S2, and offered optimal root growth in the superficial soil layer, though not in the harder and compacted subsoil layers which may have imposed mechanical impedance to root growth. Conversely, the better soil structure of S2 may have offered more favorable conditions to root growth in deeper soil strata, which is supported by studies that observed higher topsoil root concentration in intensively managed agricultural fields, in contrast to decreased penetration resistance of root growth in soils of better structural quality (Correa et al., 2019; Cavalieri-Polizeli et al., 2022). Moreover, a slightly higher proportion of fine roots were seen in S2 across all climates, confirming the observation of steeper root systems in S2 and its correlation with very fine roots. A possible explanation to that could be the result of microbial biochemical signaling in theses soils that contained higher MBC, which could have stimulated root branching frequency (Wen et al., 2022; Gonin et al., 2023; Galindo-Castañeda et al., 2024).

6.4 Glucose and nitrate concentrations increase in soil pore interstitial water under future climates, especially in S1 soils.

Soil nitrate concentrations increased under future climates for the two soils (2013<2068<2085), with slightly higher concentrations in S1 soils across all climates. Unplanted soil cubes consistently showed higher nitrate concentrations compared to planted cubes, likely due to the absence of root uptake to deplete them. The linear increase in soil nitrate under future climatic conditions possibly points to an enhanced microbial turnover of SOM in cause of higher temperatures and CO_2 levels, which would render more nitrate available in the soil solution, especially if this is coupled with a reduced plant uptake due to lower root development. In fact, a negative correlation was seen between nitrate soil concentration and root proliferation, proving how nitrate is left in the soil solution when roots are not present to absorb it. However, the enhanced root development found in 2068 contradicts this hypothesis as it still led to enhanced nitrate soil concentration compared to 2013, suggesting that nitrate accumulation isn't solely due to root uptake failure, but could also be due to microbial nitrification or reduced uptake efficiency.

Previous studies support the fact that SOM turnover is enhanced under increased temperature conditions, resulting in an increased nitrogen mineralization and nitrate availability in soils (Rustad et al., 2001). However, this depends very much on the type of ecosystem studied and the nature of SOM degraded, as different forms of SOM are more or less accessible to decomposition than others (Davidson et al., 2006). Moreover, increases in soil temperature due to climate change enhances the nitrification rate of microbes, and nitrate availability, which can lead to poor NUE if not absorbed by roots (Govindasamy et al., 2023). The higher nitrate concentrations found in S1 could also be explained by their shallower root systems, which did not grow deep enough to capture mobile nitrate in deeper soil strata. This is supported by the negative correlations of soil nitrate concentration with rooting depth (-0.63), compared to a weaker correlation with crown width (-0.27).

Therefore, deeper S2 root systems would tend to absorb more soluble nitrate, and decrease nitrate concentration in the soil solution, whereas shallower S1 root systems would not be able to capture such mobile nitrate, leading to its accumulation in soil pore water. This is supported by a study made on cereal crops which showed that plants adopting steep RSA in low-N environments absorbed more nitrate in deeper soil strata (Trachsel et al., 2013). The lower nitrate soil concentration found in S2 may as well point to its enhanced SOM, which could have slowed the process of SOM decomposition and coordinated better the release of soluble nitrogen with plant uptakes, thereby reducing the amount of labile nitrate in the soil solution. Moreover, the enhanced MBC found in S2 may have retained nitrogen in more stable forms, as is supported by the negative correlation between MBC and soil nitrate (-0.75) .

Glucose soil concentration also increased under future climates (2013<2068<2085), though only in soils S1 as glucose levels stayed stable in S2 across all climates, suggesting a buffering capacity of S2 to retain SOM in stable forms, possibly due to its enhanced MBC. Indeed, MBC was significantly higher in S2 and remained stable under future climates. Therefore, soil microbes may have likely contributed to the formation of persistent SOM via their necromass, and stabilized soil organic carbon through the formation of microaggregates, protecting SOM from rapid decomposition (Gougoulias et al., 2014b). Soil glucose concentration was also

slightly correlated with root proliferation (>0.3), just as with MBC (0.33). MBC was itself strongly correlated with root development traits, most particularly with the number of root tips (0.97), which possibly indicates root exudation processes in the root tips. However, this is uncertain, as unplanted cubes showed higher glucose concentration compared to planted cubes, suggesting that soil glucose concentration rather comes from SOM degradation than exudation processes. Moreover, glucose concentration was rather associated with thick roots of diameter range 4 (0.36) compared to thinner diameter classes (+-0.3), which contradicts the hypothesis that glucose concentration comes from root exudation, which in the latter case would be associated with thinner root diameters.

The fact that glucose soil concentration increased under future climates supports this idea, as microbial turnover of SOM is known to be enhanced under both higher temperatures and CO_2 levels. Indeed, the majority of models on soil C dynamics showed an increased decomposition rate of SOM under increasing temperature, even though this is debatable as some organic matter forms are more easily decomposed than others (Davidson et al., 2006). Elevated CO_2 levels have also shown to stimulate soil microbial respiration due to increased root exudation processes and rhizosphere carbon input from plants, which boost SOM metabolization and the release of labile sugars into the soil solution (van Groenigen et al., 2014; Pellitier et al., 2022). Therefore, the increased soil glucose concentration seen under future climates could result from a complex interaction process between soil, plant, and microbes.

6.5 Impact of RSA on grain yield

Overall, grain nitrogen content (GNC) was slightly negatively associated with root development, while the contrary was observed with grain yield. Notably, GNC and grain yield did not correlate together (r= -0.36), indicating a possible trade-off between yield quantity and quality, which was already observed in previous studies where increases in wheat yields penalized final grain protein in a dilution effect (Asseng et al., 2019; de Oliveira Silva et al., 2020; Ainsworth et al., 2025). Although one might expect that the higher grain yield seen in soils S1 would result from an increased root proliferation in those, this was not demonstrated. However, higher density of roots was observed in medium root growth angle (0.24), potentially explaining why shallower root systems in S1 induced higher grain yield and GNC, as these absorbed more nitrate thanks to a relative enhanced root proliferation in the topsoil - supported by the negative correlation between nitrate soil concentration and medium angle frequency (-0.28). Nevertheless, labile nitrate was still left in the soil solution, increasing the risk of nitrate leaching (Michel et al., 2025). Conversely, root systems in S2 appeared to slightly buffer the enhanced N mineralization seen under future climates, possibly due to their greater rooting depth. However, this did not translate into a higher grain yield nor GNC, suggesting that nitrate uptake might have been impaired by other mechanisms, possibly by competition for N with soil microbes which were effectively enhanced in S2. This is supported by some studies which found that readily made available nitrate by soil microorganisms is immediately taken up by them. However, this is nuanced by the facts that these are short-lived compared to plants, and that the latter ones are those benefitting from increased SOM turnover in the long run (Kuzyakov et al., 2013). This microbial-plant competition for N may partly explain the yield reduction in S2 despite deeper rooting. Nevertheless, these processes are also counteracted by microbial immobilization, which nuance this (Zak et al., 2000).

7 Conclusion and perspectives

This study advances our understanding about the intricate relations between soil abiotic factors, Root System Architecture (RSA), rhizosphere processes, and wheat yield under climate change. Elevated CO_2 and warming conditions were found to modulate carbon allocation in wheat, with an overall trend towards reduced root-to-shoot ratios under future climates, though root proliferation showed contrasting results in 2068 and 2085, revealing a non-linear plasticity in root development and yield outcomes to escalating climatic stresses.

While deeper RSA traits were predominantly associated with organic soils (S2), these did not confer yield advantages. On the contrary, grain yield and nitrogen content (GNC) were higher in conventionally managed soils (S1). A plausible explanation for this lies in the enhanced microbial activity in S2 soils, which could have induced competition for N between plants and soil microbes, highlighting the sometimes-contradictory role of soil microbiota in regulating nutrient availability under climate stress. However, the steeper root systems in S2 did help to reduce nitrate leaching, pointing to their potential in limiting ecosystem pollution.

A possible solution to ally the needs of maintaining wheat yield with reduced environment pollution would be to breed dimorphic wheat ideotypes capable of constructing both superficial and deep roots, as proposed by (Lynch, 2019). However, this shouldn't come at a cost of grain yield. Caution is needed when interpreting present findings as these may have been influenced by the cultivar used in the experiment (Bektas et al., 2023). Future research is thus needed to decipher the complex interplay in soil-plant-microbes interactions under adverse climates using other cultivars, and adapt breeding objectives accordingly. Finally, this experiment lacked from enough replicates to draw robust conclusions, underscoring the need for long-term field trials with enough replicates to cross-validate these Ecotron-based observations, which will be essential to guide sustainable wheat production under CC.

8 Personal contribution

During this master thesis, I had the chance to collaborate with team members of the 'Plant Science' research axis at the faculty of Gembloux Agro Bio Tech from the ULiège, which gave me valuable insights into the study of root systems and the practical cues related to it. Although I did not participate in the active sampling of root soil cores, plant aboveground biomass, nor soil interstitial pore water - which were performed prior to the start of my thesis by my co-promotor Jennifer Michel and former master students Simon Biver and Alice Quenon - I was the main person in charge of treating these samples and extract data from them. This work could not have been possible without the assistance of Jimmy Bin and Sébastien Cougnet who occasional helped me retrieve roots from the soil samples and offered me important information concerning the use of the flatbed scanner and crown imaging setup. Regarding the quantification of glucose and nitrate concentrations in soil interstitial pore water, I received practical support from Jennifer Michel and useful tips from Sok Lay. Additionally, I benefited from theoretical advice from my statistical teacher Yves Brostaux throughout the data analysis phase, as well as the continuous support of my co-promoters Jennifer Michel and Pierre Delaplace who provided me crucial feedback on my work. Lastly, the root data I obtained contributed to the writing of two research articles within the BIOFAIR project.

9 Appendices

9.1 Historical management of soil S1 (50°38'35.1474"N, 4°37'22.0123"E)

Date	Intervention	Doses	Comments/Details
2015	Wheat		
2016	Chicories		
2017	Wheat		
06/04/18	Nitrogen (N27 %)	350 kg/h	Fertilizer
15/04/18	CARYX®	1,25 L/ha	Growth Regulator + Fungicide
04/05/18	Tangus Gold	0,5 kg/ha	Fungicide
14/07/18	Canola harvest		
21/08/18	Harrowing.		Soil work
03/10/18	Tillage		Soil work
03/10/18	Sowing six-row barley		
06/11/18	HEROLD®	0,5 L /ha	Herbicide
06/11/18	Chlortoluron	1,2 L/ha	Herbicide
06/11/18	Patriot®	0,32 L/ha	Herbicide
26/02/19	Nitrogen N27 %	250 kg/ha	Fertilizer
28/03/19	KANTIK®	1 L/ha	Fungicide
28/03/19	MEDAX® TOP	1,2 L/ha	Growth regulator
28/03/19	magnesia	2,5 kg/ ha	Fertilizer
02/04/19	SULFAZOTE 22%N (28,6 U)	200 L/ha	Fertilizer
20/04/19	TERPAL®	1,2L /ha	Growth regulator
02/05/19	VELOGY ERA®	0,7L / ha	Fungicide
02/05/19	BRAVO®	1,2L /ha	Fungicide
02/05/19	magnesia	2,5KG /ha	Fertilizer
02/05/19	Patriot®	0,2L /ha	Herbicide
08/07/19	Harvest six-row barley		
24/08/19	Glyfall plus®	6L/ha	Herbicide
02/09/19	Harrowing		Soil work
09/09/19	Harrowing		Soil work
11/09/19	Sowing cover crop (radish, clover, phacelia)."	12kg/ha	
2021	Sugar beet/wheat culture		variety BTS 4860 + KWS tessilia + caprianna kws + bts 3480 (6 boxes of each)
03/04/20	Suger beet sowing		
21/08/20	Fertilizer 0-5-16+15 CaO+2 MgO+12 EB.	1113 kg/ha	Fertilizer
02/09/20	Harrowing		Soil work
07/09/20	Harrowing		Soil work
07/09/20	Liquid nitrogen	120 l/ha	Fertilizer
07/09/20	Green manure seeding (base 5kg + early 10kg) brand Lemken®	15kg/ha	
31/10/20	Fast plow		Soil work
06/12/20	Tillage		Soil work
23/03/21	Sulfur "7 So3"	800 kg/ha	Fertilizer
23/03/21	Nitrogen "N27"	150 kg/ha	Fertilizer
23/03/21	Sulfur "7 So3"	800 kg/ha	Fertilizer
26/03/21	Liquid nitrogen	350 L/ha	Fertilizer
02/04/21	Soil preparation		Soil work
04/04/21	Beetix®	1,75 L/kg	Herbicide
04/04/21	Centium®	0,05 L/kg	Herbicide

Date	Intervention	Doses	Comments/Details
01/05/21	Dianal 160®	0,9 L/ha	Herbicide
01/05/21	Ethomat®	0,3	Herbicide
01/05/21	Safari®	15 gr/ha	Herbicide
01/05/21	Goltix® Queen	1 L/ha	Herbicide
01/05/21	Vegetop	0,5 L/ha	Additive to enhance herbicide performance.
01/05/21	magnesia	2,3kg /ha	Fertilizer
07/05/21	Dianal 160®	0,9 L/ha	Herbicide
07/05/21	Ethomat 500	0,3	Herbicide
07/05/21	Goltix® Queen	1 L/ha	Herbicide
07/05/21	Vegetop	0,5 L/ha	Additive to enhance herbicide performance.
07/05/21	magnesia	2,3kg /ha	Fertilizer
11/05/21	Hoeing		Soil work
29/05/21	Dianal 160®	0,9 L/ha	Herbicide
29/05/21	Ethomat 500	0,3	Herbicide
29/05/21	Beetix®	0,6 L/ha L/kg	Herbicide
29/05/21	Tanaris®	0,6 L/ha	Herbicide
29/05/21	Lenazar®	150 gr/ha	Herbicide
07/05/21	Vegetop	0,5 L/ha	Additive to enhance herbicide performance.
15/06/21	Centium®	0,05 L/kg	Herbicide
15/06/21	Frontier® Optima	0,5 L/ha	Herbicide
15/06/21	Boron	3 L/ha	Fertilizer
15/06/21	magnesia	2,3kg /ha	Fertilizer
05/08/21	Agora	0,35l /ha	Fungicide
05/08/21	magnesia	5,9kg /ha	Fertilizer
01/09/21	Bicanta	1 L/ha	Fungicide
01/09/21	magnesia	5 kg/ha	Fertilizer
16/10/21	Harverst		
15/11/21	Harverst		
2022	Wheat		
18/10/21	Sowing wheat	153 kg/ha	Variety/ Campesino PMG:44 gr
06/11/21	Thin sowing wheat		
01-03-22	Sulfur "18 SO3"	260 kg/ha	Fertilizer
15-03-22	Sulfazote 22%	200 l/ha	Fertilizer
23-03-22	Osmose	0,2 l/ha	Fertilizer
23-03-22	SAVVY®	20 gr/ha	Herbicide
23-03-22	Sigma® Maxx	1,1 L/ha	Herbicide
23-03-22	magnesia	2 kg/ha	Fertilizer
05-04-22	Nitrogen N27 %	194 kg/ha	Fertilizer
18-04-22	FERTILEADER® Trio		Fertilizer
18-04-22	magnesia	2,3 kg/ha	Fertilizer
18-04-22	Osmose	0,2 l/ha	Fertilizer
18-04-22	Chlormequat Chloride (CCC)	1 L/ha	Growth regulator
27-04-22	Tebecur	2,7 kg/ha	Fungicide
27-04-22	Osmose	0,2 l/ha	Fertilizer
27-04-22	magnesia	2,7 kg/ha	Fertilizer
15-05-22	Nitrogen N38	31 L/ha	Fertilizer
18-05-22	Osmose	0,2 l/ha	Fertilizer
18-05-22	magnesia	3,6 kg/ha	Fertilizer
18-05-22	REVYTREX®	1,1 L/ha	Fungicide
18-05-22	COMET ®	0,4 L/ha	Fungicide
29/07/22	Harverst wheat		
05/08/22	Harrowing		Soil work
05-08-22	KALCIPHOS P-K (S)	(0-5-15) 1000 kg/ha	Fertilizer
19/08/22	Cattle manure	15t/ha	Fertilizer
24/09/22	Green fertilizer	11,6 kg/ha	Fertilizer
24/09/22	Fast plowing		Soil work

9.2 Historical management of soil S2 (50°39'12.8668"N, 4°38'10.7664"E)

Date	Intervention	Doses	Comments/Details
2017	Beet culture		
2018	Wheat culture		
2018	Cover crop (oats, mustard, radish, clover, sunflower, peas).		
2019	Potato culture		
2019-2020	wheat		
20/10/19	Mixed vegetation seeding	145 kg/ha	
02/03/20	Nitrogen N39	175 L/kg	Fertilizer
01/02/20	TMS	80 kg/ha	Fertilizer
16/03/20	Sigma® Flex	140 g/ha	Herbicide
16/03/20	Brodway	150 g/ha	Herbicide
06/04/20	Cycocel		Growth regulator
18/04/20	Nitrogen N39	170 L/ha	
18/04/20	Humic and fulvic acids	1 L/ha	Fertilizer
16/05/20	Tebuzol	04 L/ha	Fungicide
16/05/20	TMF	1L/ha	Fertilizer
16/05/20	MgSo4	1,8 kg/ha	Fertilizer
20/05/20	Nitrogen N 27	200 kh/ha	Fertilizer
02/06/20	MgSo4	1,8 kg/ha	Fertilizer
02/06/20	TMF	1L/ha	Fertilizer
02/06/20	opustear	0,35 l/ha	?
02/06/20	sportitck	0,36 l/ha	?
02/06/20	Kestrel	0,36 l/ha	Fungicide
20/08/20	Cow manure	12000L	Fertilizer
?	Cover crop seeding (phacelia, oats, radish, clover)		
?	Grazing of cover crops, CRAW Janart trials		
08/03/21	Glypho	1L/ha	Herbicide
23/02/21	TMS	80 kg/ha	Fertilizer
18/03/21	Nitrogen	100L/ha	Fertilizer
18/03/21	Humactiv	3,5 L/ha	Root stimulant
11/05/21	Flax		Fertilizer
11/05/21	TMS	1 L/ha	Fertilizer
11/05/21	MgSo4	3kg/ha	Fertilizer
11/06/21	Rudis®	1 L/ha	Fungicide
11/06/21	TMF	0,4 L/ha	Fertilizer
11/06/21	éthéplum (?)	4 L/ha	
15/06/21	TOPREX	0,3 L/ha	Growth regulator
15/06/21	Flax	(?)	Fertilizer
16/10/21	Wheat Sowing		
05/11/21	Liberator + Flufenacet	0,58 L/ha	Herbicide
05/11/21	Mateno® Duo	0,35 L/ha	Herbicide
26/02/22	TMS	80 kg/ha	Fertilizer
14/03/22	Nitrogen N39	200 L/ha	Fertilizer
05/04/22	Nitrogen N39	175 L/ha	Fertilizer
13/04/22	MgSO4	3,5 kg/ha	Fertilizer
13/04/22	TMF	1 L/ha	Fertilizer
13/04/22	Cycocel	1L /ha	Growth regulator
25/04/22	Nitrogen N39	125 L/ha	Fertilizer
22/05/22	Kestrel	1 L/ha	Fungicide
22/05/22	MGSO4	3kg/ha	Fertilizer
22/05/22	TMF	1L/ha	Fertilizer
01/06/22	Tebusip	0,7 L/ha	Fungicide
01/06/22	TMF	1L/ha	Fertilizer
01/06/22	Primus	0,1 (?)	Herbicide
	Wheat	108 Qx/ha	
15/08/22	Horse manure	15 T/ha	Fertilizer
17/09/22	Mixture Scam Selfie		cover crop

9.3 Soil physical, biological and chemical properties for both S1 and S2 at the onset of the experiment. Sampling depth: 0-20 cm.

Soil parameters	S1	S2
Sand (%)	20.7	7.6
Silt (%)	67.1	78.8
Clay (%)	12.1	13.5
P (mg/100g)	13.6	39.8
K (mg/100g)	31.2	72.5
Mg (mg/100g)	8.4	14.7
Ca (mg/100g)	218.3	534.4
pH (KCL)	7.4	7.5
C:N	11.7	10.2
Mesofauna (na)	36	46
Water Holding Capacity (% w/w)	53.8	64.2
dry weight cover crop (g)	350	2645
Leaves of oak tree (%)	40	0
Wheat straw (%)	45	40
Grass (%)	2	40
ELSE (twigs, weeds…) (%)	8	5
Raddish (%)	0	10
Legume (%)	0	5

9.4 Composition of the remaining cover crop litter for soils S1 and S2 at the onset of the experiment (expressed in % biomass).

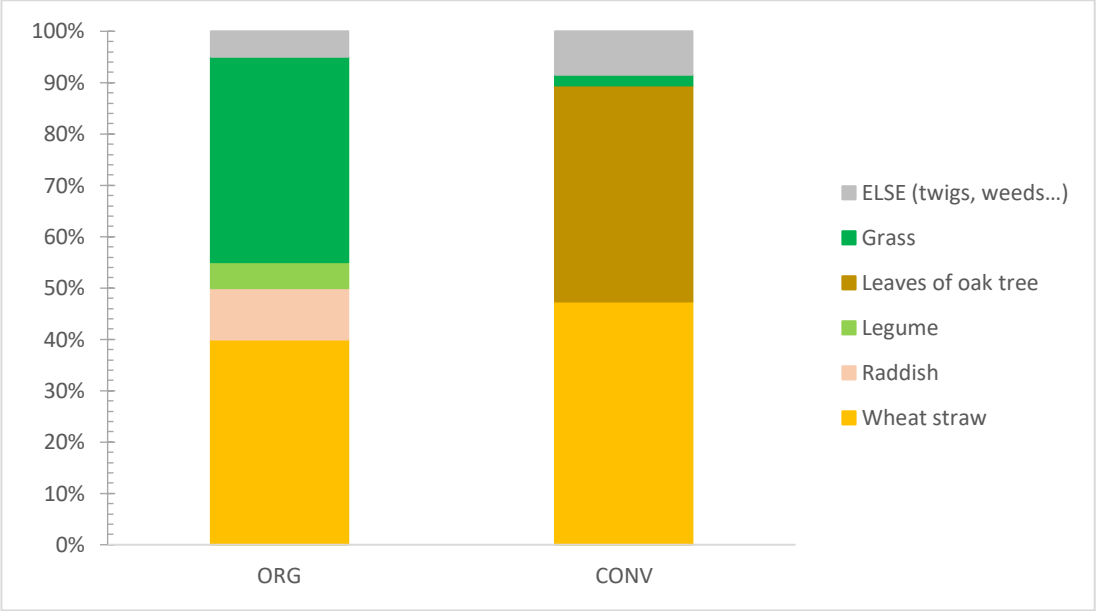

9.5 Anthrone test – lab protocol

For the anthrone test, a glucose stock solution of concentration 1 mg/mL was initially prepared by dissolving 100 mg of anhydrous glucose into 100 mL Milli-Q® distilled water. This stock solution was then diluted to create a series of standard solutions with varying concentrations. Specifically, aliquots of 5µL, 50µL, 100µL, 150µL, 200µL, 250 µL, and 500 µL of the stock solution were diluted with distilled water to a final volume of 1000 µL, giving glucose concentrations of 0.005, 0.05, 0.1, 0.15, 0.2, 0.25, and 0.5 mg/mL. However, these concentrations were later adjusted to 0.001, 0.005, 0.01, 0.05, 0.1, 0.15, and 0.2 mg/mL, as the initial values were found to be too high compared to the concentrations of the samples for which they intended to be a reference.

The anthrone solution was prepared by dissolving anthrone reagent in sulfuric acid to a concentration of 0.2%. For the assay, 50 µL of each sample and standard solution were pipetted into a 96-well plate, making sure replicates were performed for each sample. Then, 150 µl of anthrone reagent was added to each well, ensuring handling was performed under a fume hood for safety measures.The solutions were thoroughly mixed by pipetting up and down 10 times. The plate was then incubated at 100°C for 20 minutes. Finally, it was inserted in a Spark® Multimode Microplate Reader (Tecan Trading AG, Männedorf, Switzerland) spectrophotometer to measure the absorbance of the solutions. The absorbance values obtained from the standard solutions were plotted against the used sugar concentrations to get a calibration curve for each plate and determinate the carbohydrate content in each sample accordingly, expressed as glucose equivalence (Yemm et al., 1954; Gerwig, 2021).

9.6 Formula used for to calculate the average and median diameters of whole root samples based on measurements of their sub-samples.

Formula:

$$\text{Weighted Average Diameter} = \frac{(D1 \times L1) + (D2 \times L2)}{L1 + L2}$$

Where:

- $D1$ and $D2$ are the average diameters of the sub-samples.
- $L1$ and $L2$ are the total root lengths of the sub-samples.

("ChatGPT (GPT-4)," 2023).

9.7 Screeplot of eigenvalues according to the Kaiser rule

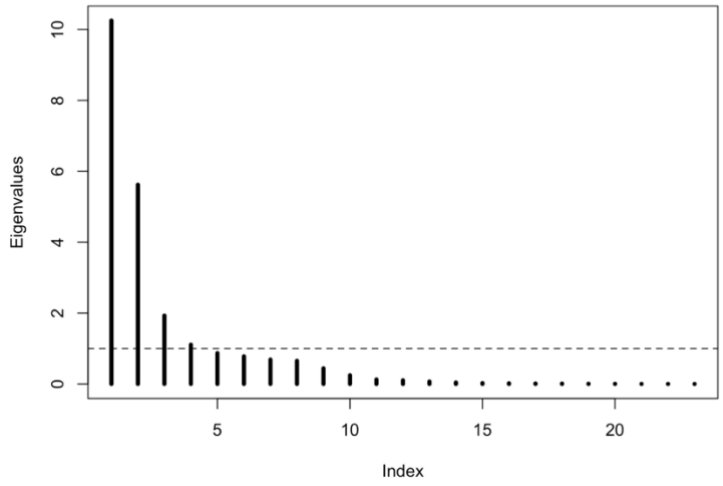

9.8 Statistically significant correlations of root parameters with principal components from the PCA

$Dim.1

Link between the variable and the continuous variables (R-square)

	correlation	p.value
Total,Root,Length,mm.x	0.9816387	4.557928e-104
Network_Area_roots	0.9800623	1.495572e-101
Number,of,Root,Tips.x	0.9778782	2.223450e-98
Poids (mg)	0.9530583	1.469081e-75
Diameter_3	0.9407506	1.437368e-68
Diameter_2	0.9301981	1.117636e-63
Surface,Area,mm2.x	0.9020367	1.145960e-53
Diameter_1	0.8906555	1.856156e-50
Diameter_4	0.8737410	2.720979e-46
Solidity	0.6597408	2.416514e-19
Network_Area_crowns	0.6092021	5.410745e-16
Branching,frequency,per,mm	0.5599344	2.956703e-13
Medium,Angle,Frequency	0.5218836	1.975647e-11
Volume,mm3.x	0.5105936	6.234599e-11
Shallow,Angle,Frequency	0.2989606	2.727779e-04
Average,Diameter,mm.x	-0.1803145	3.056621e-02
Median,Diameter,mm.x	-0.2863757	5.019196e-04
Average,Root,Orientation,deg	-0.4493114	1.614689e-08
Steep,Angle,Frequency	-0.4956082	2.689478e-10

$Dim.2

Link between the variable and the continuous variables (R-square)

	correlation	p.value
Depth,mm	0.9350975	7.589073e-66
Convex,Area,mm2	0.8649592	2.331139e-44
Average,Root,Orientation,deg	0.7678602	2.983305e-29
Steep,Angle,Frequency	0.7298259	3.192134e-25
Network_Area_crowns	0.5986013	2.301936e-15
Maximum,Width,mm	0.4257004	1.042472e-07
Diameter_1	0.1675332	4.474051e-02
Diameter_2	0.1654347	4.752513e-02
Medium,Angle,Frequency	-0.2973274	2.957079e-04
Solidity	-0.3886484	1.481237e-06
Width-to-Depth,Ratio	-0.6181024	1.537726e-16
Median,Diameter,mm.x	-0.6495932	1.278660e-18
Average,Diameter,mm.x	-0.7212390	2.091255e-24
Shallow,Angle,Frequency	-0.8033001	9.108174e-34

$Dim.3

Link between the variable and the continuous variables (R-square)

	correlation	p.value
Maximum,Width,mm	0.8445697	2.370194e-40
Width-to-Depth,Ratio	0.5724030	6.619713e-14
Convex,Area,mm2	0.3958787	9.047258e-07
Medium,Angle,Frequency	0.3290172	5.661635e-05
Shallow,Angle,Frequency	0.2710996	1.013998e-03
Network_Area_crowns	0.1827084	2.838837e-02
Median,Diameter,mm.x	-0.1651148	4.796193e-02
Volume,mm3.x	-0.2318652	5.168410e-03
Average,Diameter,mm.x	-0.2380680	4.061460e-03
Solidity	-0.2649371	1.331596e-03
Average,Root,Orientation,deg	-0.3479116	1.930201e-05
Steep,Angle,Frequency	-0.3687409	5.425430e-06

9.9 PCA plot on the second factorial plane (PC2 & PC3)

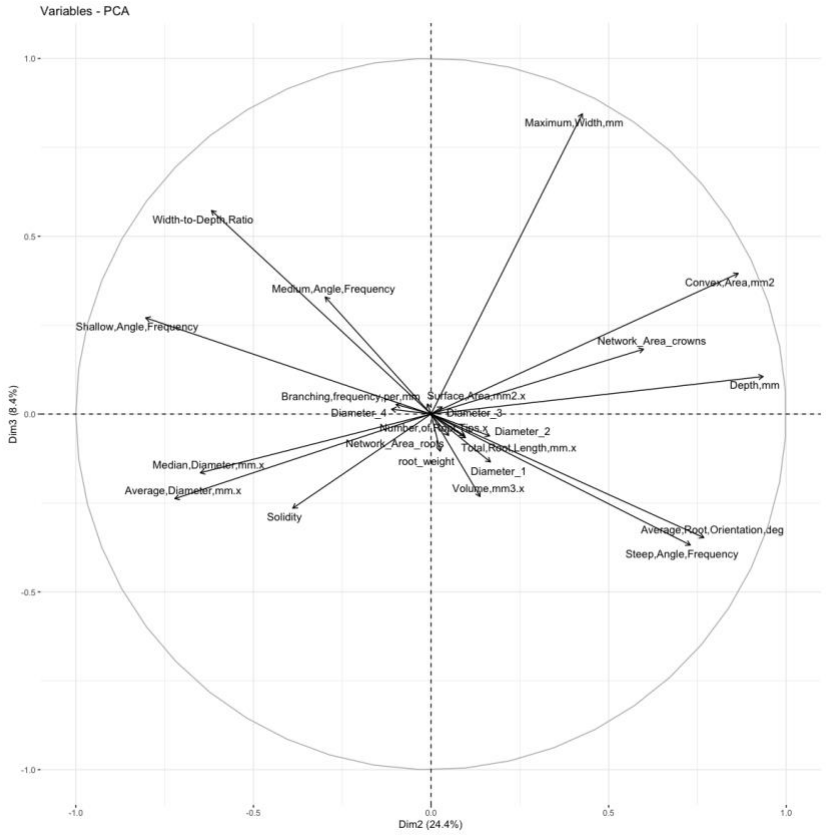

9.10 Results of the post-hoc pairwise comparisons on the centroids' coordinates of each modality relative to PC1 and PC2.

```
        Pairwise comparisons using permutation MANOVAs (test: Pillai)

data:  response_matrix by group_factor
999 permutations

        2013_S1 2013_S2 2068_S1 2068_S2 2085_S1
2013_S2 0.705   -       -       -       -
2068_S1 1.000   1.000   -       -       -
2068_S2 1.000   1.000   1.000   -       -
2085_S1 0.540   1.000   0.090   0.585   -
2085_S2 0.345   1.000   0.015   0.315   1.000

P value adjustment method: bonferroni
```

9.11 Euclidian distance matrix of modalities centroids' coordinates, relative to PC1 and PC2.

	2013_S1	2013_S2	2068_S1	2068_S2	2085_S1	2085_S2
2013_S1	0,0					
2013_S2	1,6	0,0				
2068_S1	1,1	1,3	0,0			
2068_S2	1,3	1,6	0,3	0,0		
2085_S1	2,1	1,3	2,4	2,7	0,0	
2085_S2	2,0	1,6	2,5	2,8	0,4	0,0

9.12 Mathematical computation of root traits extracted from a scanned image, using RhizoVision Explorer.

Feature extracted	Description
Number of Root Tips	The number of root tips is pixels in identified root topology that have only one neighbouring skeletal pixel.
Total Root Length (px, mm)	The sum of the Euclidean distances between the connected skeletal pixels in the entire root topology of the plant root image.
Network Area (px^2, mm^2)	The total number of pixels in the segmented image.
Average, Median and Maximum Diameter (px, mm)	The distance transform value at each skeletal pixel is the radius at that pixel and is doubled to give the diameter. The average, median and maximum diameters are computed across all these skeleton pixels.
Perimeter (px, mm)	The sum of the Euclidean distances between the connected contour pixels in the entire segmented image of the plant root.
Volume (px^3, mm^3) and Surface Area (px^2, mm^2)	Using the radii for each skeletal pixel determined earlier, the volume at the skeletal pixel is calculated as the length of the pixel multiplied by the cross-sectional area of the root at that pixel. Similarly, the surface area is calculated as the length of the pixel multiplied by the circumference of the cross-section of the root at that pixel. Volume and surface area are calculated as the sum of values from all skeletal pixels.
Computation Time (s)	The time taken to analyse a plant root image is noted as computation time in seconds.
Root Length, Projected Area, Surface Area and Volume histograms	For each skeletal pixel, the root length, projected area on the surface of the image plane, surface area and volume of the root at that pixel are computed. These values are binned according to the diameter ranges specified by the user.
Number of Branch Points*	The number of branch points is pixels in the identified root topology that have at least three neighbouring skeletal root segments.
Branching Frequency (px^{-1}, mm^{-1})*	The number of branch points per unit root length.
Median and Maximum number of roots**	For each row in the segmented image, a horizontal line scanning is performed that records the number of pixel transitions from a background to a root pixel. This list of pixel transitions is sorted and the median and the maximum number of roots are noted.
Depth, Maximum Width (px, mm)**	The maximum vertical and horizontal distance the root crown grew at the time of imaging are noted as Depth and Maximum Width, respectively.
Width-to-Depth Ratio**	The ratio of Maximum Width to Depth is noted as the Width-to-Depth ratio.
Convex Area (px^2, mm^2) and Solidity**	The area of the convex hull that is fit to include the entire root crown system is noted as Convex Area. Solidity is the ratio of the Network Area to Convex Area.
Lower Root Area (px^2, mm^2)**	For a root crown image, the skeletal pixel that has the maximum radius is located. The network area of the root system that is below the skeletal pixel located above is noted as Lower Root Area.
Holes and Average Hole Size (px^2, mm^2)**	Holes are background components between roots in a segmented image. These holes are counted, and their average size is determined.
Steep Angle Frequency, Medium Angle Frequency, Shallow Angle Frequency and Average Root Orientation**	Within 40 × 40 pixel locality for every skeletal pixel in the centre, we get the coordinates of all the skeletal pixels in that locality and compute the angular orientation for the locality. We group these orientations in bins of 0–30°, 30–60° and 60–90° and note the frequencies as Steep, Medium and Shallow Angle Frequencies. The average of these orientations is noted as Average Root Orientation.

Root traits extracted from broken root scans are marked with (*), and those stemming from crown root images are marked with (**) (Seethepalli, Dhakal, et al., 2021).

9.13 Random effects of the LMM fitted on TRL_log & residual plot (taking ID as the experimental unit)

```
Scaled residuals:
     Min       1Q   Median       3Q      Max
-2.21725 -0.44975  0.05214  0.51758  1.84320

Random effects:
 Groups   Name        Variance  Std.Dev. Corr
 ID       (Intercept) 0.000e+00 0.000000
          Depth10_20  1.442e-01 0.379791  NaN
 ID.1     (Intercept) 4.477e-02 0.211599
          Timepointt2 2.336e-06 0.001528  1.00
          Timepointt3 5.619e-01 0.749606 -1.00 -1.00
 CER      (Intercept) 6.147e-02 0.247936
 Residual             1.627e-01 0.403409
Number of obs: 126, groups:  ID, 24; CER, 6
```

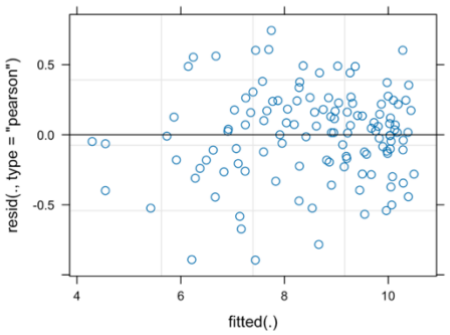

9.14 Biplot of each modality centroids with their confidence ellipses on PC1 & PC2.

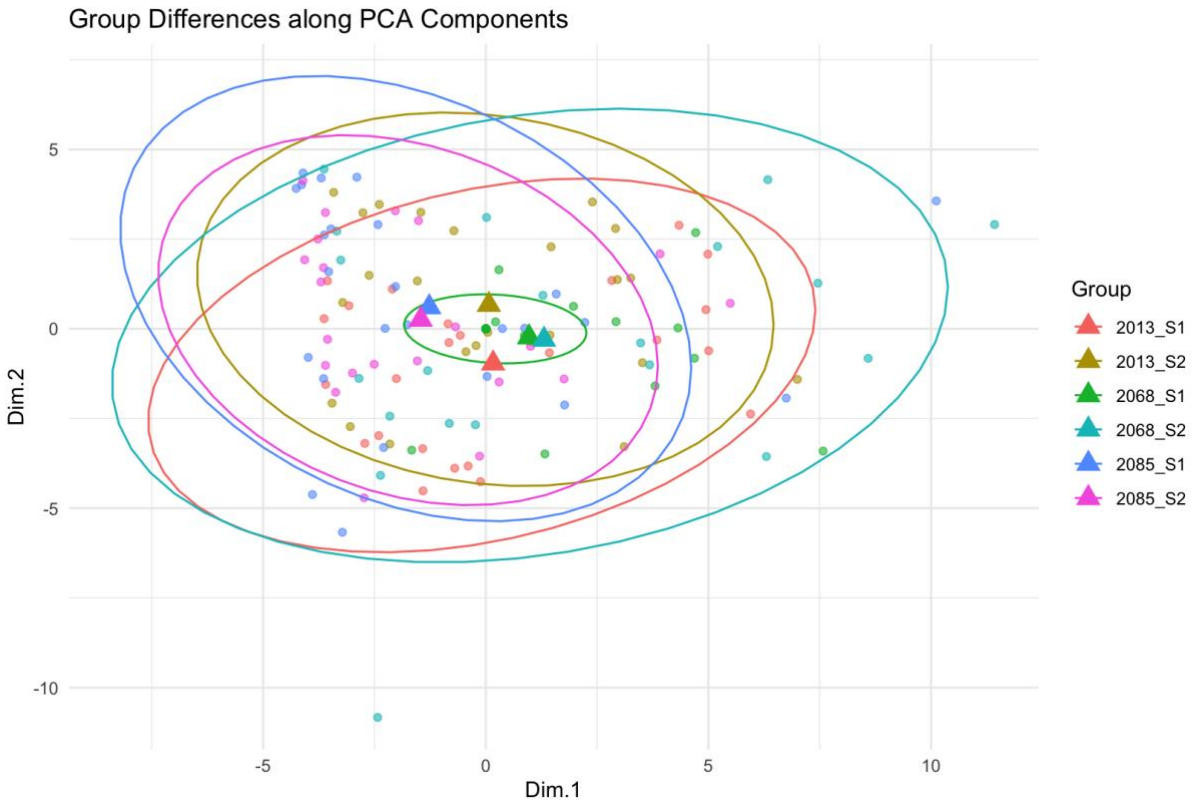

9.15 Bar plots showing non-significant effects of Year-Soil on root average diameter, crown depth, width, and width:depth ratio

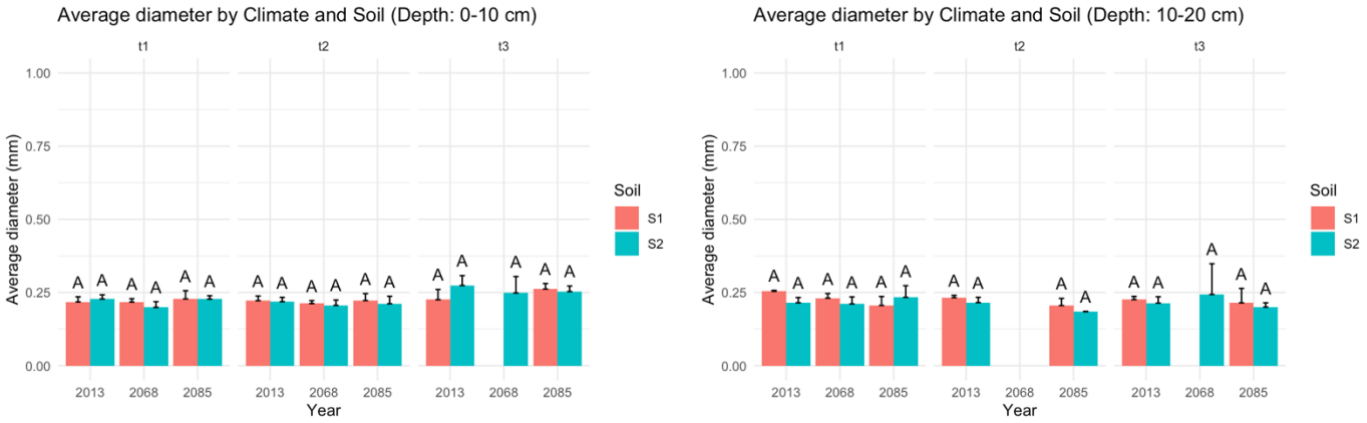

Appendix 9.15.1: bar plots showing root average diameter across years and soil types (S1 = conventional, S2 = organic), segregated between timepoints, and depths (left: 0-10 cm; right: 10-20 cm). Bars represent means plus standard deviations (Mean + SD). Groups sharing same letters are not statistically different.

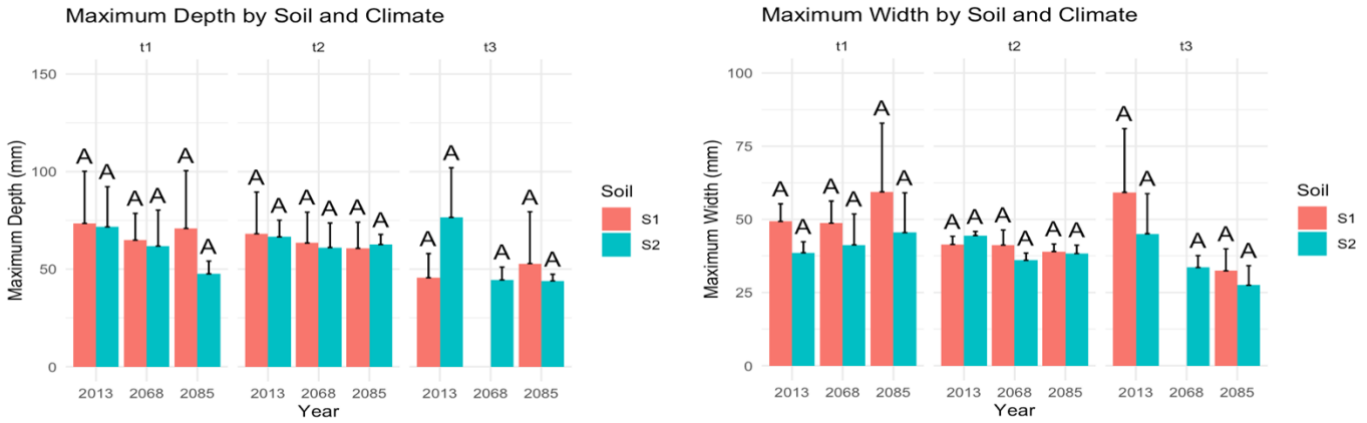

Appendix 9.15.2: bar plots showing root crown width (right) and depth (left) across years and soil types (S1 = conventional, S2 = organic), segregated between timepoints, and depths (left: 0-10 cm; right: 10-20 cm). Bars represent means plus standard deviations. Groups sharing same letters are not statistically different.

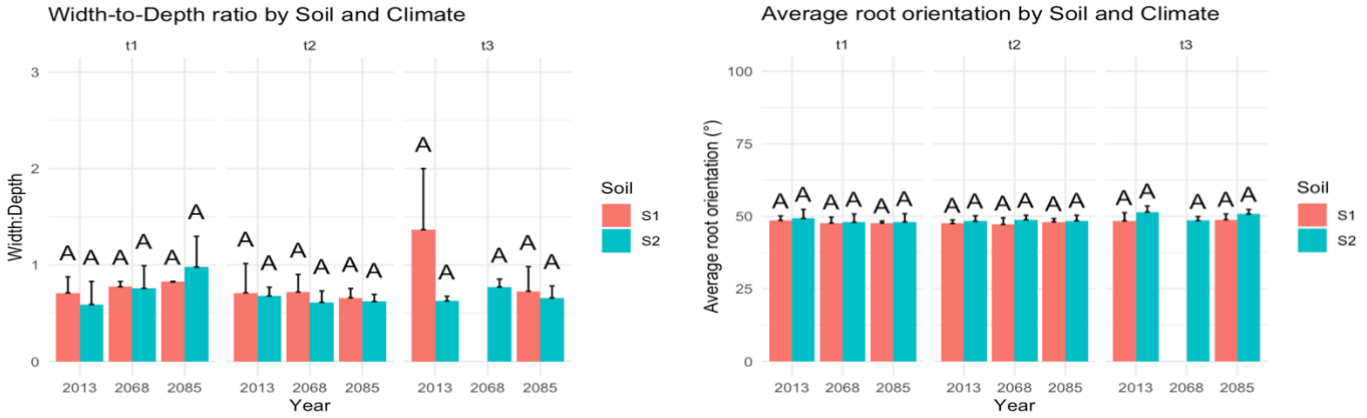

Appendix 9.15.3: bar plots showing width-to-depth ratio (left) and average root orientation (right) across years and soil types (S1 = conventional, S2 = organic), separated by timepoint. Groups sharing the same letter prove to not be statistically different from each other. Bars represent means plus standard deviations (Mean + SD). Groups sharing same letters are not statistically different.

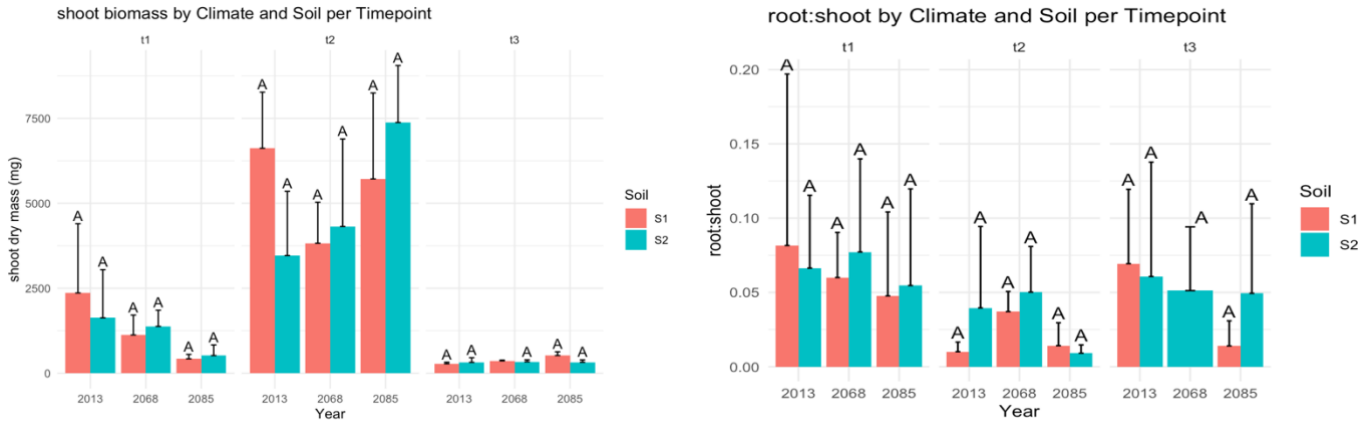

Appendix 9.15.4: Shoot Dry Weight (in mg) and root-to-shoot ratio across years and soil types separated by timepoints and soil depths (missing data at t3). Bars represent means plus the upper half of standard deviations (Mean + SD). Groups sharing same letters are not statistically different from each other.

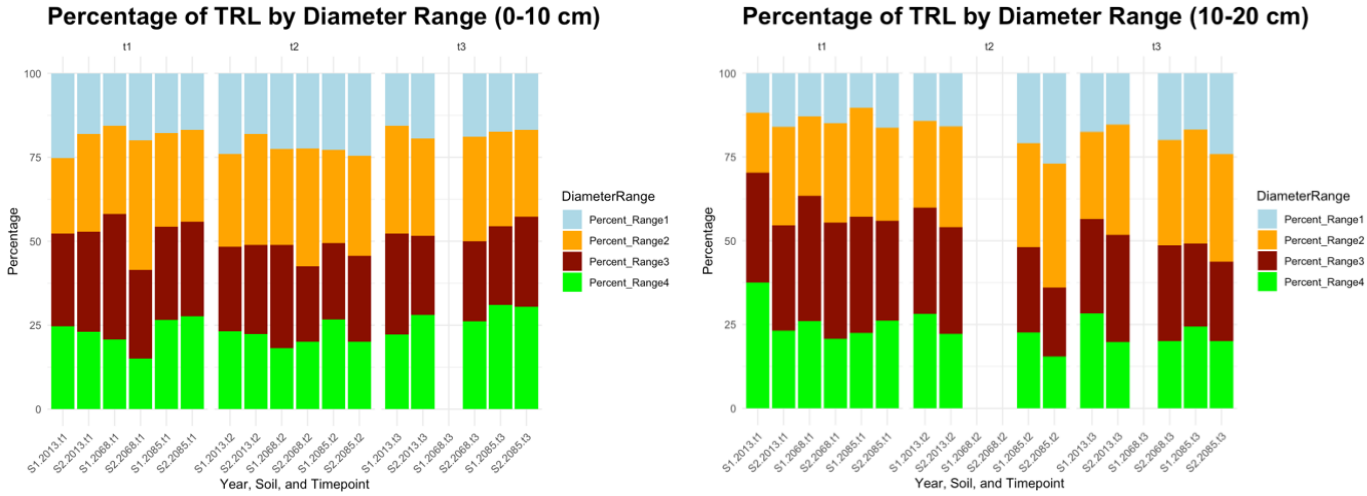

Appendix 9.15.5: Distribution of diameter ranges (normalized by TRL), across Year x Soil modalities, by timepoint and depth (left: 0-10 cm and right: 10-20 cm). Diameter range 1 : [0–0.09] mm; Diameter range 2 : [0.09–0.18] mm; Diameter range 3 : [0.18–0.26] mm; Diameter range 4 : [0.26 mm and above].

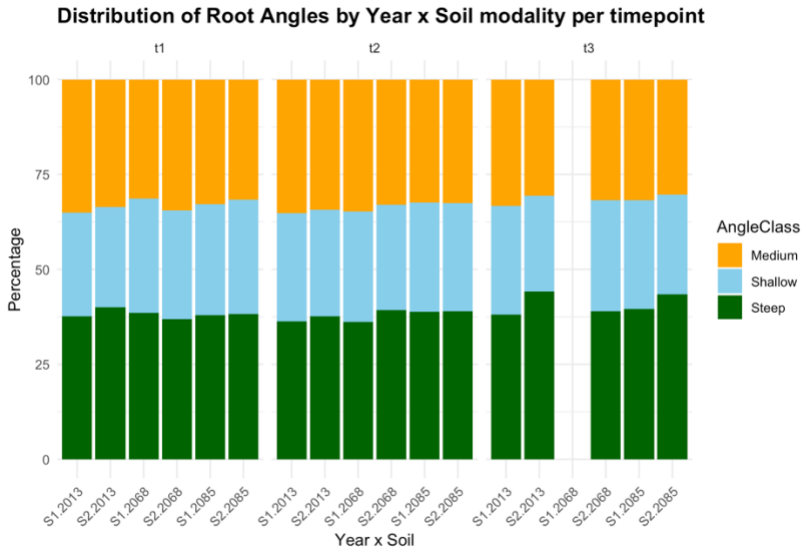

Appendix 9.15.6: Distribution of root angles frequencies across Year x Soil modalities, by timepoint. Shallow Angle comprises the angular range [0–30°]; Medium Angle [30–60°]; and Steep Angle [60–90°].

9.16 Means, standard error (SE), and significance groupings letters for *Year* and *Soil* effects on root traits within each combination of timepoint and depth.

t1		2013						2068						2085					
		S1			S2			S1			S2			S1			S2		
	Depth	Mean	SE	group	Mean	SE	group	Mean	SE	group	Mean	SE	group	Mean	SE	group	Mean	SE	group
TRL (mm)	0-10 cm	19187,6	2079,1	A	19771,0	1414,0	A	18091,1	2138,9	A	36729,1	6762,8	A	10583,9	4165,4	A	7921,2	1032,6	A
	10-20 cm	7800,6	745,2	B	12152,7	1491,4	B	11330,8	1974,7	B	11902,0	1764,9	B	1809,6	1043,0	A	945,4	96,6	A
BF (mm^-1)	0-10 cm	1,893	0,234	A	1,312	0,106	A	1,110	0,139	A	1,011	0,085	A	1,175	0,063	A	1,343	0,328	A
	10-20 cm	0,999	0,091	A	0,989	0,080	A	1,044	0,110	A	0,930	0,132	A	0,521	0,052	A	0,803	0,215	A
NbRT	0-10 cm	6135,8	988,2	A	5509,8	444,6	A	5336,8	902,7	A	9115,8	1772,3	A	2556,3	983,8	A	2052,3	287,3	A
	10-20 cm	2182,0	175,7	B	3168,8	547,8	B	3008,3	559,1	B	3183,0	478,5	B	380,3	207,3	A	239,8	27,1	A
volume (mm^3)	0-10 cm	1068,9	152,1	A	1249,7	121,2	A	893,9	112,4	A	9357,3	8082,4	A	687,6	296,8	A	1769,2	1327,4	A
	10-20 cm	502,4	54,9	A	607,9	118,0	A	582,5	94,2	A	492,0	58,7	A	92,8	66,5	A	55,4	13,5	A
AvD (mm)	0-10 cm	0,218	0,009	A	0,228	0,007	A	0,217	0,006	A	0,199	0,010	A	0,228	0,014	A	0,228	0,006	A
	10-20 cm	0,254	0,001	A	0,215	0,009	A	0,231	0,008	A	0,211	0,012	A	0,206	0,015	A	0,234	0,020	A
Width:Depth	0-10 cm	0,71	0,10	A	0,59	0,12	A	0,77	0,03	A	0,76	0,12	A	0,82	0,00	A	0,98	0,16	A
Angle (°)	0-10 cm	48,6	0,9	A	49,3	1,6	A	47,7	1,0	A	47,9	1,4	A	47,7	0,5	A	48,0	1,4	A

t2		2013						2068						2085					
		S1			S2			S1			S2			S1			S2		
	Depth	Mean	SE	group	Mean	SE	group	Mean	SE	group	Mean	SE	group	Mean	SE	group	Mean	SE	group
TRL (mm)	0-10 cm	24381,7	2293,6	A	21627,0	3233,6	A	26561,7	1757,4	A	30640,8	4136,0	A	23981,3	8577,1	A	19487,8	4160,0	A
	10-20 cm	6963,1	1464,5	A	8909,3	577,6	A	NA	NA	NA	NA	NA	NA	3981,9	1054,0	A	6267,0	727,0	A
BF (mm^-1)	0-10 cm	1,827	0,145	A	1,208	0,087	A	1,164	0,128	A	1,249	0,104	A	1,409	0,163	A	1,237	0,079	A
	10-20 cm	1,061	0,045	A	1,156	0,201	A	NA	NA	NA	NA	NA	NA	1,084	0,150	A	1,283	0,137	A
NbRT	0-10 cm	7626,5	963,2	A	6155,3	871,2	A	7820,3	841,1	A	8663,0	1138,3	A	7395,8	2796,2	A	6220,5	1377,9	A
	10-20 cm	1985,8	378,8	A	2510,8	211,8	A	NA	NA	NA	NA	NA	NA	1208,3	344,7	A	1719,5	188,5	A
volume (mm^3)	0-10 cm	1553,1	160,2	A	1316,6	210,9	A	4718,2	3405,4	A	1556,8	401,1	A	8211,3	7025,9	A	1081,7	199,1	A
	10-20 cm	375,7	74,6	A	431,5	62,0	A	NA	NA	NA	NA	NA	NA	186,5	64,7	A	255,1	61,4	A
AvD (mm)	0-10 cm	0,222	0,008	A	0,219	0,007	A	0,212	0,005	A	0,206	0,009	A	0,222	0,012	A	0,212	0,013	A
	10-20 cm	0,233	0,004	A	0,216	0,009	A	NA	NA	NA	NA	NA	NA	0,205	0,012	A	0,185	0,001	A
Width:Depth	0-10 cm	0,71	0,18	A	0,68	0,05	A	0,72	0,09	A	0,61	0,06	A	0,66	0,05	A	0,62	0,04	A
Angle (°)	0-10 cm	47,5	0,7	A	48,3	0,9	A	47,2	1,1	A	48,8	0,8	A	48,1	0,5	A	48,5	1,0	A

t3		2013						2068						2085					
		S1			S2			S1			S2			S1			S2		
	Depth	Mean	SE	group	Mean	SE	group	Mean	SE	group	Mean	SE	group	Mean	SE	group	Mean	SE	group
TRL (mm)	0-10 cm	4478,2	1136,1	A	3175,4	1057,7	A	NA	NA	NA	3271,4	222,1	A	1183,7	359,0	A	2389,2	236,4	A
	10-20 cm	868,9	324,2	A	2249,5	883,2	A	NA	NA	NA	1309,5	361,9	A	244,9	171,2	A	433,1	162,7	A
BF (mm^-1)	0-10 cm	0,984	0,075	A	0,914	0,137	A	NA	NA	NA	1,003	0,212	A	0,854	0,140	A	0,934	0,187	A
	10-20 cm	0,746	0,095	A	1,085	0,170	A	NA	NA	NA	0,948	0,222	A	0,441	0,145	A	0,594	0,134	A
NbRT	0-10 cm	1376,5	287,8	A	830,5	216,2	A	NA	NA	NA	1136,0	48,5	A	419,5	128,8	A	811,0	42,6	A
	10-20 cm	281,5	103,1	A	803,0	308,4	A	NA	NA	NA	394,8	121,6	A	87,0	59,5	A	146,0	58,0	A
volume (mm^3)	0-10 cm	244,9	53,7	A	364,9	116,9	A	NA	NA	NA	290,7	86,6	A	94,1	27,3	A	203,0	39,5	A
	10-20 cm	48,2	20,4	A	92,5	30,3	A	NA	NA	NA	72,5	18,6	A	10,6	7,2	A	18,1	7,2	A
AvD (mm)	0-10 cm	0,226	0,017	A	0,274	0,017	A	NA	NA	NA	0,248	0,028	A	0,262	0,010	A	0,253	0,009	A
	10-20 cm	0,226	0,005	A	0,214	0,011	A	NA	NA	NA	0,243	0,052	A	0,215	0,025	A	0,200	0,007	A
Width:Depth	0-10 cm	1,37	0,32	A	0,63	0,03	A	NA	NA	NA	0,77	0,04	A	0,73	0,13	A	0,66	0,06	A
Angle (°)	0-10 cm	48,4	1,4	A	51,5	1,2	A	NA	NA	NA	48,5	0,7	A	48,8	1,0	A	50,8	0,8	A

t1		2013						2068						2085					
		S1			S2			S1			S2			S1			S2		
	Depth	Mean	SE	group	Mean	SE	group	Mean	SE	group	Mean	SE	group	Mean	SE	group	Mean	SE	group
RL_D1(%)	0-10 cm	24,5	3,6	A	17,8	1,4	A	15,2	2,2	A	23,3	5,6	A	19,1	1,9	A	19,4	3,0	A
	10-20 cm	11,9	0,9	A	16,2	1,3	A	12,2	1,8	A	14,6	2,8	A	12,5	2,2	A	15,8	2,0	A
RL_D2(%)	0-10 cm	22,48	0,85	A	28,95	1,94	A	26,31	2,06	A	35,47	3,03	A	30,24	3,12	A	27,37	1,12	A
	10-20 cm	17,53	1,56	A	30,24	2,39	A	23,10	1,92	A	28,33	3,60	A	35,73	6,08	A	27,77	3,48	A
RL_D3(%)	0-10 cm	28,01	1,58	A	29,97	0,90	A	37,44	0,77	A	24,86	4,25	A	26,33	2,53	A	25,68	2,44	A
	10-20 cm	32,54	0,80	A	31,24	1,04	A	37,68	0,96	A	35,14	2,31	A	33,33	4,47	A	29,94	3,58	A
RL_D4(%)	0-10 cm	25,02	1,74	A	23,26	1,91	A	21,07	1,87	A	13,25	3,72	A	24,35	4,33	A	27,51	0,60	A
	10-20 cm	38,02	1,94	A	22,36	2,50	A	27,04	2,63	A	21,98	3,87	A	18,47	4,14	A	26,46	5,77	A
root_weight (mg)	0-10 cm*	77,28	10,25	B	83,13	4,15	B	69,23	8,74	B	146,29	24,30	C	25,63	10,83	A	36,46	6,59	B
	10-20 cm	40,23	6,62	B	51,78	7,89	B	44,01	6,76	C	42,51	5,45	C	9,04	5,79	A	4,28	0,22	A
shoot_weight (mg)	0-10 cm	2361,5	1100,7	A	1629,5	765,4	A	1125,3	315,7	A	1378,8	256,4	A	422,5	71,3	A	520,0	168,1	A
MBC	0-10 cm*	68,15	5,31	B	90,62	6,89	B	70,76	7,34	B	86,94	17,46	B	63,77	4,72	A	96,83	8,78	C
	10-20 cm	70,85	6,26	A	59,20	9,00	A	64,34	4,33	A	66,53	8,39	A	44,73	3,87	A	54,47	8,17	A

t2		2013						2068						2085					
		S1			S2			S1			S2			S1			S2		
	Depth	Mean	SE	group	Mean	SE	group	Mean	SE	group	Mean	SE	group	Mean	SE	group	Mean	SE	group
RL_D1(%)	0-10 cm	24,0	2,1	A	17,9	0,8	A	14,4	1,1	A	22,3	0,6	A	25,3	2,9	A	24,2	2,5	A
	10-20 cm	14,6	1,1	A	15,7	2,6	A	NA	NA	NA	NA	NA	NA	20,6	0,5	A	26,6	3,3	A
RL_D2(%)	0-10 cm	27,28	1,80	A	34,42	4,52	A	31,57	2,57	A	35,62	1,72	A	28,08	2,53	A	29,86	0,37	A
	10-20 cm	24,76	1,90	A	30,19	4,03	A	NA	NA	NA	NA	NA	NA	32,21	4,23	A	37,23	2,19	A
RL_D3 (%)	0-10 cm	24,86	1,79	B	26,63	0,09	B	34,42	0,60	C	22,72	1,15	B	21,44	2,21	A	25,48	1,49	B
	10-20 cm	30,71	1,60	A	31,76	2,79	A	NA	NA	NA	NA	NA	NA	26,72	1,98	A	20,81	2,01	A
RL_D4 (%)	0-10 cm	23,89	2,64	A	21,10	3,93	A	19,62	1,49	A	19,35	2,37	A	20,76	5,40	A	20,46	1,50	A
	10-20 cm	29,98	2,94	A	22,37	4,22	A	NA	NA	NA	NA	NA	NA	20,42	4,71	A	15,41	0,85	A
root_weight (mg)	0-10 cm	121,61	17,60	A	113,84	14,80	A	129,15	4,89	A	160,03	12,81	A	117,63	37,79	A	91,48	14,14	A
	10-20 cm	36,39	6,22	A	32,29	1,44	A	NA	NA	NA	NA	NA	NA	14,25	4,22	A	19,35	3,75	A
shoot_weight (mg)	0-10 cm	6620,0	1430,0	A	3462,7	1219,3	A	3824,5	651,7	A	4317,3	1391,2	A	5527,3	1491,0	A	7377,0	1082,8	A
MBC	0-10 cm	74,30	11,25	A	90,81	11,87	A	80,63	4,29	A	98,13	4,44	A	68,01	7,18	A	95,43	5,59	A
	10-20 cm	58,83	7,83	A	53,74	9,71	A	68,11	2,77	A	78,07	7,14	A	50,31	1,57	A	61,31	5,93	A

t3		2013						2068						2085					
		S1			S2			S1			S2			S1			S2		
	Depth	Mean	SE	group	Mean	SE	group	Mean	SE	group	Mean	SE	group	Mean	SE	group	Mean	SE	group
RL_D1 (%)	0-10 cm	16,3	1,2	A	15,6	3,2	A	NA	NA	NA	18,8	0,6	A	15,1	2,7	A	17,5	2,3	A
	10-20 cm	15,5	2,7	A	15,9	0,9	A	NA	NA	NA	20,7	3,2	A	19,8	6,3	A	21,7	4,1	A
RL_D2 (%)	0-10 cm	30,64	2,99	A	25,63	3,40	A	NA	NA	NA	30,98	4,96	A	25,69	2,84	A	25,88	1,96	A
	10-20 cm	26,12	1,36	A	29,34	3,55	A	NA	NA	NA	28,86	4,49	A	27,88	6,10	A	29,05	3,17	A
RL_D3 (%)	0-10 cm	29,22	1,36	A	26,75	4,63	A	NA	NA	NA	24,01	1,58	A	24,39	1,46	A	26,23	2,07	A
	10-20 cm	30,67	2,32	A	31,40	0,74	A	NA	NA	NA	25,69	3,54	A	24,21	6,22	A	26,74	3,28	A
RL_D4 (%)	0-10 cm	23,83	3,85	A	31,97	5,71	A	NA	NA	NA	26,18	5,77	A	34,85	4,32	A	30,44	1,33	A
	10-20 cm	27,69	1,67	A	23,33	3,99	A	NA	NA	NA	24,80	8,25	A	28,07	8,02	A	22,50	2,50	A
root_weight (mg)	0-10 cm	33,66	3,43	A	24,17	6,15	A	NA	NA	NA	36,10	5,86	A	10,36	3,26	A	24,33	5,85	A
	10-20 cm	8,92	2,08	A	5,81	0,71	A	NA	NA	NA	9,63	0,77	A	1,98	0,73	A	2,78	0,85	A
shoot_weight (mg)	0-10 cm	NA	NA	NA	NA	NA	NA	NA	NA	NA	NA	NA	NA	NA	NA	NA	NA	NA	NA
MBC	0-10 cm*	57,63	1,62	A	61,21	6,33	A	62,83	1,11	A	62,98	11,57	A	48,24	4,08	A	58,77	9,93	A
	10-20 cm	43,22	7,74	A	41,27	6,76	A	43,96	4,56	A	48,92	6,23	A	32,10	5,52	A	47,60	4,08	A

9.17 Scatter plot between glucose and nitrate soil concentrations

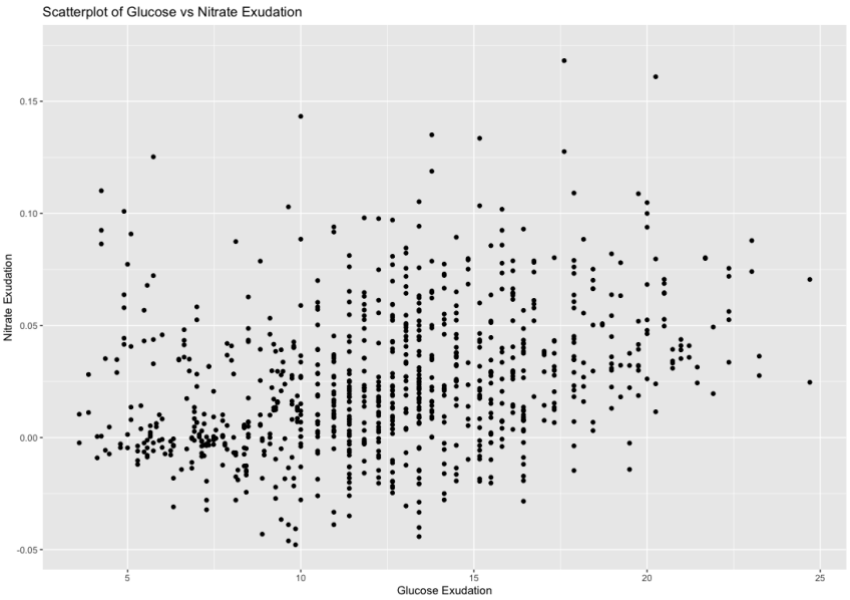

9.18 Loadings of variables on the first two principal components from the probabilistic PCA (pPCA).

	PC1	PC2
Number of root tips (na)	0.334	-0.013
Branching frequency (mm^{-1})	0.194	0.017
Root volume (mm^3)	0.176	-0.113
Surface area (mm^2)	0.305	0.055
Root length – diameter range 1 (mm)	0.306	-0.068
Root length – diameter range 2 (mm)	0.318	-0.058
Root length – diameter range 3 (mm)	0.318	0.030
Root length – diameter range 4 (mm)	0.293	0.098
Root dry biomass (mg)	0.322	0.018
Total root length (mm)	0.162	-0.238
Root crown depth (mm)	0.115	-0.320
Root crown width (mm)	0.018	0.058
Shallow angle frequency (%)	0.009	0.461
Medium angle frequency (%)	0.112	0.352
Steep angle frequency (%)	-0.082	-0.569
Shoot dry biomass (mg)	0.150	0.001
Glucose concentration (mg mL^{-1})	0.020	0.170
Nitrate concentration (mg mL^{-1})	-0.069	0.052
MBC (µg C g^{-1} dry soil)	0.384	0.000
Grain yield (t ha^{-1})	0.073	-0.079
Grain.N (%)	-0.033	0.323

9.19 Biplot of variables and individuals from the pPCA, grouped by Soil with 95% confidence ellipses

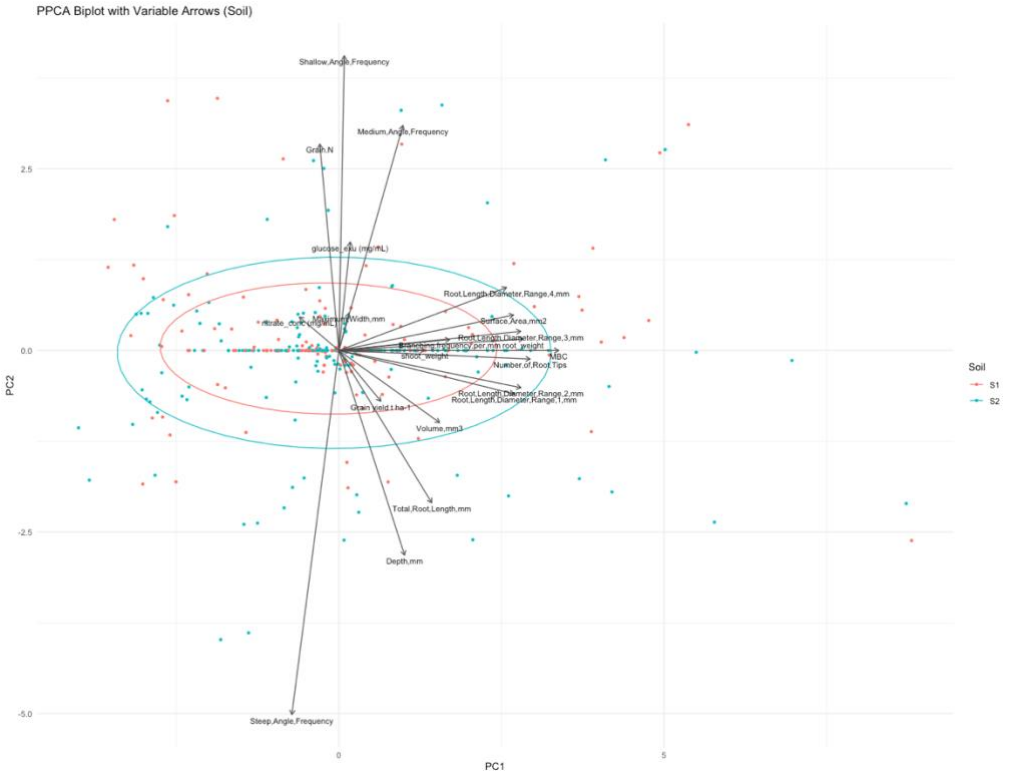

9.20 Biplot of variables and individuals from the pPCA, grouped by Year with 95% confidence ellipses

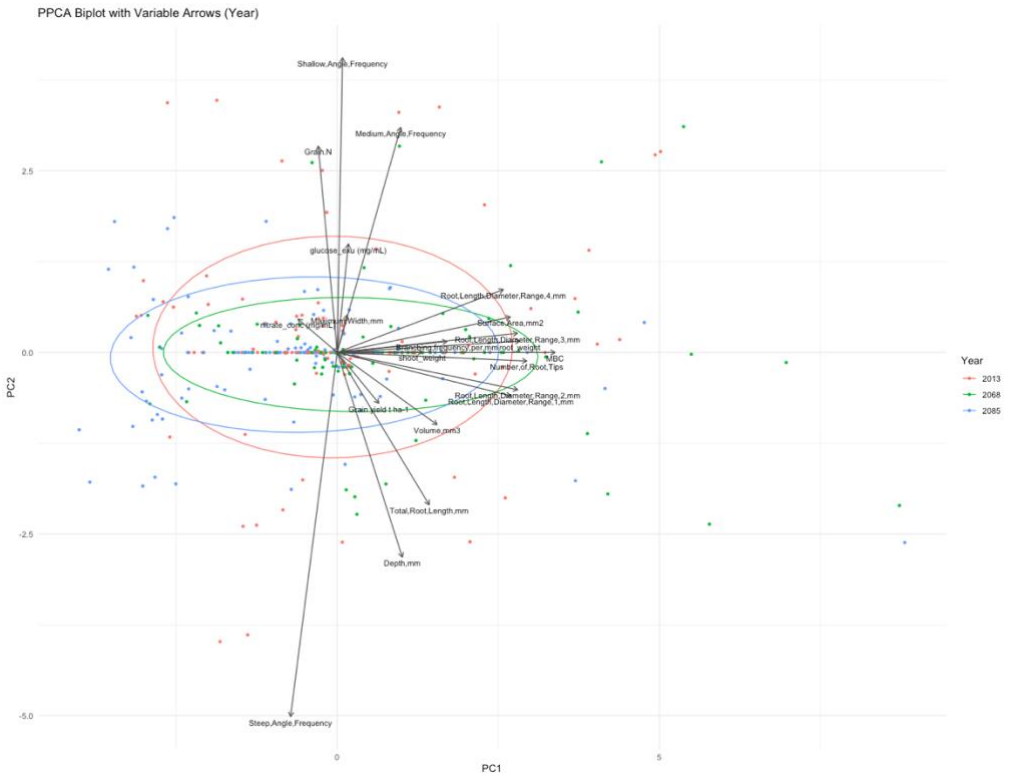

9.21 Coordinates of ellipse centroids representing Soil x Climate modalities along PC1 & PC2 of the pPCA.

Modality	Dim.1	Dim.2
2013.S1	0.038	0.337
2013.S2	0.049	-0.085
2068.S1	0.558	0.049
2068.S2	0.566	-0.108
2085.S1	-0.662	-0.032
2085.S2	-0.430	-0.136

9.22 Spearman's correlation plot between variables derived from the probabilistic Principal Component Analysis (pPCA).

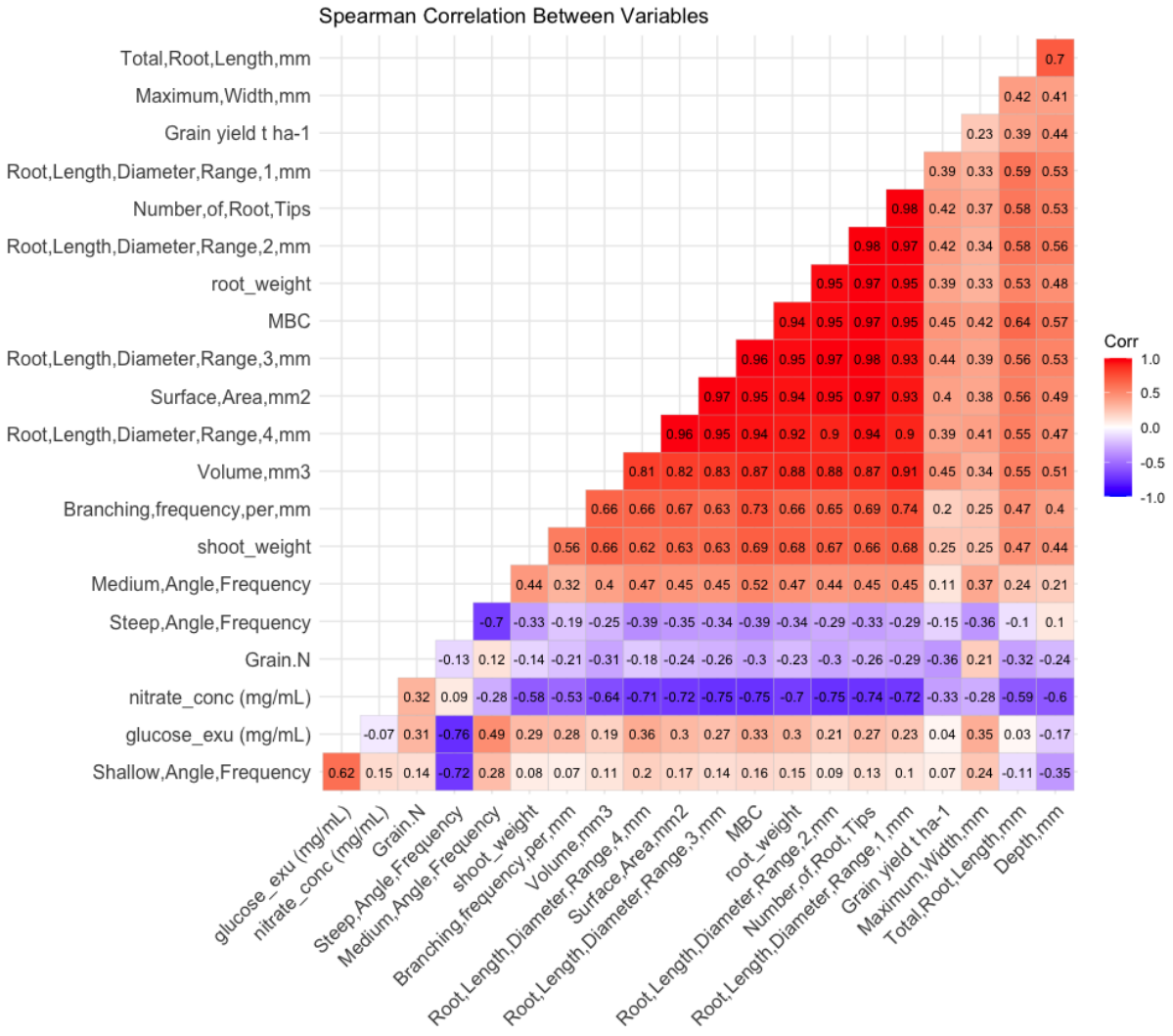

Red squares indicate positive correlations, while blue squares indicate negative correlations. The intensity of the color reflects the strength of the correlation.

10 Bibliography

Agler M.T., Ruhe J., Kroll S., Morhenn C., Kim S.-T., Weigel D. & Kemen E.M., 2016. Microbial Hub Taxa Link Host and Abiotic Factors to Plant Microbiome Variation. *PLOS Biol.* **14**(1), e1002352, DOI:10.1371/journal.pbio.1002352.

Ainsworth E., Sanz-Sáez A. & Leisner C., 2025. Crops and rising atmospheric CO2: friends or foes? *Philos. Trans. B* **380**, DOI:10.1098/rstb.2024.0230.

Altieri M.A., 2018. *Agroecology: The Science Of Sustainable Agriculture, Second Edition*, Boca Raton: CRC Press, 448.

An H.-Y., Han J.-J., He Q.-N., Zhu Y.-L., Wu P., Wang Y.-C., Gao Z.-Q., Du T.-Q. & Xue J.-F., 2024. Influence of Nitrogen Application Rate on Wheat Grain Protein Content and Composition in China: A Meta-Analysis. *Agronomy* **14**(6), 1164, DOI:10.3390/agronomy14061164.

Asseng S., Jamieson P.D., Kimball B., Pinter P., Sayre K., Bowden J.W. & Howden S.M., 2004. Simulated wheat growth affected by rising temperature, increased water deficit and elevated atmospheric CO2. *Field Crops Res.* **85**(2), 85–102, DOI:10.1016/S0378-4290(03)00154-0.

Asseng S., Martre P., Maiorano A., Rötter R.P., O'Leary G.J., Fitzgerald G.J., Girousse C., Motzo R., Giunta F., Babar M.A., Reynolds M.P., Kheir A.M.S., Thorburn P.J., Waha K., Ruane A.C., Aggarwal P.K., Ahmed M., Balkovič J., Basso B., Biernath C., Bindi M., Cammarano D., Challinor A.J., De Sanctis G., Dumont B., Eyshi Rezaei E., Fereres E., Ferrise R., Garcia-Vila M., Gayler S., Gao Y., Horan H., Hoogenboom G., Izaurralde R.C., Jabloun M., Jones C.D., Kassie B.T., Kersebaum K.-C., Klein C., Koehler A.-K., Liu B., Minoli S., Montesino San Martin M., Müller C., Naresh Kumar S., Nendel C., Olesen J.E., Palosuo T., Porter J.R., Priesack E., Ripoche D., Semenov M.A., Stöckle C., Stratonovitch P., Streck T., Supit I., Tao F., Van der Velde M., Wallach D., Wang E., Webber H., Wolf J., Xiao L., Zhang Z., Zhao Z., Zhu Y. & Ewert F., 2019. Climate change impact and adaptation for wheat protein. *Glob. Change Biol.* **25**(1), DOI:10.1111/gcb.14481.

Badri D.V. & Vivanco J.M., 2009. Regulation and function of root exudates. *Plant Cell Environ.* **32**(6), 666–681, DOI:10.1111/j.1365-3040.2009.01926.x.

Bais H.P., Weir T.L., Perry L.G., Gilroy S. & Vivanco J.M., 2006. The role of root exudates in rhizosphere interactions with plants and other organisms. *Annu. Rev. Plant Biol.* **57**, 233–266, DOI:10.1146/annurev.arplant.57.032905.105159.

Bates D., M{\"a}chler M., Bolker B. & Walker S., 2015. Fitting Linear Mixed-Effects Models Using {lme4}. *J. Stat. Softw.* 1--48.

B.C. Curtis, February-6-2025. Wheat in the world. https://www.fao.org/4/y4011e/y4011e04.htm, (06/02/2025).

Bektas H., Hohn C.E., Lukaszewski A.J. & Waines J.G., 2023. On the Possible Trade-Off between Shoot and Root Biomass in Wheat. *Plants* **12**(13), 2513, DOI:10.3390/plants12132513.

Ben-Ari T., Boé J., Ciais P., Lecerf R., Van der Velde M. & Makowski D., 2018. Causes and implications of the unforeseen 2016 extreme yield loss in the breadbasket of France. *Nat. Commun.* **9**(1), 1627, DOI:10.1038/s41467-018-04087-x.

Benayas J., Newton A., Diaz A. & Bullock J., 2009. Enhancement of Biodiversity and Ecosystem Services by Ecological Restoration: A Meta-Analysis. *Science* **325**, 1121–4, DOI:10.1126/science.1172460.

Biel W., Kazimierska K. & Bashutska U., 2020. Nutritional value of wheat, triticale, barley and oat grains. *Acta Sci. Pol. Zootech.* **19**(2), 19–28.

Biodiversa+, 2024. . *Biodiversa +*. https://www.biodiversa.eu/, (25/06/2024).

BIOFAIR, 2023. . https://www.biofair.uliege.be/cms/c_6757815/en/biofair, (25/06/2024).
Böhm W., 1979. Techniques of Root Washing. *In*: Böhm, W. ed. *Methods of Studying Root Systems*. Berlin, Heidelberg: Springer, 115–124.
Calvin K., Dasgupta D., Krinner G., Mukherji A., Thorne P.W., Trisos C., Romero J., Aldunce P., Barrett K., Blanco G., Cheung W.W.L., Connors S., Denton F., Diongue-Niang A., Dodman D., Garschagen M., Geden O., Hayward B., Jones C., Jotzo F., Krug T., Lasco R., Lee Y.-Y., Masson-Delmotte V., Meinshausen M., Mintenbeck K., Mokssit A., Otto F.E.L., Pathak M., Pirani A., Poloczanska E., Pörtner H.-O., Revi A., Roberts D.C., Roy J., Ruane A.C., Skea J., Shukla P.R., Slade R., Slangen A., Sokona Y., Sörensson A.A., Tignor M., Van Vuuren D., Wei Y.-M., Winkler H., Zhai P., Zommers Z., Hourcade J.-C., Johnson F.X., Pachauri S., Simpson N.P., Singh C., Thomas A., Totin E., Arias P., Bustamante M., Elgizouli I., Flato G., Howden M., Méndez-Vallejo C., Pereira J.J., Pichs-Madruga R., Rose S.K., Saheb Y., Sánchez Rodríguez R., Ürge-Vorsatz D., Xiao C., Yassaa N., Alegría A., Armour K., Bednar-Friedl B., Blok K., Cissé G., Dentener F., Eriksen S., Fischer E., Garner G., Guivarch C., Haasnoot M., Hansen G., Hauser M., Hawkins E., Hermans T., Kopp R., Leprince-Ringuet N., Lewis J., Ley D., Ludden C., Niamir L., Nicholls Z., Some S., Szopa S., Trewin B., Van Der Wijst K.-I., Winter G., Witting M., Birt A., Ha M., Romero J., Kim J., Haites E.F., Jung Y., Stavins R., Birt A., Ha M., Orendain D.J.A., Ignon L., Park S., Park Y., Reisinger A., Cammaramo D., Fischlin A., Fuglestvedt J.S., Hansen G., Ludden C., Masson-Delmotte V., Matthews J.B.R., Mintenbeck K., Pirani A., Poloczanska E., Leprince-Ringuet N. & Péan C., 2023. IPCC, 2023: Climate Change 2023: Synthesis Report. Contribution of Working Groups I, II and III to the Sixth Assessment Report of the Intergovernmental Panel on Climate Change [Core Writing Team, H. Lee and J. Romero (eds.)]. IPCC, Geneva, Switzerland., Intergovernmental Panel on Climate Change (IPCC).
Canarini A., Kaiser C., Merchant A., Richter A. & Wanek W., 2019. Root Exudation of Primary Metabolites: Mechanisms and Their Roles in Plant Responses to Environmental Stimuli. *Front. Plant Sci.* **10**, DOI:10.3389/fpls.2019.00157.
Cangioli L., Mancini M., Napoli M., Fagorzi C., Orlandini S., Vaccaro F. & Mengoni A., 2022. Differential Response of Wheat Rhizosphere Bacterial Community to Plant Variety and Fertilization. *Int. J. Mol. Sci.* **23**(7), 3616, DOI:10.3390/ijms23073616.
Carvalhais L.C., Dennis P.G., Fan B., Fedoseyenko D., Kierul K., Becker A., Wiren N. von & Borriss R., 2013. Linking Plant Nutritional Status to Plant-Microbe Interactions. *PLOS ONE* **8**(7), e68555, DOI:10.1371/journal.pone.0068555.
Castrillo G., Teixeira P.J.P.L., Paredes S.H., Law T.F., De Lorenzo L., Feltcher M.E., Finkel O.M., Breakfield N.W., Mieczkowski P., Jones C.D., Paz-Ares J. & Dangl J.L., 2017. Root microbiota drive direct integration of phosphate stress and immunity. *Nature* **543**(7646), 513–518, DOI:10.1038/nature21417.
Cavalieri-Polizeli K.M.V., Marcolino F.C., Tormena C.A., Keller T. & Moraes A. de, 2022. Soil Structural Quality and Relationships With Root Properties in Single and Integrated Farming Systems. *Front. Environ. Sci.* **10**, DOI:10.3389/fenvs.2022.901302.
Ceglar A., Zampieri M., Toreti A. & Dentener F., 2019. Observed Northward Migration of Agro-Climate Zones in Europe Will Further Accelerate Under Climate Change. *Earths Future* **7**(9), 1088–1101, DOI:10.1029/2019EF001178.
Chang J., Havlík P., Leclère D., de Vries W., Valin H., Deppermann A., Hasegawa T. & Obersteiner M., 2021. Reconciling regional nitrogen boundaries with global food security. *Nat. Food* **2**(9), 700–711, DOI:10.1038/s43016-021-00366-x.
Chantigny M.H., Olk D.C. & Angers D.A., 2025. Investigating the nature of soil carbohydrates and amino compounds with liquid chromatography. *Soil Sci. Soc. Am. J.* **89**(1), e270018, DOI:10.1002/saj2.70018.
Chaparro J.M., Badri D.V. & Vivanco J.M., 2014. Rhizosphere microbiome assemblage is

affected by plant development. *ISME J.* **8**(4), 790–803, DOI:10.1038/ismej.2013.196.
ChatGPT (GPT-4), 2023. .
Chen H., Dai Z., Veach A.M., Zheng J., Xu J. & Schadt C.W., 2020. Global meta-analyses show that conservation tillage practices promote soil fungal and bacterial biomass. *Agric. Ecosyst. Environ.* **293**, 106841, DOI:10.1016/j.agee.2020.106841.
Christenhusz M.J.M., 2010. The Kew Plant Glossary, an illustrated dictionary of plant terms. *Bot. J. Linn. Soc.* **164**(4), 440–441, DOI:10.1111/j.1095-8339.2010.01099.x.
Correa J., Postma J.A., Watt M. & Wojciechowski T., 2019. Soil compaction and the architectural plasticity of root systems. *J. Exp. Bot.* **70**(21), 6019–6034, DOI:10.1093/jxb/erz383.
Davidson E.A. & Janssens I.A., 2006. Temperature sensitivity of soil carbon decomposition and feedbacks to climate change. *Nature* **440**(7081), 165–173, DOI:10.1038/nature04514.
Dawson J., Huggins D. & Jones S., 2008. Characterizing nitrogen use efficiency in natural and agricultural ecosystems to improve the performance of low input and organic agricultural systems. *Field Crops Res.* **107**, 89–101, DOI:10.1016/j.fcr.2008.01.001.
de Oliveira Silva A., Ciampitti I.A., Slafer G.A. & Lollato R.P., 2020. Nitrogen utilization efficiency in wheat: A global perspective. *Eur. J. Agron.* **114**, 126008, DOI:10.1016/j.eja.2020.126008.
DeAngelis K.M., Brodie E.L., DeSantis T.Z., Andersen G.L., Lindow S.E. & Firestone M.K., 2009. Selective progressive response of soil microbial community to wild oat roots. *ISME J.* **3**(2), 168–178, DOI:10.1038/ismej.2008.103.
DeLong C., Cruse R. & Wiener J., 2015. The Soil Degradation Paradox: Compromising Our Resources When We Need Them the Most. *Sustainability* **7**(1), 866–879, DOI:10.3390/su7010866.
DESA, 2017. World Population Prospects: The 2017 Revision - Key Findings and Advance Tables - World | ReliefWeb, UN Department of Economic and Social Affairs.
DigiCamControl, n.d. DigiCamControl software (Version 2.1.2) ComputersoftwareComputersoftware. SourceForge.
Dijkstra F.A., Carrillo Y., Pendall E. & Morgan J.A., 2013. Rhizosphere priming: a nutrient perspective. *Front. Microbiol.* **4**, DOI:10.3389/fmicb.2013.00216.
Doval C.Y., 2018. What is Sustainable Agriculture? | Sustainable Agriculture Research & Education Program. https://sarep.ucdavis.edu/sustainable-ag, (05/02/2025).
Drinkwater L.E. & Snapp S.S., 2007. Nutrients in Agroecosystems: Rethinking the Management Paradigm. *In*: Sparks, D.L. ed. *Advances in Agronomy*. Academic Press, 163–186.
E. Weaver J., 1926. Root Development of Field Crops: Table of Contents. https://soilandhealth.org/wp-content/uploads/01aglibrary/010139fieldcroproots/010139toc.html, (09/04/2024).
Epson Europe, n.d. Epson scan 2 software. https://www.epson.eu/en_EU/faq/KA-01831/contents, (01/06/2025).
Epson Expression 12000XL Photo Scanner | Products | Epson US, n.d. . https://epson.com/For-Work/Scanners/Photo-and-Graphics/Epson-Expression-12000XL-Photo-Scanner/p/12000XL-PH, (01/06/2025).
Erisman J.W., Galloway J., Seitzinger S., Bleeker A. & Butterbach-Bahl K., 2011. Reactive nitrogen in the environment and its effect on climate change. *Curr. Opin. Environ. Sustain.*, Carbon and nitrogen cycles **3**(5), 281–290, DOI:10.1016/j.cosust.2011.08.012.
European Commission, June-25-2024. Consequences of climate change. https://climate.ec.europa.eu/climate-change/consequences-climate-change_en, (25/06/2024).
Eurostat, February-8-2025. Statistics | Eurostat. https://ec.europa.eu/eurostat/databrowser/view/APRO_CPSH1__custom_15296702/default/ta

ble?lang=en, (08/02/2025).
FAO, 2021. The state of the world's land and water resources for food and agriculture – Systems at breaking point. Synthesis report 2021., Rome.
FAO, 2025. Tobacco | Land & Water | Food and Agriculture Organization of the United Nations | Land & Water | Food and Agriculture Organization of the United Nations. https://www.fao.org/land-water/databases-and-software/crop-information/wheat/en/, (08/02/2025).
FAOSTAT, 2023. . https://www.fao.org/faostat/en/#data/QCL/visualize, (26/06/2024).
Folegatti M.V., Blanco F.F., Boaretto R.M. & Boaretto A.E., 2005. Calibration of cardy-ion meters to measure nutrient concentrations in soil solution an in plant sap. *Sci. Agric.* **62**, 8–11, DOI:https://doi.org/10.1590/S0103-90162005000100002.
Foley J.A., DeFries R., Asner G.P., Barford C., Bonan G., Carpenter S.R., Chapin F.S., Coe M.T., Daily G.C., Gibbs H.K., Helkowski J.H., Holloway T., Howard E.A., Kucharik C.J., Monfreda C., Patz J.A., Prentice I.C., Ramankutty N. & Snyder P.K., 2005. Global Consequences of Land Use. *Science* **309**(5734), 570–574, DOI:10.1126/science.1111772.
Fox J. & Weisberg S., 2019. An {R} Companion to Applied Regression.
Freschet G.T., Pagès L., Iversen C.M., Comas L.H., Rewald B., Roumet C., Klimešová J., Zadworny M., Poorter H., Postma J.A., Adams T.S., Bagniewska-Zadworna A., Bengough A.G., Blancaflor E.B., Brunner I., Cornelissen J.H.C., Garnier E., Gessler A., Hobbie S.E., Meier I.C., Mommer L., Picon-Cochard C., Rose L., Ryser P., Scherer-Lorenzen M., Soudzilovskaia N.A., Stokes A., Sun T., Valverde-Barrantes O.J., Weemstra M., Weigelt A., Wurzburger N., York L.M., Batterman S.A., Gomes de Moraes M., Janeček Š., Lambers H., Salmon V., Tharayil N. & McCormack M.L., 2021. A starting guide to root ecology: strengthening ecological concepts and standardising root classification, sampling, processing and trait measurements. *New Phytol.* **232**(3), 973–1122, DOI:10.1111/nph.17572.
Fumures – Livre Blanc Céréales, n.d. .
Galindo-Castañeda T., Hartmann M. & Lynch J.P., 2024. Location: root architecture structures rhizosphere microbial associations. *J. Exp. Bot.* **75**(2), 594–604, DOI:10.1093/jxb/erad421.
Galindo-Castañeda T., Lynch J.P., Six J. & Hartmann M., 2022. Improving Soil Resource Uptake by Plants Through Capitalizing on Synergies Between Root Architecture and Anatomy and Root-Associated Microorganisms. *Front. Plant Sci.* **13**, DOI:10.3389/fpls.2022.827369.
Gerwig G.J., 2021. Detection of Carbohydrates by Colorimetric Methods. *In*: Gerwig, G.J. ed. *The Art of Carbohydrate Analysis*. Cham: Springer International Publishing, 61–88.
Giot O., Termonia P., Degrauwe D., De Troch R., Caluwaerts S., Smet G., Berckmans J., Deckmyn A., De Cruz L., De Meutter P., Duerinckx A., Gerard L., Hamdi R., Van den Bergh J., Van Ginderachter M. & Van Schaeybroeck B., 2016. Validation of the ALARO-0 model within the EURO-CORDEX framework. *Geosci. MODEL Dev.* **9**(3), 1143–1152, DOI:10.5194/gmd-9-1143-2016.
Gonin M., Salas-González I., Gopaulchan D., Frene J.P., Roden S., Van de Poel B., Salt D.E. & Castrillo G., 2023. Plant microbiota controls an alternative root branching regulatory mechanism in plants. *Proc. Natl. Acad. Sci.* **120**(15), e2301054120, DOI:10.1073/pnas.2301054120.
González-Miranda I., Vidal K., Peñaloza P., González-Miranda I., Vidal K. & Peñaloza P., 2021. Comparing nitrate leaching in lettuce crops cultivated under agroecological, transition, and conventional agricultural management in central Chile. *Chil. J. Agric. Res.* **81**(2), 210–219, DOI:10.4067/S0718-58392021000200210.
Gougoulias C., Clark J.M. & Shaw L.J., 2014a. The role of soil microbes in the global carbon cycle: tracking the below-ground microbial processing of plant-derived carbon for

manipulating carbon dynamics in agricultural systems. *J. Sci. Food Agric.* **94**(12), 2362–2371, DOI:10.1002/jsfa.6577.
Gougoulias C., Clark J.M. & Shaw L.J., 2014b. The role of soil microbes in the global carbon cycle: tracking the below-ground microbial processing of plant-derived carbon for manipulating carbon dynamics in agricultural systems. *J. Sci. Food Agric.* **94**(12), 2362–2371, DOI:10.1002/jsfa.6577.
Govindasamy P., Muthusamy S., Bagavathiannan M., Mowrer J., Jagannadham P.T.K., Maity A., Halli H.M., K. S., Vadivel R., Das T.K., Raj R., Pooniya V., Babu S., Rathore S., L. M. & Tiwari G., 2023. Nitrogen use efficiency—a key to enhance crop productivity under a changing climate. *Front. Plant Sci.* **14**, 1121073, DOI:10.3389/fpls.2023.1121073.
Gruber N. & Galloway J.N., 2008. An Earth-system perspective of the global nitrogen cycle. *Nature* **451**(7176), 293–296, DOI:10.1038/nature06592.
Han X., Zhou G., Luo Q., Ferlian O., Zhou L., Meng J., Qi Y., Pei J., He Y., Liu R., Du Z., Long J., Zhou X. & Eisenhauer N., 2023. Plant biomass responses to elevated CO2 are mediated by phosphorus uptake. *Sci. Total Environ.* **863**, 160775, DOI:10.1016/j.scitotenv.2022.160775.
Hansen B., Kristensen E.S., Grant R., Høgh-Jensen H., Simmelsgaard S.E. & Olesen J.E., 2000. Nitrogen leaching from conventional versus organic farming systems — a systems modelling approach. *Eur. J. Agron.* **13**(1), 65–82, DOI:10.1016/S1161-0301(00)00060-5.
Herve M., 2025. RVAideMemoire: Testing and Plotting Procedures for Biostatistics.
Hobbs P.R., Sayre K. & Gupta R., 2008. The role of conservation agriculture in sustainable agriculture. *Philos. Trans. R. Soc. B Biol. Sci.* **363**(1491), 543–555, DOI:10.1098/rstb.2007.2169.
Hossard L., Archer D.W., Bertrand M., Colnenne-David C., Debaeke P., Ernfors M., Jeuffroy M.-H., Munier-Jolain N., Nilsson C., Sanford G.R., Snapp S.S., Jensen E.S. & Makowski D., 2016. A Meta-Analysis of Maize and Wheat Yields in Low-Input vs. Conventional and Organic Systems. *Agron. J.* **108**(3), 1155–1167, DOI:10.2134/agronj2015.0512.
Hütsch B., Augustin J. & Merbach W., 2002. Plant rhizodeposition - An important source for carbon turnover in soils. *J. Plant Nutr. Soil Sci.* **165**, 397–407, DOI:10.1002/1522-2624(200208)165:4<397::AID-JPLN397>3.0.CO;2-C.
Impact drivers, 2024. . https://climate-adapt.eea.europa.eu/en/eu-adaptation-policy/key-eu-actions/european-climate-risk-assessment/eucra-viewer-impact-drivers, (12/02/2025).
IPCC, 2014. AR5 Synthesis Report: Climate Change.
IPCC, 2021. Climate Change - The Physical Science Basis. Working Group I Contribution to the Sixth Assessment Report of the Intergovernmental Panel on Climate Change.
IPCC, n.d. SIXTH ASSESSMENT REPORT. Regional fact sheet - Europe.
ISRIC, February-27-2025. Luvisols. *www.isric.org*. https://www.isric.org/explore/world-soil-distribution/luvisols, (27/02/2025).
Jackson R.B., Lajtha K., Crow S.E., Hugelius G., Kramer M.G. & Piñeiro G., 2017. The Ecology of Soil Carbon: Pools, Vulnerabilities, and Biotic and Abiotic Controls. *Annu. Rev. Ecol. Evol. Syst.* **48**(Volume 48, 2017), 419–445, DOI:10.1146/annurev-ecolsys-112414-054234.
Jacob D., Petersen J., Eggert B., Alias A., Christensen O.B., Bouwer L.M., Braun A., Colette A., Déqué M., Georgievski G., Georgopoulou E., Gobiet A., Menut L., Nikulin G., Haensler A., Hempelmann N., Jones C., Keuler K., Kovats S., Kröner N., Kotlarski S., Kriegsmann A., Martin E., van Meijgaard E., Moseley C., Pfeifer S., Preuschmann S., Radermacher C., Radtke K., Rechid D., Rounsevell M., Samuelsson P., Somot S., Soussana J.-F., Teichmann C., Valentini R., Vautard R., Weber B. & Yiou P., 2014. EURO-CORDEX: new high-resolution climate change projections for European impact research. *Reg. Environ. Change* **14**(2), 563–578, DOI:10.1007/s10113-013-0499-2.

Jetten M.S.M., 2008. The microbial nitrogen cycle. *Environ. Microbiol.* **10**(11), 2903–2909, DOI:10.1111/j.1462-2920.2008.01786.x.
Jones D.L., Hodge A. & Kuzyakov Y., 2004. Plant and mycorrhizal regulation of rhizodeposition. *New Phytol.* **163**(3), 459–480, DOI:10.1111/j.1469-8137.2004.01130.x.
Jones D.L., Nguyen C. & Finlay R.D., 2009. Carbon flow in the rhizosphere: carbon trading at the soil–root interface. *Plant Soil* **321**(1), 5–33, DOI:10.1007/s11104-009-9925-0.
Josse J. & Husson F., 2016. {missMDA}: A Package for Handling Missing Values in Multivariate Data Analysis. *J. Stat. Softw.* 1--31.
Josse J., Husson F. & Lê S., 2008. {FactoMineR}: A Package for Multivariate Analysis. *J. Stat. Softw.* 1--18.
Karlen D.L., Peterson G.A. & Westfall D.G., 2014. Soil and Water Conservation: Our History and Future Challenges. *Soil Sci. Soc. Am. J.* **78**(5), 1493–1499, DOI:10.2136/sssaj2014.03.0110.
Karlen D.L. & Rice C.W., 2015. Soil Degradation: Will Humankind Ever Learn? *Sustainability* **7**(9), 12490–12501, DOI:10.3390/su70912490.
Kawasaki A., Dennis P.G., Forstner C., Raghavendra A.K.H., Richardson A.E., Watt M., Mathesius U., Gilliham M. & Ryan P.R., 2021. The microbiomes on the roots of wheat (Triticum aestivum L.) and rice (Oryza sativa L.) exhibit significant differences in structure between root types and along root axes. *Funct. Plant Biol. FPB* **48**(9), 871–888, DOI:10.1071/FP20351.
Khan A., Ahmad M., Ahmed M. & Iftikhar Hussain M., 2020. Rising Atmospheric Temperature Impact on Wheat and Thermotolerance Strategies. *Plants* **10**(1), 43, DOI:10.3390/plants10010043.
Kopittke P.M., Menzies N.W., Wang P., McKenna B.A. & Lombi E., 2019a. Soil and the intensification of agriculture for global food security. *Environ. Int.* **132**, 105078, DOI:10.1016/j.envint.2019.105078.
Kopittke P.M., Menzies N.W., Wang P., McKenna B.A. & Lombi E., 2019b. Soil and the intensification of agriculture for global food security. *Environ. Int.* **132**, 105078, DOI:10.1016/j.envint.2019.105078.
Kuznetsova A., Brockhoff P.B. & Christensen R.H.B., 2017. lmerTest Package: Tests in Linear Mixed Effects Models. *J. Stat. Softw.* **82**, 1–26, DOI:10.18637/jss.v082.i13.
Kuzyakov Y. & Xu X., 2013. Competition between roots and microorganisms for nitrogen: mechanisms and ecological relevance. *New Phytol.* **198**(3), 656–669, DOI:10.1111/nph.12235.
Lal R., 2015. Restoring Soil Quality to Mitigate Soil Degradation. *Sustainability* **7**(5), 5875–5895, DOI:10.3390/su7055875.
LAQUAtwin NO3-11C/NO3-11S/NO3-11, May-19-2025. . https://www.horiba.com/int/water-quality/products/detail/action/show/Product/laquatwin-no3-11c-no3-11s-no3-11-794/, (19/05/2025).
Lehman R.M., Cambardella C.A., Stott D.E., Acosta-Martinez V., Manter D.K., Buyer J.S., Maul J.E., Smith J.L., Collins H.P., Halvorson J.J., Kremer R.J., Lundgren J.G., Ducey T.F., Jin V.L. & Karlen D.L., 2015. Understanding and Enhancing Soil Biological Health: The Solution for Reversing Soil Degradation. *Sustainability* **7**(1), 988–1027, DOI:10.3390/su7010988.
Lenth R.V., 2024. emmeans: Estimated Marginal Means, aka Least-Squares Means.
Lobell D.B., Hammer G.L., McLean G., Messina C., Roberts M.J. & Schlenker W., 2013. The critical role of extreme heat for maize production in the United States. *Nat. Clim. Change* **3**(5), 497–501, DOI:10.1038/nclimate1832.
Lynch J., 1995. Root Architecture and Plant Productivity. *Plant Physiol.* **109**(1), 7–13, DOI:10.1104/pp.109.1.7.

Lynch J.P., 2019. Root phenotypes for improved nutrient capture: an underexploited opportunity for global agriculture. *New Phytol.* **223**(2), 548–564, DOI:10.1111/nph.15738.
Lynch J.P., 2022a. Harnessing root architecture to address global challenges. *Plant J.* **109**(2), 415–431, DOI:10.1111/tpj.15560.
Lynch J.P., 2022b. Harnessing root architecture to address global challenges. *Plant J.* **109**(2), 415–431, DOI:10.1111/tpj.15560.
Mäkinen H., Kaseva J., Trnka M., Balek J., Kersebaum K.C., Nendel C., Gobin A., Olesen J.E., Bindi M., Ferrise R., Moriondo M., Rodríguez A., Ruiz-Ramos M., Takáč J., Bezák P., Ventrella D., Ruget F., Capellades G. & Kahiluoto H., 2018. Sensitivity of European wheat to extreme weather. *Field Crops Res.* **222**, 209–217, DOI:10.1016/j.fcr.2017.11.008.
Matson P.A., Parton W.J., Power A.G. & Swift M.J., 1997. Agricultural Intensification and Ecosystem Properties. *Science* **277**(5325), 504–509, DOI:10.1126/science.277.5325.504.
McGrath J.M. & Lobell D.B., 2013. Reduction of transpiration and altered nutrient allocation contribute to nutrient decline of crops grown in elevated CO(2) concentrations. *Plant Cell Environ.* **36**(3), 697–705, DOI:10.1111/pce.12007.
Micallef S.A., Shiaris M.P. & Colón-Carmona A., 2009. Influence of Arabidopsis thaliana accessions on rhizobacterial communities and natural variation in root exudates. *J. Exp. Bot.* **60**(6), 1729–1742, DOI:10.1093/jxb/erp053.
Michel J., Leemans V., Weinmann M., Balanzategui I., Bin J., Biver S., Blum A., Börger R., Cao D., Him S., Kirbas G., Le Gouis J., Moya-Larano J., Persyn M., Pierreux J., Quenon A., Sánchez-Moreno S., Symanczik S., Brande F. & Delaplace P., 2024. *Low-input soil management increases yield and decreases CO2-emissions but aggravates risk of nitrate leaching and diseases in winter wheat cropping systems under climate change*.
Michel J., Leemans V., Weinmann M., Balanzategui-Guijarro I., Bin J., Biver S., Blum A., Börger R., Cao D., Him S.-L., Kirbas G., Gouis J.L., Moya-Laraño J., Persyn M., Pierreux J., Quenon A., Sanchez-Moreno S., Symanczik S., Brande F.V., Straeten D.V.D., Wagner M., Waibel M., Xayphrarath A., Vanderschuren H., Thonar C. & Delaplace P., 2025. Trade-offs associated with higher winter wheat yields in low soil organic matter cropping systems under climate change.
Mönchgesang S., Strehmel N., Schmidt S., Westphal L., Taruttis F., Müller E., Herklotz S., Neumann S. & Scheel D., 2016. Natural variation of root exudates in Arabidopsis thaliana-linking metabolomic and genomic data. *Sci. Rep.* **6**(1), 29033, DOI:10.1038/srep29033.
Moore F.C. & Lobell D.B., 2015. The fingerprint of climate trends on European crop yields. *Proc. Natl. Acad. Sci.* **112**(9), 2670–2675, DOI:10.1073/pnas.1409606112.
Müller K., Vaughan D., Wickham H., François R. & Henry L., 2023. dplyr: A Grammar of Data Manipulation.
Mundt F. & Kassambara A., 2020. factoextra: Extract and Visualize the Results of Multivariate Data Analyses.
Myers S. & Smith M., 2018. Impact of anthropogenic CO2 emissions on global human nutrition. *Nat. Clim. Change* **8**, DOI:10.1038/s41558-018-0253-3.
Myers S.S., Zanobetti A., Kloog I., Huybers P., Leakey A.D.B., Bloom A.J., Carlisle E., Dietterich L.H., Fitzgerald G., Hasegawa T., Holbrook N.M., Nelson R.L., Ottman M.J., Raboy V., Sakai H., Sartor K.A., Schwartz J., Seneweera S., Tausz M. & Usui Y., 2014. Increasing CO2 threatens human nutrition. *Nature* **510**(7503), 139–142, DOI:10.1038/nature13179.
Nations U., June-24-2024. What Is Climate Change? *U. N.* https://www.un.org/en/climatechange/what-is-climate-change, (24/06/2024).
Noel S., Mikulcak F., Etter H. & Stewart N., 2015. Economics of Land Degradation Initiative: Report for policy and decision makers_ Reaping economic and environmental benefits from sustainable land management (Report), ELD Initiative and Deutsche Gesellschaft für

Internationale Zusammenarbeit (GIZ) GmbH.
OECD & Food and Agriculture Organization of the United Nations, 2022. *OECD-FAO Agricultural Outlook 2022-2031*, OECD-FAO Agricultural Outlook, OECD.
Pachauri R.K., Mayer L., & Intergovernmental Panel on Climate Change (Eds.), 2015. *Climate change 2014: synthesis report*, Geneva, Switzerland: Intergovernmental Panel on Climate Change, 151.
Palacin H., 2024. Les importations et exportations de céréales dans l'Union européenne. *Touteleurope.eu*. https://www.touteleurope.eu/agriculture-et-peche/les-importations-et-exportations-de-cereales-dans-l-union-europeenne/, (09/02/2025).
Parry M.A.J., Reynolds M., Salvucci M.E., Raines C., Andralojc P.J., Zhu X.-G., Price G.D., Condon A.G. & Furbank R.T., 2011. Raising yield potential of wheat. II. Increasing photosynthetic capacity and efficiency. *J. Exp. Bot.* **62**(2), 453–467, DOI:10.1093/jxb/erq304.
Pellitier P. & Jackson R., 2022. Microbes modify soil nutrient availability and mediate plant responses to elevated CO2. *Plant Soil* **483**, 1–8, DOI:10.1007/s11104-022-05807-5.
Piepho H.-P., Selzer L. & Graves S., 2024. multcompView: Visualizations of Paired Comparisons.
Porter J., Xie L., Challinor A., Chhetri N., Nepal U., Garrett K., Aggarwal P.K., Hakala K., Jordan J., Barros R., Dokken D., Mach K., Mastrandrea T., Bilir M., Chatterjee K., Ebi Y., Estrada R., Genova B., Girma E., & White, 2014. 7 Food Security and Food Production Systems Coordinating Lead Authors: Lead Authors: Contributing Authors: Review Editors: Volunteer Chapter Scientist. 485–533.
Pradhan G.P., Prasad P.V.V., Fritz A.K., Kirkham M.B. & Gill B.S., 2012. Effects of drought and high temperature stress on synthetic hexaploid wheat. *Funct. Plant Biol. FPB* **39**(3), 190–198, DOI:10.1071/FP11245.
Qin M., Zheng E., Hou D., Meng X., Meng F., Gao Y., Chen P., Qi Z. & Xu T., 2023. Response of Wheat, Maize, and Rice to Changes in Temperature, Precipitation, CO2 Concentration, and Uncertainty Based on Crop Simulation Approaches. *Plants* **12**(14), 2709, DOI:10.3390/plants12142709.
R Core Team, 2024. R: A Language and Environment for Statistical Computing.
Rahmann G., 2011. Biodiveristy and Organic farming : What do we know? *Landbauforsch. - VTI Agric. For. Res.* **3**(61), 189–208.
Rama B., Pörtner H.-O., Roberts D.C., Tignor M., Poloczanska E.S., Mintenbeck K., Alegría A., Craig M., Langsdorf S., Löschke S., Möller V. & Okem A. (Eds.), 2023. *Climate Change 2022:Impacts, Adaptation and Vulnerability. Contribution of Working Group II to the Sixth Assessment Report of the Intergovernmental Panel on Climate Change*, Cambridge: Cambridge University Press.
Regulation - 889/2008 - EN - EUR-Lex, June-24-2024. . https://eur-lex.europa.eu/eli/reg/2008/889/oj, (24/06/2024).
Rengel Z. & Römheld V., 2000. Root exudation and Fe uptake and transport in wheat genotypes differing in tolerance to Zn deficiency. *Plant Soil* **222**(1/2), 25–34.
Reynolds M., Bonnett D., Chapman S.C., Furbank R.T., Manès Y., Mather D.E. & Parry M.A.J., 2011. Raising yield potential of wheat. I. Overview of a consortium approach and breeding strategies. *J. Exp. Bot.* **62**(2), 439–452, DOI:10.1093/jxb/erq311.
Riahi K., Rao S., Krey V., Cho C., Chirkov V., Fischer G., Kindermann G., Nakicenovic N. & Rafaj P., 2011. RCP 8.5—A scenario of comparatively high greenhouse gas emissions. *Clim. Change* **109**(1), 33, DOI:10.1007/s10584-011-0149-y.
Richardson A.E., Barea J.-M., McNeill A.M. & Prigent-Combaret C., 2009. Acquisition of phosphorus and nitrogen in the rhizosphere and plant growth promotion by microorganisms. *Plant Soil* **321**(1), 305–339, DOI:10.1007/s11104-009-9895-2.
Riedesel L., Möller M., Horney P., Golla B., Piepho H.-P., Kautz T. & Feike T., 2023.

Timing and intensity of heat and drought stress determine wheat yield losses in Germany. *PLOS ONE* **18**(7), e0288202, DOI:10.1371/journal.pone.0288202.
Ripley B.D. & Venables W.N., 2002. *Modern Applied Statistics with S*, Springer, New York.
Rolfe S.A., Griffiths J. & Ton J., 2019. Crying out for help with root exudates: adaptive mechanisms by which stressed plants assemble health-promoting soil microbiomes. *Curr. Opin. Microbiol.*, Environmental Microbiology **49**, 73–82, DOI:10.1016/j.mib.2019.10.003.
Rudrappa T., Czymmek K.J., Paré P.W. & Bais H.P., 2008. Root-Secreted Malic Acid Recruits Beneficial Soil Bacteria. *Plant Physiol.* **148**(3), 1547–1556, DOI:10.1104/pp.108.127613.
Rustad L., Campbell J., Marion G., Norby R., Mitchell M., Hartley A., Cornelissen J., Gurevitch J., & GCTE-NEWS, 2001. A meta-analysis of the response of soil respiration, net nitrogen mineralization, and aboveground plant growth to experimental ecosystem warming. *Oecologia* **126**(4), 543–562, DOI:10.1007/s004420000544.
Sasse J., Martinoia E. & Northen T., 2018. Feed Your Friends: Do Plant Exudates Shape the Root Microbiome? *Trends Plant Sci.* **23**(1), 25–41, DOI:10.1016/j.tplants.2017.09.003.
Scavo A., Abbate C. & Mauromicale G., 2019. Plant allelochemicals: agronomic, nutritional and ecological relevance in the soil system. *Plant Soil* **442**, DOI:10.1007/s11104-019-04190-y.
Schützenmeister A. & Piepho H.-P., 2012. Residual analysis of linear mixed models using a simulation approach. *Comput. Stat. Data Anal.* **56**(6), 1405–1416, DOI:10.1016/j.csda.2011.11.006.
Seethepalli A., Dhakal K., Griffiths M., Guo H., Freschet G.T. & York L.M., 2021. RhizoVision Explorer: open-source software for root image analysis and measurement standardization. *AoB Plants* **13**(6), plab056, DOI:10.1093/aobpla/plab056.
Seethepalli A., Guo H., Liu X., Griffiths M., Almtarfi H., Li Z., Liu S., Zare A., Fritschi F.B., Blancaflor E.B., Ma X.-F. & York L.M., 2020. RhizoVision Crown: An Integrated Hardware and Software Platform for Root Crown Phenotyping. *Plant Phenomics* **2020**, DOI:10.34133/2020/3074916.
Seethepalli A. & York L.M., 2021. RhizoVision Explorer - Interactive software for generalized root image analysis designed for everyone.
Seidel S.J., Ahmadi S.H., Weihermüller L., Couëdel A., Lopez G., Behrend D., Kamali B., Gaiser T. & Hernández-Ochoa I.M., 2024. The overlooked effects of environmental impacts on root:shoot ratio in experiments and soil-crop models. *Sci. Total Environ.* **955**, 176738, DOI:10.1016/j.scitotenv.2024.176738.
Sheoran et al., 2019. Impact of organic and conventional farming practices on soil quality: a global review, Budapest, Hungary, APPLIED ECOLOGY AND ENVIRONMENTAL RESEARCH.
Shiferaw B., Smale M., Braun H.-J., Duveiller E., Reynolds M. & Muricho G., 2013. Crops that feed the world 10. Past successes and future challenges to the role played by wheat in global food security. *Food Secur.* **5**(3), 291–317, DOI:10.1007/s12571-013-0263-y.
Smith S.E. & Read D., 2008. INTRODUCTION. *In*: Smith, S.E., Read, D. eds. *Mycorrhizal Symbiosis (Third Edition)*. London: Academic Press, 1–9.
Stocker T.F., D. Qin G.-K., Plattner M., Tignor S.K., Allen J., Boschung A., Nauels Y., Xia V., Midgley B. & Midgley P.M., 2013. Climate Change 2013: The Physical Science Basis. Contribution of Working Group I to the Fifth Assessment Report of the Intergovern- mental Panel on Climate Change, Cambridge University Press, Cambridge, United Kingdom and New York, NY, USA.
Sun C.-H., Yu J.-Q. & Hu D.-G., 2017. Nitrate: A Crucial Signal during Lateral Roots Development. *Front. Plant Sci.* **8**, DOI:10.3389/fpls.2017.00485.
Terrer C., Jackson R.B., Prentice I.C., Keenan T.F., Kaiser C., Vicca S., Fisher J.B., Reich

P.B., Stocker B.D., Hungate B.A., Peñuelas J., McCallum I., Soudzilovskaia N.A., Cernusak L.A., Talhelm A.F., Van Sundert K., Piao S., Newton P.C.D., Hovenden M.J., Blumenthal D.M., Liu Y.Y., Müller C., Winter K., Field C.B., Viechtbauer W., Van Lissa C.J., Hoosbeek M.R., Watanabe M., Koike T., Leshyk V.O., Polley H.W. & Franklin O., 2020. Author Correction: Nitrogen and phosphorus constrain the CO2 fertilization of global plant biomass. *Nat. Clim. Change* **10**(7), 696–697, DOI:10.1038/s41558-020-0808-y.
Trachsel S., Kaeppler S.M., Brown K.M. & Lynch J.P., 2013. Maize root growth angles become steeper under low N conditions. *Field Crops Res.* **140**, 18–31, DOI:10.1016/j.fcr.2012.09.010.
USDA, February-8-2025. Crop Explorer - Europe. https://ipad.fas.usda.gov/cropexplorer/imageview.aspx?regionid=europe, (08/02/2025).
van der Velde M., Baruth B., Bussay A., Ceglar A., Garcia Condado S., Karetsos S., Lecerf R., Lopez R., Maiorano A., Nisini L., Seguini L. & van den Berg M., 2018. In-season performance of European Union wheat forecasts during extreme impacts. *Sci. Rep.* **8**(1), 1–10, DOI:10.1038/s41598-018-33688-1.
van Groenigen K.J., Qi X., Osenberg C.W., Luo Y. & Hungate B.A., 2014. Faster decomposition under increased atmospheric CO_2 limits soil carbon storage. *Science* **344**(6183), 508–509, DOI:10.1126/science.1249534.
Vandenkoornhuyse P., Quaiser A., Duhamel M., Le Van A. & Dufresne A., 2015. The importance of the microbiome of the plant holobiont. *New Phytol.* **206**(4), 1196–1206, DOI:10.1111/nph.13312.
Wagg C., Bender S.F., Widmer F. & van der Heijden M.G.A., 2014. Soil biodiversity and soil community composition determine ecosystem multifunctionality. *Proc. Natl. Acad. Sci.* **111**(14), 5266–5270, DOI:10.1073/pnas.1320054111.
Wen Z., White P.J., Shen J. & Lambers H., 2022. Linking root exudation to belowground economic traits for resource acquisition. *New Phytol.* **233**(4), 1620–1635, DOI:10.1111/nph.17854.
What Is Climate Change? - NASA Science, June-24-2024. . https://science.nasa.gov/climate-change/what-is-climate-change/, (24/06/2024).
Whatman prepleated qualitative filter paper for technical use, Grade 0858 1/2, grained circles, diam. 320 mm, pack of 100 Whatman paper, May-21-2025. . https://www.sigmaaldrich.com/BE/en/product/aldrich/wha10334353, (21/05/2025).
Wickham H., 2016. ggplot2: Elegant Graphics for Data Analysis. Springer-Verlag New York.
Wickham H. & Bryan J., 2025. readxl: Read Excel Files.
Wickham H., Girlich M. & Vaughan D., 2024. tidyr: Tidy Messy Data.
Yemm E.W. & Willis A.J., 1954. The estimation of carbohydrates in plant extracts by anthrone. *Biochem. J.* **57**(3), 508–514.
Zai X., Luo W., Bai W., Li Y., Xiao X., Gao X., Wang E., Wei G. & Chen W., 2021. Effect of Root Diameter on the Selection and Network Interactions of Root-Associated Bacterial Microbiomes in Robinia pseudoacacia L. *Microb. Ecol.* **82**(2), 391–402, DOI:10.1007/s00248-020-01678-4.
Zak D.R., Pregitzer K.S., King J.S. & Holmes W.E., 2000. Elevated atmospheric CO2, fine roots and the response of soil microorganisms: a review and hypothesis. *New Phytol.* **147**(1), 201–222, DOI:10.1046/j.1469-8137.2000.00687.x.
Zampieri M., Ceglar A., Dentener F. & Toreti A., 2017. Wheat yield loss attributable to heat waves, drought and water excess at the global, national and subnational scales. *Environ. Res. Lett.* **12**(6), 064008, DOI:10.1088/1748-9326/aa723b.